A premotor connectome reveals circuits for rapid, flexible, and precise wing control in *Drosophila*

Ellen Lesser

A dissertation
submitted in partial fulfillment of the
requirements for the degree of

Doctor of Philosophy

University of Washington

2024

Reading Committee:

John Tuthill, Chair

Tom Daniel

Nino Ramirez

Jim Truman

Jay Parrish

Program Authorized to Offer Degree:
Neuroscience

University of Washington

Abstract

A premotor connectome reveals circuits for rapid, flexible, and precise wing control in *Drosophila*

Ellen Lesser

Chair of the Supervisory Committee:
Associate Professor John Tuthill
Physiology and Biophysics

The nerve cord[1] processes information from sensory systems and controls muscles. These computations are implemented by neural circuits: networks of neurons with synapses between them. This project seeks to gain insight into features of neural circuit organization that allow an animal to rapidly respond to a changing environment. Even a fly, which has a fraction of the number of neurons as a human, has neural circuits that give rise to highly precise control of muscles informed by complex sensory inputs. This precision is especially important when a fly is in flight, as the animal actively controls its path by making small adjustments in muscles that controls the wings[1,2]. To gain insight into the anatomical circuits that coordinate flight, we reconstructed neurons in sensorimotor circuits that control the wing. We identified muscle targets of all the wing motor neurons, analyzed the synaptic weights between premotor neurons and motor neurons, and mapped sensory axons to the structures on the wing that they innervate. By analyzing wing circuitry alongside leg circuitry in the same animal, we found evidence that premotor circuit organization is dictated by the biomechanical properties of the joint it controls. This project demonstrates that the synaptic structure of sensorimotor circuits can vary even within the same animal. We propose that the specific circuit architectures we observe correspond to the biomechanical constraints of

[1]known as the spinal cord in vertebrates

different types of joints. By analyzing circuits at the level of single neurons and synapses, this work seeks to expand our understanding of the many ways sensorimotor circuits can be organized.

BIBLIOGRAPHY

[1] M. H. Dickinson, F. O. Lehmann, and K. G. Götz. "The active control of wing rotation by Drosophila". In: *The Journal of Experimental Biology* 182 (Sept. 1993), pp. 173–189. ISSN: 0022-0949. DOI: 10.1242/jeb.182.1.173.

[2] Bradley H. Dickerson et al. "Flies Regulate Wing Motion via Active Control of a Dual-Function Gyroscope". In: *Current biology: CB* 29.20 (Oct. 21, 2019), 3517–3524.e3. ISSN: 1879-0445. DOI: 10.1016/j.cub.2019.08.065.

TABLE OF CONTENTS

LIST OF FIGURES

LIST OF TABLES

ACKNOWLEDGMENTS

I am incredibly grateful for the mentorship, support, and community that I've found at UW. First, for the mentorship of my advisor, John Tuthill. Your commitment to scientific rigor combined with curiosity and creativity inspires me to be the kind of scientist I hope to be. I am grateful to the energy and thought you continue to put towards creating a lab environment that is equal parts challenge and encouragement. I am also grateful for the mentorship of Tony Azevedo - for your advice, thoughtfulness, and patience. I've learned a ton from you.

I am fortunate to have received invaluable guidance from scientists outside of the Tuthill Lab. Thank you to my Committee – Tom Daniel, Jim Truman, Nino Ramirez, and Jay Parrish, for all of your advice throughout this project. Thank you, as well, to Wei-Chung Lee and the FANC community. Exploring the FANC dataset had a huge influence on the way I think about research and changed the trajectory of my projects for the better. Thank you as well to Michael Dickinson, for guidance and feedback on manuscripts, and for driving the flight muscle project at MBL, which was a highlight of my time in graduate school.

Thank you to the entire Tuthill Lab, past and present, which is a hub of motivation and energy. Every lab meeting I am impressed by the care and effort each person puts into developing projects and communicating. A special thank you to Anne, for answering way too many questions and always finding new ways to capture better images. And to Su-Yee, Brandon, and Lylah, for so much kindness when I needed it most.

To my close Seattle community – Hadley, thank you for co-creating our home and filling it with art nights and chocolate; and Melissa, for running hundreds of miles with me and still being a great friend. And of course Trevor, who makes every day better and consistently brings contagious joy to everyone around.

Finally, to my family, who is always there for me and for each other.

Chapter 1

INTRODUCTION

1.1 Background

Every animal, including humans, shares the same basic blueprint for sensing and moving. A large part of this shared blueprint is the nervous system, which integrates information from disparate sensory systems and distributes commands to coordinate muscles. In a passionate treatise on mayflies, the anatomist Jan Swammerdam wrote "[animals] here and there differ in some accidents yet in the chief parts they all agree, which is one of Gods greatest wonders in nature; so that it might be said that he had Created but one Animal hidden under several outward shapes, and endless wonderful accidents."[1] Although his scientific intuition was undoubtedly influenced by the religious cult of which he was a member during this time[2], he saw past animals' exotic outsides by noticing similarities in their internal structures. It's not surprising that Swammerdam's muse was an insect in flight.

1.1.1 Motor control

Whether flying, walking, or dancing, muscles move the body according to instructions from the nervous system. Motor neurons are specialized neurons that have dendrites in the central nervous system and extend axons across the body to innervate muscles[3]. A single motor neuron and the muscle fibers that it innervates are called a motor unit (**Figure 1.1A**). Groups of motor units that innervate the same muscle make up a motor pool (**Figure 1.1B**). The nervous system coordinates activity across motor units to scale how many muscle fibers are recruited and thus how much force is produced[4]. It also coordinates activity across motor pools to produce movements that require the use of more than one muscle (e.g. most natural movements)[5]. At both the level of motor units as well as motor pools, the nervous system

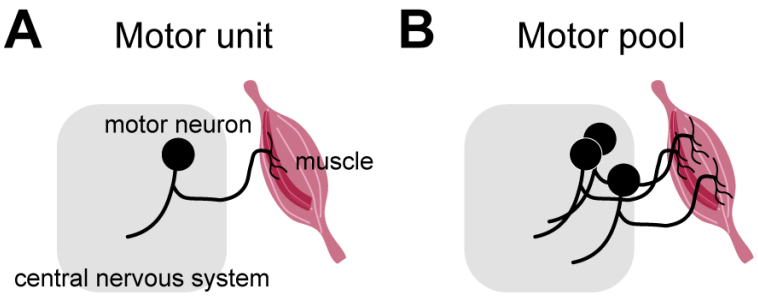

Figure 1.1: A. A motor unit is a single motor neuron and the muscle fibers that it innervates. **B.** A motor pool is a group of motor units that innervate the same muscle.

is organized such that the complexity of control is reduced, for example by forming circuits that co-activate muscles that are often contracted at the same time for specific movements[6,7].

1.1.2 Insect flight

Just as neural commands from our spinal cord instruct our muscles how to walk, winged insects' nervous systems direct flight by sending signals to muscles. Unlike our legs or the wings of pterosaurs, bats, or birds, though, insect wings have no muscles within them. Instead, muscles in the thorax cause wings to move. Small insects have small wings and smaller muscles, and possess a specialized neuro-muscular system to beat their wings at high enough frequencies to stay in the air. To efficiently provide enough power for wings to beat at frequencies over 100 Hz, two-winged insects (*diptera*) devote most of their thorax space to muscles that cause the thorax to oscillate, which causes the wings to move back and forth[8,9]. These muscles are physiologically specialized to be stretch-activated so that they can oscillate at high frequencies[8]. This specialization means that the muscles don't need neural input for every contraction. They contract asynchronously with the neural input they receive[10]. The oscillating thorax transfers power to the wing hinge, an enigmatic joint made up of mechanically linked cuticular folds where the wing attaches to the thorax[11,12]. Some of the cuticular folds, called sclerites, have muscles attached to them[13,14,15,16], which

allow the animal to modify the conformation of the wing hinge and thus alter the wing's trajectory for low-latency steering maneuvers[17]. The two specialized and separate motor systems, in addition to a third motor system for terrestrial locomotion, makes *diptera* an excellent model system for understanding neural control of muscles across a range of types of joints and movements.

1.1.3 Sensory Feedback and Central Pattern Generators

Most forms of locomotion consist of repeating a basic cycle of movement, such as steps for walking and wing strokes for flying. One way to simplify the neural commands for a repetitive movement is to have a circuit that gives rise to cyclic activity without needing constant input, known as a central pattern generator (CPG)[18]. In locusts, particular interneurons in motor circuits produce cyclical firing patterns when activated by a neurotransmitter, octopamine, which floods the nervous system during flight[19]. These oscillatory neurons are not the only input to motor neurons, though. Motor neurons also receive direct and indirect sensory feedback that can cause them to activate in advance or at a delay from their usual timing during a movement's phase[20]. Steady input from pattern-generating interneurons with signals from sensory axons allows motor networks to be both robust and responsive to changing conditions.

1.1.4 Circuits, Anatomy and Function

Neural circuits are physical structures made up of cells and the synapses between them. This project aims to analyze the physical anatomy of neural circuits - from peripheral sensory structures to muscles - to build intuition and address central questions about neural circuits. By analyzing neural circuits used to control the wing, we build on what is already known about insect flight to determine **what features of neural circuit organization allow an animal to rapidly respond to a changing environment**. First, we determine the outputs of the system, e.g. what muscle does each motor neuron innervate? Next, we determine the inputs to motor neurons and analyze their cell class, developmental identity,

neurotransmitter, and connectivity. Finally, we determine the inputs of the system, e.g. from which sensory structure on the wing does each sensory axon arise? We take advantage of new connectomic tools to look deeper into enduring questions about motor control of insect flight.

1.2 Research methods

Historically, a major advantage of studying neural systems in *Drosophila* is the accessibility of large libraries of genetic tools. Recently, advances in connectomics have led to full, dense reconstructions of the *Drosophila* brain and nerve cord at high resolution, such that single synapses can be identified[21,22,23,24]. By combining these resources, researchers can both target the same particular cell across flies, as well as query its connectivity with other cells. This project uses FANC, a community-driven connectome project, which includes a number of tools built to explore and analyze the dataset[25,26,27]. This project also relies on the FlyLight public collection of Gal4 lines and images stacks, especially the large library of images of single-cell labeling of driver lines[28]. It cannot be overstated the degree to which accessible resources like these make exploratory research feasible.

1.3 Key results

We established public resources for mapping motor and sensory neurons in the *Drosophila* ventral nerve cord to their peripheral origins or terminals. We found that groups of two to four wing steering motor neurons receive synaptic input from common premotor neurons, providing a physical substrate for harnessing ensembles of muscles that are not necessarily attached to the same wing hinge sclerite. We also found that the premotor input to these groups does not mirror the stereotyped circuits we observe in circuits for leg control, suggesting that there may be a higher degree of flexibility in the recruitment order of wing steering motor neurons. Finally, by identifying many of the axon morphologies of wing sensory neurons, we determined that a majority of direct sensory input to wing motor neurons is from the field of campaniform sensilla on the tegula. We also found that campaniform sensilla

within the same field along the radial vein can have different axon morphologies in the nerve cord, suggesting a circuit mechanism for parallelizing sensory information to different parts of the nervous system. Together, this project demonstrates how connectomics can inform research questions as well as determining features of the *Drosophila* nervous system that allow fruit flies to navigate the air with agility and grace.

References

[1] Jan Swammerdam. *Ephemeri vita, or, The natural history and anatomy of the Ephemeron, a fly that lives but five hours*. 1675. URL: https://quod.lib.umich.edu/e/eebo/A62018.0001.001?view=toc (visited on 02/27/2024).

[2] Matthew Cobb. *Generation*. Bloomsbury. 2008. URL: https://www.bloomsbury.com/us/generation-9781608190010/ (visited on 02/27/2024).

[3] Charles Scott Sherrington. *The integrative action of the nervous system*. Yale paper-bound ; Y-35. New Haven: Yale University Press, 1906.

[4] D. Kernell and H. Sjöholm. "Recruitment and firing rate modulation of motor unit tension in a small muscle of the cat's foot". In: *Brain Research* 98.1 (Nov. 7, 1975), pp. 57–72. ISSN: 0006-8993. DOI: 10.1016/0006-8993(75)90509-0. URL: http://www.sciencedirect.com/science/article/pii/0006899375905090 (visited on 07/10/2019).

[5] M. C. Tresch, P. Saltiel, and E. Bizzi. "The construction of movement by the spinal cord". In: *Nature Neuroscience* 2.2 (Feb. 1999), pp. 162–167. ISSN: 1097-6256. DOI: 10.1038/5721.

[6] Matthew C Tresch et al. "Coordination and localization in spinal motor systems". In: *Brain Research Reviews*. The Segerfalk symposium on Principles of Spinal Cord Function, Plasticity and Repair 40.1 (Oct. 1, 2002), pp. 66–79. ISSN: 0165-0173. DOI: 10.1016/S0165-0173(02)00189-3. URL: https://www.sciencedirect.com/science/article/pii/S0165017302001893 (visited on 01/13/2023).

[7] Emma F. Hodson-Tole and James M. Wakeling. "Motor unit recruitment for dynamic tasks: current understanding and future directions". In: *Journal of Comparative Physiology B* 179.1 (Jan. 1, 2009), pp. 57–66. ISSN: 1432-136X. DOI: 10.1007/s00360-008-0289-1. URL: https://doi.org/10.1007/s00360-008-0289-1 (visited on 04/10/2023).

[8] J. W. S. Pringle. "The excitation and contraction of the flight muscles of insects". In: *The Journal of Physiology* 108.2 (1949). _eprint: https://onlinelibrary.wiley.com/doi/pdf/10.1113/jp pp. 226–232. ISSN: 1469-7793. DOI: 10.1113/jphysiol.1949.sp004326. URL: https://onlinelibrary.wiley.com/doi/abs/10.1113/jphysiol.1949.sp004326 (visited on 04/10/2023).

[9] Tanvi Deora, Namrata Gundiah, and Sanjay P. Sane. "Mechanics of the thorax in flies". In: *The Journal of Experimental Biology* 220 (Pt 8 Apr. 15, 2017), pp. 1382–1395. ISSN: 1477-9145. DOI: 10.1242/jeb.128363.

[10] J. C. Coggshall. "Neurons associated with the dorsal longtitudinal flight muscles of Drosophilla melanogaster". In: *The Journal of Comparative Neurology* 177.4 (Feb. 15, 1978), pp. 707–720. ISSN: 0021-9967. DOI: 10.1002/cne.901770410.

[11] F. O. Lehmann and M. H. Dickinson. "The production of elevated flight force compromises manoeuvrability in the fruit fly Drosophila melanogaster". In: *The Journal of Experimental Biology* 204 (Pt 4 Feb. 2001), pp. 627–635. ISSN: 0022-0949. DOI: 10.1242/jeb.204.4.627.

[12] F. O. Lehmann and M. H. Dickinson. "The changes in power requirements and muscle efficiency during elevated force production in the fruit fly Drosophila melanogaster". In: *The Journal of Experimental Biology* 200 (Pt 7 Apr. 1997), pp. 1133–1143. ISSN: 0022-0949. DOI: 10.1242/jeb.200.7.1133.

[13] Edward G. Boettiger and Edwin Furshpan. "The mechanics of flight movements in diptera". In: *The Biological Bulletin* 102.3 (June 1952). Publisher: The University of

Chicago Press, pp. 200–211. ISSN: 0006-3185. DOI: 10.2307/1538368. URL: https://www.journals.uchicago.edu/doi/abs/10.2307/1538368 (visited on 05/16/2023).

[14] J. A. Miyan and A. W. Ewing. "How Diptera move their wings: a re-examination of the wing base articulation and muscle systems concerned with flight". In: *Philosophical Transactions of the Royal Society of London. B, Biological Sciences* 311.1150 (Nov. 19, 1985). Publisher: Royal Society, pp. 271–302. DOI: 10.1098/rstb.1985.0154. URL: https://royalsocietypublishing.org/doi/10.1098/rstb.1985.0154 (visited on 10/19/2022).

[15] J. R. Trimarchi and A. M. Schneiderman. "The motor neurons innervating the direct flight muscles of Drosophila melanogaster are morphologically specialized". In: *The Journal of Comparative Neurology* 340.3 (Feb. 15, 1994), pp. 427–443. ISSN: 0021-9967. DOI: 10.1002/cne.903400311.

[16] Carroll M. Williams and Muriel Voter Williams. "The flight muscles of Drosophila repleta". In: *Journal of Morphology* 72.3 (1943). _eprint: https://onlinelibrary.wiley.com/doi/pdf/10.10 pp. 589–599. ISSN: 1097-4687. DOI: 10.1002/jmor.1050720308. URL: https://onlinelibrary.wiley.com/doi/abs/10.1002/jmor.1050720308 (visited on 05/16/2023).

[17] Michael H Dickinson and Michael S Tu. "The Function of Dipteran Flight Muscle". In: *Comparative Biochemistry and Physiology Part A: Physiology* 116.3 (Mar. 1, 1997), pp. 223–238. ISSN: 0300-9629. DOI: 10.1016/S0300-9629(96)00162-4. URL: https://www.sciencedirect.com/science/article/pii/S0300962996001624 (visited on 02/14/2024).

[18] Eve Marder and Dirk Bucher. "Central pattern generators and the control of rhythmic movements". In: *Current Biology* 11.23 (Nov. 27, 2001). Publisher: Elsevier, R986–R996. ISSN: 0960-9822. DOI: 10.1016/S0960-9822(01)00581-4. URL: https://www.cell.com/current-biology/abstract/S0960-9822(01)00581-4 (visited on 02/29/2024).

[19] Jan-Marino Ramirez and Keir G. Pearson. "Octopamine induces bursting and plateau potentials in insect neurones". In: *Brain Research* 549.2 (May 24, 1991), pp. 332–337. ISSN: 0006-8993. DOI: 10.1016/0006-8993(91)90477-D. URL: http://www.sciencedirect.com/science/article/pii/000689939190477D (visited on 07/08/2019).

[20] Donald M. Wilson. "The Central Nervous Control of Flight in A Locust". In: *Journal of Experimental Biology* 38.2 (June 1, 1961), pp. 471–490. ISSN: 0022-0949. DOI: 10.1242/jeb.38.2.471. URL: https://doi.org/10.1242/jeb.38.2.471 (visited on 02/20/2024).

[21] Jasper S. Phelps et al. "Reconstruction of motor control circuits in adult Drosophila using automated transmission electron microscopy". In: *Cell* 184.3 (Feb. 2021), 759–774.e18. ISSN: 00928674. DOI: 10.1016/j.cell.2020.12.013. URL: https://linkinghub.elsevier.com/retrieve/pii/S0092867420316834 (visited on 12/22/2023).

[22] Louis K Scheffer et al. "A connectome and analysis of the adult Drosophila central brain". In: *eLife* 9 (Sept. 3, 2020). Ed. by Eve Marder et al. Publisher: eLife Sciences Publications, Ltd, e57443. ISSN: 2050-084X. DOI: 10.7554/eLife.57443. URL: https://doi.org/10.7554/eLife.57443 (visited on 10/15/2023).

[23] Zhihao Zheng et al. "A Complete Electron Microscopy Volume of the Brain of Adult Drosophila melanogaster". In: *Cell* 174.3 (July 26, 2018), 730–743.e22. ISSN: 0092-8674. DOI: 10.1016/j.cell.2018.06.019. URL: http://www.sciencedirect.com/science/article/pii/S0092867418307876 (visited on 07/09/2019).

[24] Shin-ya Takemura et al. *A Connectome of the Male Drosophila Ventral Nerve Cord*. Pages: 2023.06.05.543757 Section: New Results. June 6, 2023. DOI: 10.1101/2023.06.05.543757. URL: https://www.biorxiv.org/content/10.1101/2023.06.05.543757v1 (visited on 02/14/2024).

[25] Anthony Azevedo et al. *Tools for comprehensive reconstruction and analysis of Drosophila motor circuits*. Pages: 2022.12.15.520299 Section: New Results. Dec. 15, 2022. DOI: 10.1101/2022.12.15.520299. URL: https://www.biorxiv.org/content/10.1101/2022.12.15.520299v1 (visited on 12/12/2023).

[26] Sven Dorkenwald et al. "FlyWire: online community for whole-brain connectomics". In: *Nature Methods* 19.1 (Jan. 2022), pp. 119–128. ISSN: 1548-7105. DOI: 10.1038/s41592-021-01330-0.

[27] Sven Dorkenwald et al. *CAVE: Connectome Annotation Versioning Engine*. Pages: 2023.07.26.550598 Section: New Results. July 28, 2023. DOI: 10.1101/2023.07.26.550598. URL: https://www.biorxiv.org/content/10.1101/2023.07.26.550598v1 (visited on 10/16/2023).

[28] Geoffrey W Meissner et al. "A searchable image resource of Drosophila GAL4 driver expression patterns with single neuron resolution". In: *eLife* 12 (Feb. 23, 2023). Ed. by Ilona C Grunwald Kadow and Claude Desplan. Publisher: eLife Sciences Publications, Ltd, e80660. ISSN: 2050-084X. DOI: 10.7554/eLife.80660. URL: https://doi.org/10.7554/eLife.80660 (visited on 02/19/2024).

Chapter 2

CONNECTOMIC RECONSTRUCTION OF *DROSOPHILA* WING MOTOR NEURONS

2.0.1 Note

This chapter is adapted from the manuscript "Tools for connectomic reconstruction and analysis of a female *Drosophila* ventral nerve cord" by Azevedo, Lesser, Phelps, Mark et. al., which has been accepted for publication at *Nature*. This adaptation focuses on the wing motor neurons and the experimental utility of the connectome, which were my contributions to the collaborative project.

The original author list appears as:

Anthony Azevedo*, Ellen Lesser*, Jasper S. Phelps*, Brandon Mark*, Leila Elabbady, Sumiya Kuroda, Anne Sustar, Anthony Moussa, Avinash Kandelwal, Chris J. Dallmann, Sweta Agrawal, Su-Yee J. Lee, Brandon Pratt, Andrew Cook, Kyobi Skutt-Kakaria, Stephan Gerhard, Ran Lu, Nico Kemnitz, Kisuk Lee, Akhilesh Halageri, Manuel Castro, Dodam Ih, Jay Gager, Marwan Tammam, Sven Dorkenwald, Forrest Collman, Casey Schneider-Mizell, Derrick Brittain, Chris S. Jordan, Michael Dickinson, Alexandra Pacureanu, H. Sebastian Seung, Thomas Macrina, Wei-Chung Allen Lee, John C. Tuthill

2.1 Abstract

Like the vertebrate spinal cord, the insect ventral nerve cord (VNC) mediates limb sensation and motor control. Here, we apply automated tools for electron microscopy volume alignment, neuron segmentation, and synapse prediction toward creating a connectome of an adult female *Drosophila* VNC[1]. To interpret a connectome, it is crucial to know its relationship with the rest of the body. We therefore mapped the muscle targets of wing motor

neurons in the connectome by reconstructing their 3D morphology and comparing across literature. Knowing the outputs of the connectome allowed us to identify neural circuits that coordinate the wings and legs during escape takeoff. Finally, we demonstrate a connectome-informed approach for *in vivo* intracellular recording from a premotor neuron in the VNC. We provide the reconstruction of VNC circuits and motor neuron atlas, along with tools for programmatic and interactive access, as community resources to support experimental and theoretical studies of how the fly nervous system controls behavior.

2.2 Introduction

A principal function of the nervous system is to move the body. A longstanding question in neuroscience is how neural circuits control adaptive motor behaviors, such as limbed locomotion. In vertebrate animals, much effort has been dedicated to understanding cortical and subcortical circuits that plan movements and issue descending commands[2,3,4]. There is also an extensive body of literature on the physiology and function of motor neurons (MNs) that directly control muscle activity[5,6]. In comparison, less is known about the function of intermediate circuits of the spinal cord, where proprioceptive feedback signals are integrated with descending motor commands to coordinate patterns of muscle activity[7,4,8]. Understanding the architecture and activity patterns of spinal circuits has been challenging due to their experimental inaccessibility, cell-type diversity, and the large number of spinal interneurons and MNs.

The adult fruit fly, *Drosophila melanogaster*, is a tractable model system to investigate neural circuits for adaptive motor control[9]. Leg and wing motor circuits in the fly are contained within the ventral nerve cord (VNC), which functions like the vertebrate spinal cord to sense and move the limbs[10]. Each of the fly's six legs is controlled by 60-70 uniquely identifiable MNs[11,12,13,1]. For comparison, a single calf muscle in the cat is innervated by 600 MNs[14].

Flies have two distinct modes of locomotion: walking and flying. Unlike the leg, the *Drosophila* wing has anatomically, physiologically, and functionally distinct muscles for power

and steering[15]. The wing's power and steering muscles attach to the thorax and wing hinge, respectively. They are controlled by just 29 MNs on each side; the dendritic anatomy and muscle innervation patterns of most of the wing MNs have been previously described from light microscopy[16,17]. As with the leg system, the number of wing MNs is remarkably small compared with their vertebrate counterparts — a single pectoralis muscle of a hummingbird is innervated by $\sim$ 2000 MNs[18].

We previously reported two advances for understanding how the fly's central nervous system controls the body[11]. First, we applied machine learning tools for automated neuron segmentation and synapse prediction to an EM volume of the *Drosophila* Female Adult Nerve Cord (FANC)[1]. We described the application of new software tools for cell-type annotation, querying connectivity, and identification of genetic driver lines based on reconstructed neuronal morphology. The FANC connectome is being actively proofread and analyzed by a consortium of 30 labs. In addition, we introduced the FANC segmentation and interactive tools as resources to the broader neuroscience community. This work complements a parallel project to reconstruct the connectome of an adult male VNC[19,20,21], as well as two existing connectomes for the adult female *Drosophila* brain[22,23].

We also address a fundamental limitation of existing EM datasets of the adult *Drosophila* brain and VNC, namely that they contain only the central nervous system. The fly's body and peripheral nervous system, including muscles, sensory neuron somas and dendrites, and MN axons, are typically dissected away during sample preparation. The inability to reconstruct the peripheral inputs and outputs of the connectome poses a particular challenge for investigating how central circuits mediate motor control of the body. Together, the reconstruction of a female VNC and the identification of the peripheral targets of MNs provide a foundation for investigating how sensorimotor circuits move the body and integrate descending signals from the brain to control behavior.

2.3 Results

Automated reconstruction and tools for analysis of an EM volume of a female fly VNC

We previously imaged an electron microscopy volume of a *Drosophila* Female Adult Nerve Cord (FANC, pronounced "fancy") and manually reconstructed a small number of VNC neurons and synapses (**Figure 2.1a,b**)[1]. To accelerate efforts to map the VNC connectome, here we applied deep-learning based approaches to automatically reconstruct neurons and synaptic connections throughout FANC. Proper alignment of serial sections is crucial for automated segmentation and data analysis, so we first refined the alignment of FANC's image data using self-supervised convolutional neural networks[24]. We then used convolutional neural networks (CNNs) to segment the dataset into neurons and fragments of neurons[25] and to predict synapse locations (**Figure 2.1c**), as well as pre- and post-synaptic partners[26]. To identify all cells intrinsic to the VNC, we detected nuclei using a separate CNN (**Figure 2.1e-f**)[27,28,11].

The automated cell segmentation was ingested into a ChunkedGraph[29], which allowed human experts to proofread errors in the reconstructions, such as attaching cell bodies and splitting neuronal processes from glia, through the web interface Neuroglancer[30]. We imported synapse and cell body predictions into the Connectome Annotation Versioning Engine (CAVE), so that the associated cell segmentation for each annotation dynamically updated during proofreading[31]. This system allowed us to query up-to-date connectivity and associated metadata, such as cell-type annotations. The suite of tools available for analysis of the FANC dataset are described in **Extended Data Figure S2.1a-e**, including a web platform (`https://braincircuits.io`) for performing color-depth MIP searches[32] to find genetic driver lines that label any neuron within the FANC dataset. Following the example of FlyWire[29], we organized a community currently comprising over 200 users from over 30 labs who use these tools to proofread the FANC cell segmentation and analyze their circuits of interest. Representative examples of proofread motor and premotor neurons are shown in **Figure 2.1g**, and **supplementary Table S2.1** provides links to 3D visualizations of

reconstructed motor neurons in Neuroglancer.

In summary, we report tools for visualizing and analyzing the entire *Drosophila* VNC. The automated segmentation, followed by appropriate proofreading (see **Extended Data Figure S2.2** and **Methods**) provides a level of accuracy comparable to manual tracing[11]. On average, proofreading MNs and their presynaptic partners required 20 edits per neuron. Proofreading automatically segmented neurons requires a fraction of the time of manual tracing, thus dramatically accelerating reconstruction of the connectome.

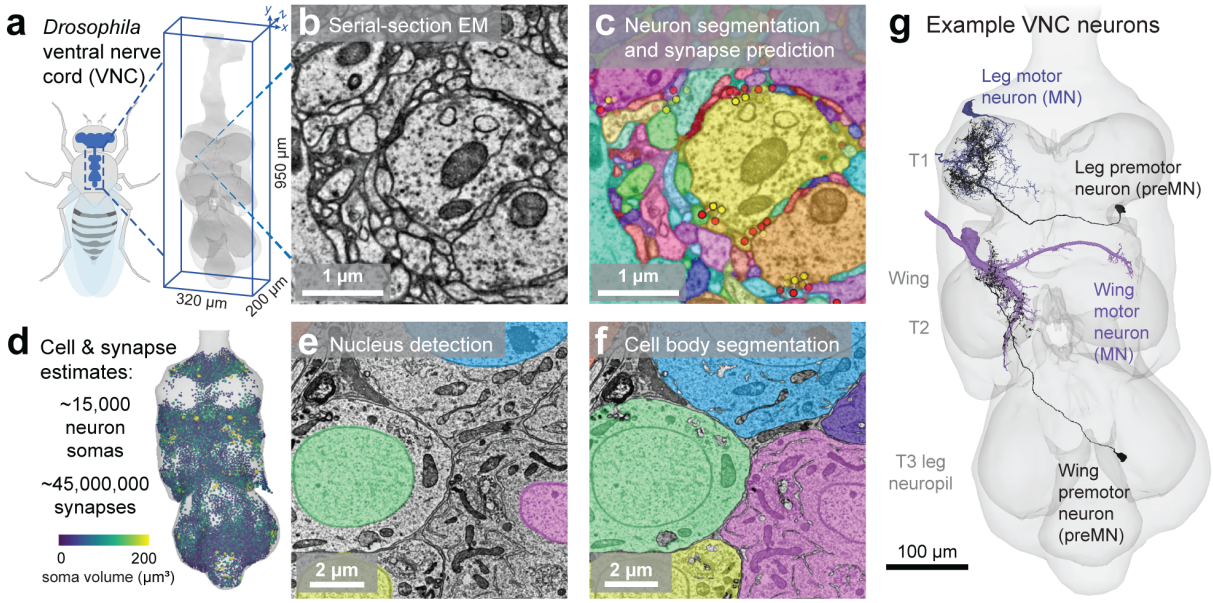

Figure 2.1: Automated tools for connectomic reconstruction of a *Drosophila* VNC. a, We aligned, segmented, and analyzed a serial-section electron microscopy dataset of a *Drosophila* Female Adult ventral Nerve Cord (FANC). **b,** Example section of raw EM image data from the FANC dataset. **c,** We automatically segmented neurons using convolutional neural nets and mean affinity agglomeration with semantic and size constraints[25]. Each segmented cell is shaded with a different color. We applied automated methods for synapse identification across the entire FANC dataset[26]. Example presynaptic sites are labeled with yellow dots and postsynaptic sites are labeled red. **d,** We counted the total number of neurons in FANC by automatically detecting cell nuclei **e** and segmenting cell bodies **f.** **g,** We visualized and proofread segmented cells in Neuroglancer, a WebGL-based viewer for volumetric data[30]

.

Identification of wing motor neurons

Wing muscles (**Figure 2.2a**) can be broadly divided into three groups based on their functional roles in flight[15,33]. First, 13 large muscle fibers power flight indirectly by causing the thorax to resonate at high frequencies, which changes the conformation of the mechanically complex wing hinge to drive the wings back and forth[34]. The 13 fibers are organized into four muscles on each side, a single dorsal-longitudinal muscle (consisting of 6 fibers, DLM1-6), and three dorsoventral muscles (consisting of three fibers (DVM1), and two fibers (DVM2 and DVM3)). A second set of 12 smaller muscles attach directly to the hardened cuticle elements (sclerites) of the wing hinge to rapidly adjust wing motion. Third, the lateral thorax is equipped with four tension muscles, which, although not directly connecting to the sclerites at the base of the wing, are thought to adjust wing motion via their effects on the mechanical stiffness of the thorax[35,33].

We identified the MNs that innervate wing muscles by locating neurons in FANC with cell bodies in the VNC and axons that leave through one of the three nerves associated with the wing neuropil (**Figure 2.2b**): the anterior dorsal mesothoracic nerve (ADMN), posterior dorsal mesothoracic nerve (PDMN), and the mesothoracic accessory nerve (mesoAN)[10,1]. We found 37 neurons on each side, 29 of which we determined to be wing MNs (the other eight are discussed below and in **Extended Data Figure S2.3a-c**). We identified left-right homologous pairs, but here we focus our analysis on the left side.

Most identifications were based on dendritic morphology from the literature, including MNs that innervate direct and tension muscles[36,16,17,37], and MNs that innervate indirect muscles[38,39] (**Figure 2.3a-c**).

The MNs of the DLMs were the only MNs we found to possess presynaptic sites in the VNC (**Extended Data Figure S2.3d**). These synapses were rare (about 10 predicted synapses in total). The presence of weak synaptic connectivity between DLM MNs complements recent work demonstrating that gap junctions between DLM MNs offset their spike timing during flight[40].

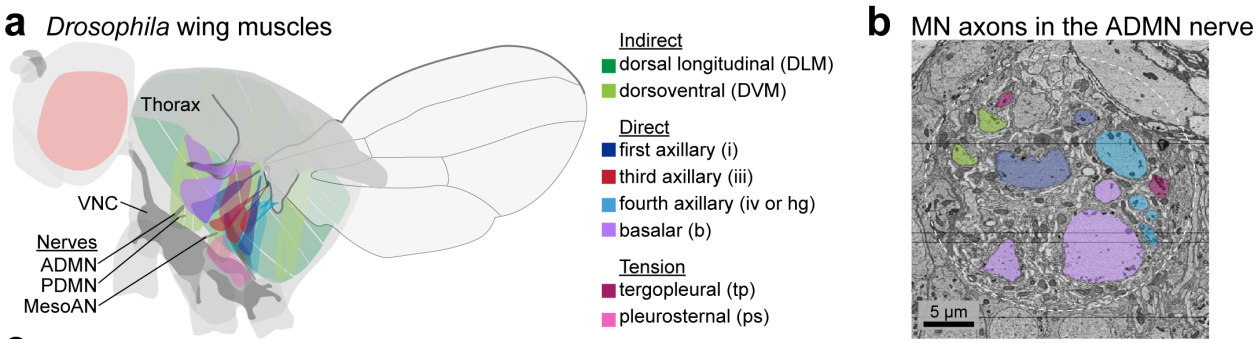

Figure 2.2: Wing control musculature. a, Schematic showing muscles that power and finely control wing motion. Indirect power muscles (green) span the thorax along the anterior-posterior and dorsal-ventral axes; their antagonistic contractions resonate the thorax at high frequencies and cause the wings to move back and forth during flight. Direct muscles attach directly to sclerites of the wing hinge and finely adjust the wing motion. Tension muscles attach to the inner wall of the thorax and internal apodemes, and their contractions are thought to alter the tension of the thorax, thus modifying the oscillations generated by the indirect power muscles. Also pictured is the VNC, with the nerves that carry MN axons to wing muscles (PDMN, ADMN, MesoAN). **b,** EM image from FANC showing a cross section of the ADMN. MN axons are colored according to the key in **a** Horizontal black lines are due to missing slices from the serial-sectioned reconstructed volume.

We found four efferent neurons that innervate peripheral nerves, but which we did not categorize as MNs. One is the previously described peripherally synapsing interneuron, which plays an important role in escape behavior[41]. Three are previously undescribed efferent neurons, one of which has a branch that ascends to the brain (**Extended Data Figure S2.3a-c**).

A neural circuit to retract the front legs during escape take-off.

With knowledge of the muscle targets of the wing MNs and front leg MNs[11], the connectome points to clear hypotheses about the physiological and behavioral function of premotor circuits. We illustrate the potential of combining the VNC connectome and MN projection map with identification and analysis of premotor neurons that coordinate the fly's legs and wings during escape takeoff (**Figure 2.4a**).

Previous research identified a class of VNC local neurons (giant fiber coupled or GFC)

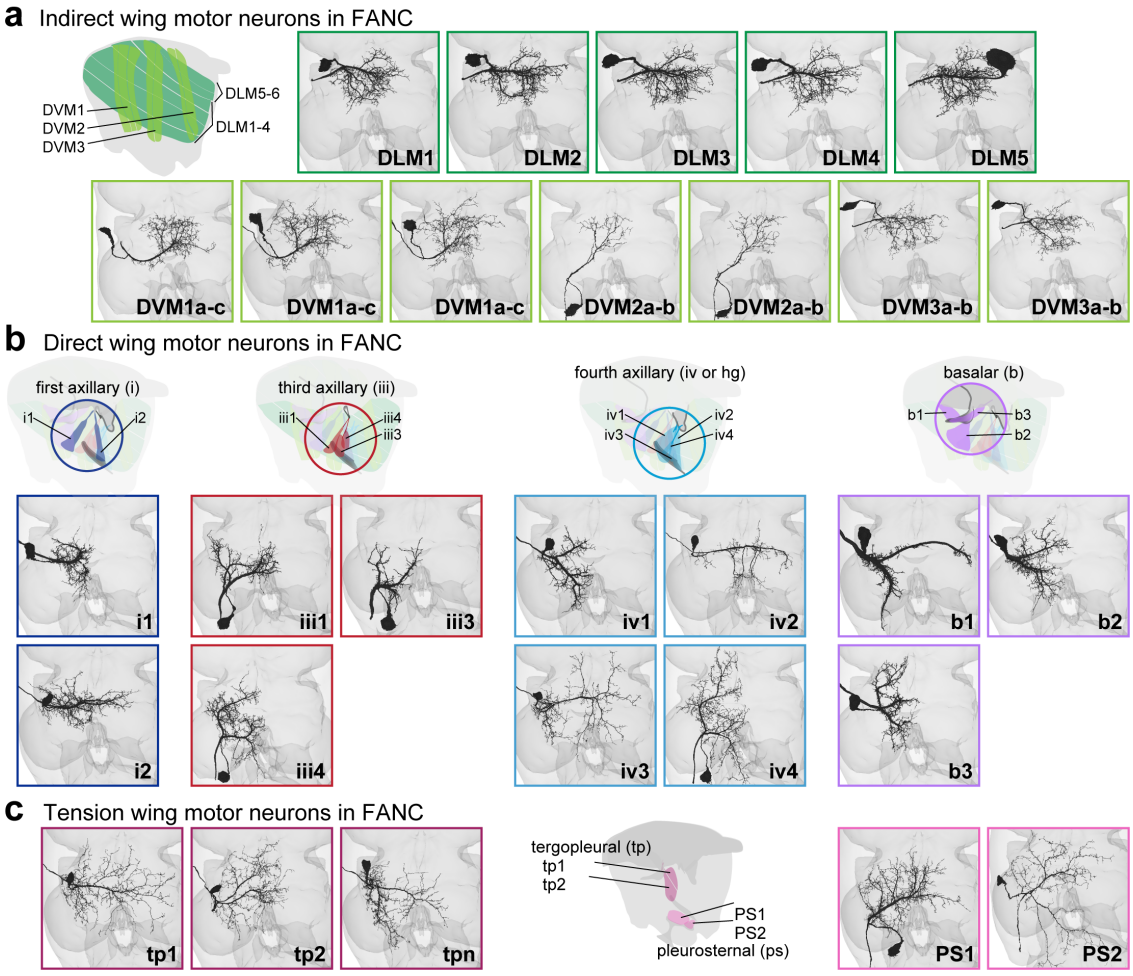

Figure 2.3: Identification of wing MNs in FANC. a, FANC MNs that innervate indirect MNs. We could not differentiate the MNs that innervate individual DVM fibers within each muscle (DVM 1, DVM 2, or DVM 3), so they share a common label (i.e. DVM 1a-c refers to all three MNs that innervate DVM 1). See methods for details on identification. **b,** FANC MNs that innervate direct muscles. **c,** FANC MNs that innervate tension muscles.

that are electrically coupled to the giant fiber[42], a large descending neuron that drives evasive escape takeoff[43,44]. In the FANC volume, we identified and proofread two subtypes of GFC interneurons (GFC2 and GFC4). We then used FANC synapse predictions to understand how they are synaptically connected to leg and wing MNs (**Figure 2.4b**). The morphology of the GFC2 and GFC4 interneurons indicates that they develop from stem cell hemilineages

(18B and 11A, respectively) that release the excitatory neurotransmitter acetylcholine[45].

We found that the GFC2 interneurons synapse onto indirect and tension wing MNs as well as tergotrochanter (TT) MNs that innervate the middle leg (T2), which is consistent with previous literature[43]. In addition to its role in T2 trochanter-femur extension during jumping, the enormous TT muscle is also thought to quickly initiate the first cycle of mechanical oscillation in the power muscles that maintain flight[35]. Thus, GFC2 interneurons are positioned to excite MNs that drive two parallel motor programs: jumping and initiation of the flight motor. The other interneuron subtype, GFC4, synapses onto front leg (T1) MNs that flex the trochanter-femur or tibia[11]. This connectivity suggests that descending input from the giant fiber drives synchronized extension of the middle legs (jumping) and flexion of the front legs (lift-off). Although the role of the T1 leg retraction during take-off has not been previously described, it is visible in high-speed videos of *Drosophila* escape (e.g. von Reyn et al. 2014, Supplementary Video 1)[46,47,44].

Leg MNs in *Drosophila* and other animals are typically recruited in a hierarchical sequence, with small, low-force producing MNs firing prior to large, high force producing MNs. In paired electrophysiological recordings from tibia flexor MNs, we previously observed occasional violations of the recruitment order, in which MNs at the top of the hierarchy fire before MNs at the bottom[48]. We hypothesized that these violations could occur during ballistic escape behaviors, such as escape takeoff. Consistent with this prediction, the only MNs that receive synaptic input from GFC interneurons are the largest MNs that innervate femur-trochanter and tibia flexor muscles (**Figure 2.4c**). Thus, our analysis of the connectome suggests that descending input from the giant fiber is positioned to subvert the standard leg MN recruitment order to drive rapid, ballistic escape behavior via the GFC4 interneurons.

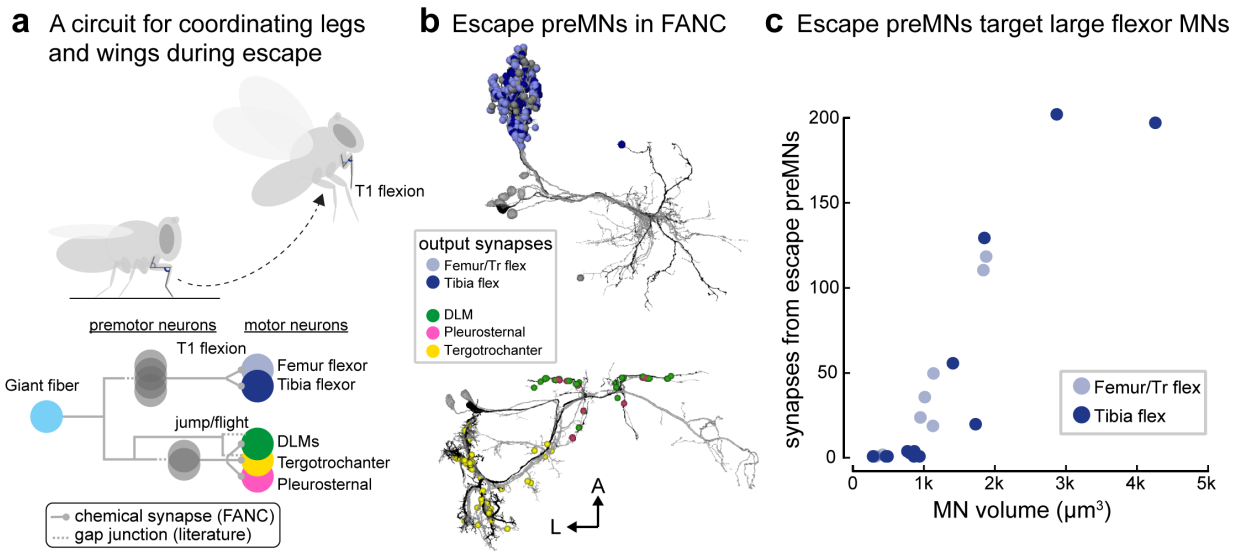

Figure 2.4: Circuits that coordinate the wings and legs during escape takeoff. a, Schematic of a proposed circuit for escape based on prior literature and FANC synapse predictions. The Giant Fiber (GF) excites wing and middle (T2) leg MNs as well as premotor neurons (preMNs) through gap junctions. In FANC, preMNs that are electrically coupled to the GF target T1 tibia and trochanter-femur flexor MNs as well as MNs that innervate T2 leg tergotrochanter muscles, DLMs, and thorax tension muscles (pleurosternal). **b,** We identified interneurons that have been previously shown to be electrically coupled to the giant fiber(Kennedy and Broadie, 2018). (Top) GFC4 preMNs from hemilineage 11A. (Bottom) GFC2 preMNs from hemilineage 18B. The interneurons make synapses (spheres) onto MNs that drive jumping in the T2 legs (yellow), flexion of the T1 legs (blue), and initiate the flight motor (green and pink). A single interneuron in each group is represented in black to show morphology. Additional colors in T1 indicate synapses onto MNs other than tibia and trochanter flexors. **c,** Premotor neurons that are electrically coupled to the giant fiber exclusively target the largest MNs innervating tibia and trochanter-femur flexor muscles, suggesting that this circuit motif bypasses the recruitment hierarchy to execute the fast high-force movements necessary for escape.

Connectome-informed targeting of interneurons for electrophysiological recordings.

Even in a pared down nervous system like that of *Drosophila*, it is not practical to record from every neuron. Connectomics offers a resource for targeting experiments to specific neurons based on their known synaptic inputs and outputs. Further, the genetic tools available in *Drosophila* make finding and recording from the same neuron across individuals feasible. Here, we show one example of how the connectome can be used to determine which specific

cells to record from intracellularly. We focused on a bilateral pair of interneurons in the flight circuit (**Figure 2.5a**). From the connectome, we found that each neuron synapses onto the same left-right pairs of direct wing MNs. We were able to find a Gal4 driver line that labels these two neurons (R50G08; Jim Truman, personal communication), among others, but their relatively large cell bodies made them recognizable for patching.

When we recorded the activity of one of the interneurons in a quiescent animal, we found that with higher amounts of input, the spike timing became more precise (**Figure 2.5b**). Using the connectome, we were also able to quantify the sources of synaptic input to these interneurons. These interneurons receive nearly half of their input from descending neurons from the brain, as well as at least 15% of their input from sensory neurons (**Figure 2.5c**). Together, we propose that these interneurons play a role in synchronizing the left and right wings, such as setting the wing stroke phase during flight.

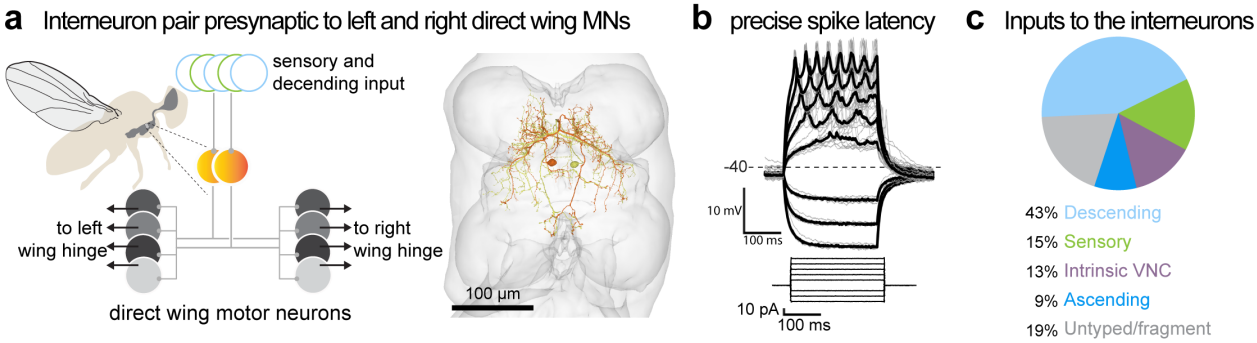

Figure 2.5: Targeting in-vivo recording based on connectomics. a, A pair of interneurons was identified in the connectome as each neuron connects to direct wing steering MNs on both sides of the body. Left: schematic of neural circuit. Right: 3d reconstructions of the pair of neurons in FANC. **b,** intracellular current-clamp recording from one of the neurons in vivo while animal is restrained and quiescent (recording from 50G08-Gal4 driving UAS-GFP). Like other neurons, as current injection increases so does firing rate. In this neuron, however, at higher firing rates the latency of spiking is highly precise, as can be seen by the single trials (gray lines) overlaying on each other for the few spikes (thick black line = mean of trials). **c,** Proportion of inputs to the pair of interneurons. They receive less input from intrinsic VNC neurons than most VNC interneurons.

2.4 Discussion

By revealing the structure of the neurons and synapses that underlie animal behavior, connectomes provide a foundation for generating and falsifying theories of neural circuit function. While comprehensive connectomes have been mapped for small crawling animals like *C. elegans*[49] and *Drosophila* larva[50], we previously lacked a synapse-level wiring diagram of motor circuits for any limbed animal. Here, we provide tools for collaboratively proofreading a draft connectome of a female adult *Drosophila* VNC, an atlas linking the outputs of the connectome to the body, and analysis of a circuit that coordinates the legs and wings during escape behavior. Our effort to reconstruct the connectome of a female VNC (FANC) complements a parallel project to reconstruct a male VNC (MANC)[51,20,21]. The existence of multiple VNC connectomes will enable comparison of neural wiring across individuals and the identification of sexually dimorphic neural circuits.

The community effort to comprehensively reconstruct neurons and measure synaptic connections within FANC is ongoing. At the time of publication, the community has proofread less than half of the total FANC dataset (**Extended Data Figure S2.2**), yet the automated reconstruction, proofreading environment, and analysis tools already enable interactive inquiry into the neurobiology of the VNC. Our work parallels similar efforts in the adult fly brain[22], the male VNC[51,20,21] and the larval nervous system[52]. Further, the distributed nature of the community-driven FANC effort is a strength, as it allows the connectome to be continuously refined as each circuit is proofread by experts in that area. Even before the connectome is complete, researchers can analyze subcircuits as a means of generating and falsifying hypotheses. Using tools to match VNC neurons reconstructed in the EM volume with GAL4 lines imaged by light microscopy (**Extended Data Figure S2.1**), it is then possible to test these hypotheses with in vivo recordings and manipulations of neural activity, as we demonstrate here. Additional software tools exist to facilitate comparison of neuronal morphology and connectivity across individual animals and to bridge EM datasets[53]. Even with a single connectome, however, it is possible to gain insight into morphology and neural

circuitry that differ between related species. For example, our reconstruction revealed independent control of the femur and trochanter leg segments, which were previously thought to be mechanically fused in *Drosophila*[54].

Many challenges remain for interpreting a synaptic wiring diagram[55]. First, synapses can be either excitatory or inhibitory. Fortunately, VNC neurons develop from stem cell hemilineages that share identifiable morphological features as well as neurotransmitter identity[45]. Therefore, hemilineage identification of VNC cell types can identify candidate neurotransmitters, as we did for the escape circuitry (**Figure 2.3**). As done previously for the whole fly brain EM dataset, we can also use hemilineage identities as ground-truth for training convolutional neural networks to predict neurotransmitter identity directly from the EM image data[22,56].

A second challenge is the inability to see electrical synapses or sites of neuromodulation in connectome datasets. The spatial resolution of existing connectomic datasets is insufficient to resolve gap junctions, which are known to play an important role in sensorimotor processing within the VNC[57,58,43]. Sample-preserving imaging approaches like serial-section transmission electron microscopy have the capacity for higher-resolution (e.g., 2 nm/pixel) imaging at identified locations, potentially allowing visualization of gap junctions. It is also not currently possible to identify sites of neuromodulation, which are essential for flexible motor control[59]. Because EM reconstruction provides a map of chemical synaptic transmission between neurons, physiological measurements will also be necessary to test for the effects of gap junctions and neuromodulators.

Many organisms use their limbs to maintain posture in the face of gravity, navigate uneven terrain, and manipulate objects in the environment. Connectomic-driven discovery represents a paradigm shift for investigating these fundamental motor control problems. Previous work on the neural control of movement has attempted to link neural dynamics to motor output, in part to infer the connectivity and function of premotor networks[60,61,62,63,64]. A connectome allows one to work backwards from the MNs to identify premotor networks that coordinate specific patterns of muscle activation and inhibition. The adult fly VNC

also provides a unique opportunity to investigate two distinct modes of limbed locomotion, walking and flight.

As we show here, connectomics can narrow the search for interneurons that with key roles in circuits function. The connectome pointed us to a pair of interneurons that are both upstream of left and right steering motor neurons. Their firing precision in response to current injection suggests that they may possess a specialized combination of ion channels which may ensure faithful signal propagation. Much of left-right wing synchronization is achieved passively, as the wings are both attached to the thorax[34]. During steering maneuvers in free flight, however, the left and right wings exhibit different trajectories[65]. These precise interneurons may be a node that ensures left and right wings re-synchronize to the same phase after unilateral adjustments.

The FANC connectome will have many uses beyond the study of limb motor control. For example, it will enable the identification and analysis of neural circuits for descending modulation[66,67], ascending communication with the brain[68,36], and sensory organs distributed across the fly limbs, thorax, and abdomen[9]. By creating a bridge between the VNC connectome and the body, the MN projection map will facilitate development and analysis of neuromechanical models for flexible motor control[69,70]. The compact sensorimotor circuits that mediate robust control of the fly leg and wing may provide inspiration for engineering of micro-scale robotic systems[71]. Matching cell types and comparing connectivity motifs to the larval connectome[72,50,73] may provide insight into the development and evolution of sensorimotor circuits[74,75]. Finally, as volumetric EM datasets from other animal species are collected, comparative connectomics provides a powerful tool to study the evolution of the nervous system[76].

2.5 Acknowledgements

We thank Rachel Wilson for financial support of SG during development of braincircuits.io (via U19NS104655 and R01NS129647 to RIW). We thank Richard Mann, Han Cheong, Erica Ehrhardt, Gwyneth Card, and Greg Jefferis for assistance with leg and wing MN

identification. This work was supported by a Searle Scholar Award, a Klingenstein-Simons Fellowship, a Pew Biomedical Scholar Award, a McKnight Scholar Award, a Sloan Research Fellowship, the New York Stem Cell Foundation, and a UW Innovation Award to JCT; a Genise Goldenson Award to WAL; NIH U19NS104655 to JCT and MD; NIH R01MH117808 to JCT, WAL, and HSS. JCT is a New York Stem Cell Foundation – Robertson Investigator.

2.6 Methods

See Azevedo et. al., 2022 for details on automatic detection of neuron nuclei, comparison to ground truth, and leg MN identification[11].

EM Dataset Alignment, Segmentation, Annotation

We refined the alignment of the FANC image data using self-supervised convolutional neural networks[24]. We next trained a CNN to identify knife marks that occurred during serial sectioning. We then used CNNs to segment the dataset into neurons and fragments of neurons and to predict synapse locations[25], excluding regions of the data with knife marks. We also used a CNN to predict pre and postsynaptic partners[26]. The automated segmentation was ingested into the ChunkedGraph data structure[29].

We imported synapse and cell body predictions into the Connectome Annotation Versioning Engine (CAVE), so that the associated cell segmentation objects for each annotation would be dynamically updated during proofreading[31]. This system allowed us to query the up-to-date connectivity graph and associated metadata, such as cell-type annotations. The suite of tools available for analysis of the FANC dataset are described in **Extended Data Figure S2.1a-e**, including a web platform (https://braincircuits.io) for performing color-depth MIP searches[32] to find genetic driver lines that label any neuron within the FANC dataset.

Proofreading

We corrected errors in the segmentation through manual proofreading with Google's Neuroglancer interface[30]. We adopted a two-pass heuristic to proofread MNs: a first pass to correct major errors, and a second pass to more closely inspect the neuron morphology. Examples of major errors included a missing soma, requiring merging two objects; a missing branch, e.g. from the primary neurite, requiring merging the branch onto the larger MN object; or incorrect merges with glia, which wrap around the MN axons in the nerve and can be segmented with the MN, requiring splitting the object (**Extended Data Figure S2.2a**)[29]. These major errors were typically due to two types of artifacts in the EM data that impacted the segmentation and reconstruction. First, the serial sectioning procedure left several knife marks that could cross an entire neuropil. These knife marks were identified and excluded from the segmentation, but branches that cross the knife marks were segmented as separate objects. The left T1 neuromere in particular had several large knife marks which could lead to somas or large branches being detached from the neurons. The second type of artifact was the darker appearance of the cytosol of many peripheral axons. This led to merges between glia and the axons of sensory and MNs.

After a first pass, e.g. to reattach somas, we made a second pass over the MN morphology to correct smaller errors like incorrectly merged branches that in fact belong to other objects (requiring a split), or merging smaller branches that branched distally from the primary neurite. Common causes of these errors include darkly stained lipid aggregates in the EM image which often occurred where two neurites were closely apposed, and the segmentation algorithm could incorrectly identify the process that emerged on the other side.

The MNs were also initially manually traced in CATMAID[1]. We took advantage of this to import the manually traced skeletons for each MN and check that no further branches were missing. Note, the four MNs we used to ground-truth synapse prediction and reconstruction were extensively manually traced to include the "twigs" at the ends of the dendrites, though some were missed in synapse dense regions (**Extended Data Figure S2.3e**). That level of

detail was too time consuming to apply to all the MNs, and unnecessary given the improved accuracy of the segmentation. As a result, proofread MNs tended to have more twigs and more extensive dendrites than the manually traced skeletons.

Currently, 30% of non-sensory neurons have been marked as proofread by the community. The distributed responsibility of community-based proofreading stems from a need to pool resources across the community, in lieu of building a dedicated connectomics team charged with proofreading. As a result, circuits of more direct interest to the community have likely received more attention. On the other hand, the proofread reconstruction remains dynamic and circuits that are particularly difficult to segment can still be proofread, like the sensory neurons in FANC.

Identification of wing MNs

Unlike the leg, previous literature has already linked fly MN morphologies to muscle targets using muscle back-fills and specific GAL4 drivers[77,17,39,37], so we were able to identify many of the neurons based on morphology alone. We identified wing and thorax MNs in FANC by finding neurons with cell bodies in the VNC and axons leaving through one of three wing-associated nerves: the anterior dorsal mesothoracic nerve (ADMN), posterior dorsal mesothoracic nerve (PDMN), and the mesothoracic accessory nerve (MesoAN)[10]. We found 37 neurons on each side. The right side MesoAN is partially severed, so some of the MNs could not be reliably traced to a cell body. We only discuss the left side, but all neurons could be paired across the midline by eye. Of the 37 neurons, three innervate the large tergotrochanter "jump" muscle unique to the middle leg and five were eliminated as non-MN efferent neurons. One is the peripherally synapsing interneuron[41], and four are previously undescribed and predicted to be neuromodulatory. We categorized the wing and thorax MNs as indirect, direct, or tension, based on their proposed function[15].

The indirect muscles contain two antagonistic groups: dorsal longitudinal muscles (DLMs) and dorsoventral muscles (DVMs). The six DLM fibers are innervated by five MNs[77]. We differentiated the first four DLMs based on the position of their axons along the anterior-

posterior axis; DLM 5, which innervates muscle fibers five and six, is identifiable by its large contralateral cell body. It also has the posterior-most axon, so we labeled the DLM MN with the anterior-most axon as DLM 1. We found three MNs in the ADMN that innervate DVM 1, two MNs in the MesoAN that innervate DVM 2, and two MNs in the PDMN that innervate DVM 3, according to the morphologies and nomenclature established in *Calliphora*[39].

Unlike in the leg, direct wing muscles are innervated by a single MN[78]. We relied on two papers to identify most of the direct MNs[37], and identified the rest based on morphology and fasciculation in FANC and consultation with other experts in the field (now published)[16,36]. The first axillary (i) muscle i1 was identified from Trimarchi and Schneiderman; i2 is identified with lower confidence due to its projection across the midline in FANC, which was not previously observed using light microscopy. It does, however, fasciculate with i1. The third axillary MNs iii1 and iii3 were identified from literature. We determined iii4 based on its similar morphology and fasciculation in the MesoAN. The fourth MN that looks similar to the iii MNs was determined to be iv4 (also known as "hg4"). The fourth axillary MNs iv1 and iv2 (hg1 and hg2) were determined based on literature; iv3 (hg3) was determined based on its similar morphology to iv2. Basalar MNs b1 and b2 were identified from literature. We identified the third basalar MN b3 based on its fasciculation with MNs b1 and b2.

There are two sets of tension muscles, defined by the sclerites they attach to: the tergopleural (tp) muscles and the pleurosternal (ps) muscles. We identified tp1, tp2, and tpn from literature, although the morphologies we observed in FANC were not as similar for tergopleural MNs as other MNs. For the pleurosternal muscles, we found three candidate MNs instead of two. One is predicted to be either neuromodulatory or may also innervate one or both of the pleurosternal muscles, like the tpn MN; it is shown in **Extended Data Figure S2.3c**.

The main tergotrochanter MN was identified based on previous literature[79]. Two small MNs whose axons travel alongside the large tergotrochanter axon are predicted to either innervate the large TT muscle or innervate the intracoxal depressor and levator, respectively (muscles 67 and 68, according to Miller)[80].

Supplementary Table T2.1 contains links to view wing motor neurons in Neuroglancer.

Electrophysiology

To gain access to the VNC in an intact animal we used the preparation described in Agrawal 2020 Figure 1a[57]. The fly was positioned ventral-side-up in the holder. We glued down the legs to avoid mechanical interference but left the thorax as free from glue as possible, so that the wings were free to move. We never observed natural wing movements once the cuticle above the VNC was dissected, but the wings often buzzed even when the fly was glued into the holder.

Data and Code Availability

The EM dataset and reconstructions are freely available[1].

Details on code for alignment, segmentation, automatic detection of synapses and cell nuclei, and annotation software (CAVE) can be found via the citations in the Methods section, "EM Dataset Alignment, Segmentation, Annotation."

The segmentation of the Female Adult Nerve Cord dataset is available by joining the FANC community. Instructions on joining the FANC community can be found at `http://github.com/htem/FANC_auto_recon/wiki#collaborative-community`. Code for interacting with FANC can be found at `http://github.com/htem/FANC_auto_recon`. Code for analysis and figures is available at `http://github.com/EllenLesser/Azevedo_Lesser_Phelps_Mark_2023/`.

2.7 Supplementary Materials

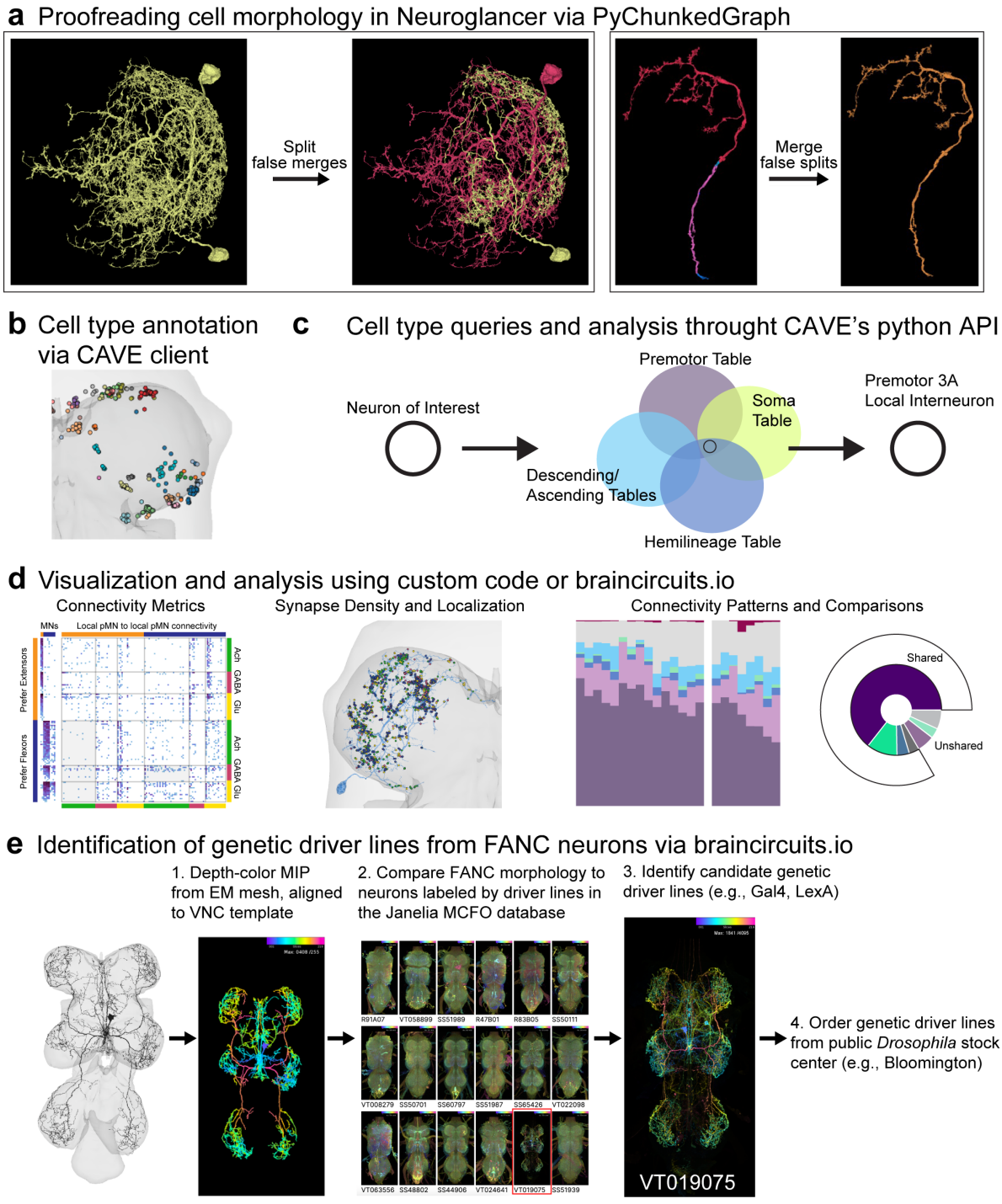

Figure S2.1: Summary of FANC software tools for cell proofreading. a, Proofreading of cell morphology in Neuroglancer via PyChunkedGraph, **b,** cell type annotation, **c,** identification, **d,** cellular and circuit analysis, and **e,** identification of genetic driver lines.

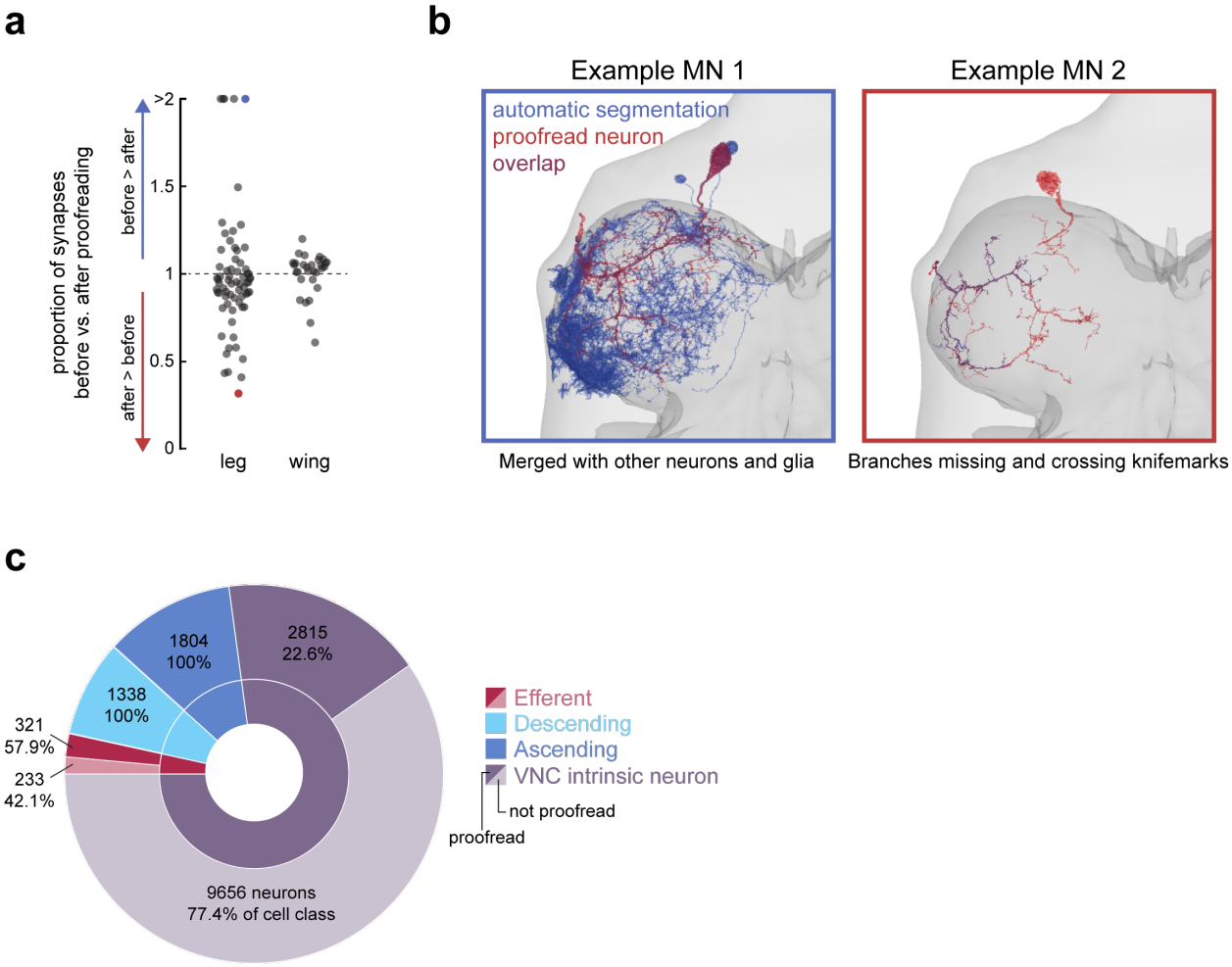

Figure S2.2: Proofreading improves neuron reconstruction. **a,** Overview of how proofreading affected the number of input synapses to each MN. Many of the MN meshes changed substantially, some increased in size as objects were merged (number of synapses before vs. after < 1), and some decreased in size as objects were split (number of synapses before vs. after > 1). Leg MNs underwent larger changes than wing MNs, relative to starting volume. **b,** Example leg MNs before and after proofreading. Left) An example MN that was initially merged with glia and other neurons (blue, extra somas are visible). Right) An example MN that required branches to be merged across knife marks. **c,** The proportions of neurons in FANC that are currently proofread, by cell class.

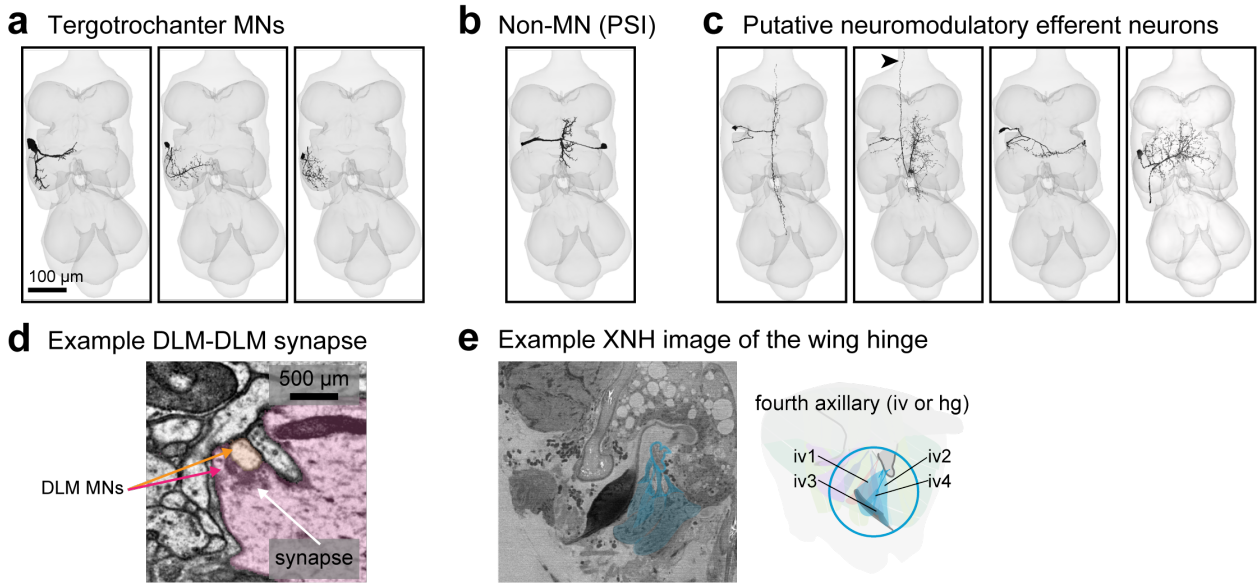

Figure S2.3: FANC efferent neurons with axons in the ADMN or PDMN that are not wing MNs. **a,** MNs that innervate the T2 tergotrochanter leg muscle send axons through the PDMN. The two small neurons have not been identified previously. We identify them as TT MNs here based on their fasciculation with the main TT MN. We predict that they also innervate the main TT muscle, or the intracoxal depressor and levator, respectively (muscles 67 and 68 according to Miller, 1950[80]. **b,** The peripherally synapsing interneuron (PSI) sends an axon into the PDMN and synapses onto DLM axons but does not innervate muscles[41]. **c,** Four other unidentified neurons have axons in the ADMN or PDMN. Their dendrites are thinner than any other motor neurons, and not like anything previously shown using light microscopy. One has an ascending process (indicated with an arrow), and its projection into PDMN does not travel to the end of the dissection so it is not an MN. One (right-most) shares a majority of its input with pleurosternal MNs, and is likely neuromodulatory or may play a similar role to the tpn MN. **d,** DLM MNs are the only MNs we observed with output synapses, and they synapse onto each other. **e,** Recently collected XNH images of the wing and wing hinge were used to help inform the anatomical cartoon schematics.

Nerve	Muscle	Insertion	MNs	view
PDMN	dorsal longitudinal	thorax	5	link
ADMN	dorsoventral 1	thorax	3	link
mesoAN	dorsoventral 2	thorax	2	link
PDMN	dorsoventral 3	thorax	2	link
ADMN	i1	first axillary	1	link
ADMN	i2	first axillary	1	link
mesoAN	iii1	third axillary	1	link
mesoAN	iii3	third axillary	1	link
mesoAN	iii4	third axillary	1	link
ADMN	iv1	fourth axillary	1	link
ADMN	iv2	fourth axillary	1	link
ADMN	iv3	fourth axillary	1	link
mesoAN	iv4	fourth axillary	1	link
ADMN	b1	basalar apophysis	1	link
ADMN	b2	basalar apophysis	1	link
ADMN	b3	basalar apophysis	1	link
ADMN	tp1	meso-scutum	1	link
ADMN	tp2	meso-scutum	1	link
ADMN	tp	tp2 meso-scutum	1	link
mesoAN	PS1	pleural apophysis	1	link
mesoAN	PS2	pleural apophysis	1	link
PDMN	middle leg tergotrochanter		3	link

Table 2.1: Neuroglancer links to wing motor neurons. Entries in the right column link to 3D views of each motor neuron or group of motor neurons.

References

[1] Jasper S. Phelps et al. "Reconstruction of motor control circuits in adult Drosophila using automated transmission electron microscopy". In: *Cell* 184.3 (Feb. 2021), 759–774.e18. ISSN: 00928674. DOI: 10.1016/j.cell.2020.12.013. URL: https://linkinghub.elsevier.com/retrieve/pii/S0092867420316834 (visited on 12/22/2023).

[2] Silvia Arber and Rui M. Costa. "Networking brainstem and basal ganglia circuits for movement". In: *Nature Reviews. Neuroscience* 23.6 (June 2022), pp. 342–360. ISSN: 1471-0048. DOI: 10.1038/s41583-022-00581-w.

[3] Hidehiko K. Inagaki et al. "Neural Algorithms and Circuits for Motor Planning". In: *Annual Review of Neuroscience* 45 (July 8, 2022), pp. 249–271. ISSN: 1545-4126. DOI: 10.1146/annurev-neuro-092021-121730.

[4] Roberto Leiras, Jared M. Cregg, and Ole Kiehn. "Brainstem Circuits for Locomotion". In: *Annual Review of Neuroscience* 45.1 (2022). _eprint: https://doi.org/10.1146/annurev-neuro-082321-025137, pp. 63–85. DOI: 10.1146/annurev-neuro-082321-025137. URL: https://doi.org/10.1146/annurev-neuro-082321-025137 (visited on 11/21/2022).

[5] Marc D. Binder, Randall K. Powers, and C. J. Heckman. "Nonlinear Input-Output Functions of Motoneurons". In: *Physiology (Bethesda, Md.)* 35.1 (Jan. 1, 2020), pp. 31–39. ISSN: 1548-9221. DOI: 10.1152/physiol.00026.2019.

[6] Daniel Kernell. *The Motoneurone and its Muscle Fibres*. Oxford University Press, Aug. 17, 2006. ISBN: 978-0-19-172389-6. URL: http://www.oxfordscholarship.com.offcampus.lib.washington.edu/view/10.1093/acprof:oso/9780198526551.001.0001/acprof-9780198526551 (visited on 01/16/2019).

[7] Martyn Goulding. "Circuits controlling vertebrate locomotion: moving in a new direction". In: *Nature Reviews Neuroscience* 10.7 (July 2009). Bandiera_abtest: a Cg_type:

Nature Research Journals Number: 7 Primary_atype: Reviews Publisher: Nature Publishing Group, pp. 507–518. ISSN: 1471-0048. DOI: 10.1038/nrn2608. URL: https://www.nature.com/articles/nrn2608 (visited on 10/27/2021).

[8] Ludwig Ruder and Silvia Arber. "Brainstem Circuits Controlling Action Diversification". In: *Annual Review of Neuroscience* 42 (July 8, 2019), pp. 485–504. ISSN: 1545-4126. DOI: 10.1146/annurev-neuro-070918-050201.

[9] John C. Tuthill and Rachel I. Wilson. "Mechanosensation and Adaptive Motor Control in Insects". In: *Current biology: CB* 26.20 (Oct. 24, 2016), R1022–R1038. ISSN: 1879-0445. DOI: 10.1016/j.cub.2016.06.070.

[10] Robert Court et al. "A Systematic Nomenclature for the Drosophila Ventral Nerve Cord". In: *Neuron* 107.6 (Sept. 23, 2020), 1071–1079.e2. ISSN: 1097-4199. DOI: 10.1016/j.neuron.2020.08.005.

[11] Anthony Azevedo et al. *Tools for comprehensive reconstruction and analysis of Drosophila motor circuits*. Pages: 2022.12.15.520299 Section: New Results. Dec. 15, 2022. DOI: 10.1101/2022.12.15.520299. URL: https://www.biorxiv.org/content/10.1101/2022.12.15.520299v1 (visited on 12/12/2023).

[12] M. Baek and R. S. Mann. "Lineage and Birth Date Specify Motor Neuron Targeting and Dendritic Architecture in Adult Drosophila". In: *Journal of Neuroscience* 29.21 (May 27, 2009), pp. 6904–6916. ISSN: 0270-6474, 1529-2401. DOI: 10.1523/JNEUROSCI.1585-09.2009. URL: http://www.jneurosci.org/cgi/doi/10.1523/JNEUROSCI.1585-09.2009 (visited on 05/18/2017).

[13] D.J. Brierley et al. "Developmental origins and architecture of Drosophila leg motoneurons". In: *The Journal of Comparative Neurology* 520.8 (June 1, 2012), pp. 1629–1649. ISSN: 1096-9861. DOI: 10.1002/cne.23003. URL: http://onlinelibrary.wiley.com/doi/10.1002/cne.23003/abstract (visited on 05/18/2017).

[14] R. E. Burke. "Motor Units: Anatomy, Physiology, and Functional Organization". In: *Comprehensive Physiology*. _eprint: https://onlinelibrary.wiley.com/doi/pdf/10.1002/cphy.cp010210 John Wiley & Sons, Ltd, 2011, pp. 345–422. ISBN: 978-0-470-65071-4. DOI: 10.1002/cphy.cp010210. URL: https://onlinelibrary.wiley.com/doi/abs/10.1002/cphy.cp010210 (visited on 11/21/2022).

[15] Michael H Dickinson and Michael S Tu. "The Function of Dipteran Flight Muscle". In: *Comparative Biochemistry and Physiology Part A: Physiology* 116.3 (Mar. 1, 1997), pp. 223–238. ISSN: 0300-9629. DOI: 10.1016/S0300-9629(96)00162-4. URL: https://www.sciencedirect.com/science/article/pii/S0300962996001624 (visited on 02/14/2024).

[16] Erica Ehrhardt et al. *Single-cell type analysis of wing premotor circuits in the ventral nerve cord of Drosophila melanogaster*. Pages: 2023.05.31.542897 Section: New Results. June 1, 2023. DOI: 10.1101/2023.05.31.542897. URL: https://www.biorxiv.org/content/10.1101/2023.05.31.542897v2 (visited on 10/23/2023).

[17] Angela O'Sullivan et al. "Multifunctional Wing Motor Control of Song and Flight". In: *Current biology: CB* 28.17 (Sept. 10, 2018), 2705–2717.e4. ISSN: 1879-0445. DOI: 10.1016/j.cub.2018.06.038.

[18] Edward R. Donovan et al. "Muscle Activation Patterns and Motor Anatomy of Anna's Hummingbirds Calypte anna and Zebra Finches Taeniopygia guttata". In: *Physiological and Biochemical Zoology* 86.1 (Jan. 2013). Publisher: The University of Chicago Press, pp. 27–46. ISSN: 1522-2152. DOI: 10.1086/668697. URL: https://www.journals.uchicago.edu/doi/10.1086/668697 (visited on 11/28/2022).

[19] H. S. J. Cheong et al. *Transforming descending input into behavior: The organization of premotor circuits in the Drosophila Male Adult Nerve Cord connectome*. Pages: 2023.06.07.543976 Section: New Results. June 7, 2023. DOI: 10.1101/2023.06.07.543976. URL: https://www.biorxiv.org/content/10.1101/2023.06.07.543976v1 (visited on 10/16/2023).

[20] Elizabeth C. Marin et al. *Systematic annotation of a complete adult male Drosophila nerve cord connectome reveals principles of functional organisation*. Pages: 2023.06.05.543407 Section: New Results. June 6, 2023. DOI: 10.1101/2023.06.05.543407. URL: https://www.biorxiv.org/content/10.1101/2023.06.05.543407v1 (visited on 08/30/2023).

[21] Shin-ya Takemura et al. *A Connectome of the Male Drosophila Ventral Nerve Cord*. Pages: 2023.06.05.543757 Section: New Results. June 6, 2023. DOI: 10.1101/2023.06.05.543757. URL: https://www.biorxiv.org/content/10.1101/2023.06.05.543757v1 (visited on 02/14/2024).

[22] Sven Dorkenwald et al. *Neuronal wiring diagram of an adult brain*. Pages: 2023.06.27.546656 Section: New Results. June 30, 2023. DOI: 10.1101/2023.06.27.546656. URL: https://www.biorxiv.org/content/10.1101/2023.06.27.546656v1 (visited on 08/30/2023).

[23] C. Shan Xu et al. *A Connectome of the Adult Drosophila Central Brain*. Pages: 2020.01.21.911859 Section: New Results. Jan. 21, 2020. DOI: 10.1101/2020.01.21.911859. URL: https://www.biorxiv.org/content/10.1101/2020.01.21.911859v1 (visited on 11/03/2023).

[24] Sergiy Popovych et al. *Petascale pipeline for precise alignment of images from serial section electron microscopy*. Pages: 2022.03.25.485816 Section: New Results. Mar. 27, 2022. DOI: 10.1101/2022.03.25.485816. URL: https://www.biorxiv.org/content/10.1101/2022.03.25.485816v1 (visited on 09/12/2022).

[25] Thomas Macrina et al. *Petascale neural circuit reconstruction: automated methods*. Pages: 2021.08.04.455162 Section: New Results. Aug. 5, 2021. DOI: 10.1101/2021.08.04.455162. URL: https://www.biorxiv.org/content/10.1101/2021.08.04.455162v1 (visited on 02/15/2024).

[26] Julia Buhmann et al. "Automatic detection of synaptic partners in a whole-brain Drosophila electron microscopy data set". In: *Nature Methods* 18.7 (July 2021). Number: 7 Publisher: Nature Publishing Group, pp. 771–774. ISSN: 1548-7105. DOI: 10.1038/s41592-021-01183-7. URL: https://www.nature.com/articles/s41592-021-01183-7 (visited on 09/12/2022).

[27] Kisuk Lee et al. *Superhuman Accuracy on the SNEMI3D Connectomics Challenge*. May 31, 2017. DOI: 10.48550/arXiv.1706.00120. arXiv: 1706.00120[cs]. URL: http://arxiv.org/abs/1706.00120 (visited on 12/05/2022).

[28] Shang Mu et al. *3D reconstruction of cell nuclei in a full Drosophila brain*. Pages: 2021.11.04.467197 Section: New Results. Nov. 4, 2021. DOI: 10.1101/2021.11.04.467197. URL: https://www.biorxiv.org/content/10.1101/2021.11.04.467197v1 (visited on 12/05/2022).

[29] Sven Dorkenwald et al. "FlyWire: online community for whole-brain connectomics". In: *Nature Methods* 19.1 (Jan. 2022), pp. 119–128. ISSN: 1548-7105. DOI: 10.1038/s41592-021-01330-0.

[30] Jeremy Maitin-Shepard et al. *google/neuroglancer:* Oct. 16, 2021. DOI: 10.5281/zenodo.5573294. URL: https://zenodo.org/record/5573294 (visited on 09/12/2022).

[31] Sven Dorkenwald et al. *CAVE: Connectome Annotation Versioning Engine*. Pages: 2023.07.26.550598 Section: New Results. July 28, 2023. DOI: 10.1101/2023.07.26.550598. URL: https://www.biorxiv.org/content/10.1101/2023.07.26.550598v1 (visited on 10/16/2023).

[32] Hideo Otsuna, Masayoshi Ito, and Takashi Kawase. *Color depth MIP mask search: a new tool to expedite Split-GAL4 creation*. Pages: 318006 Section: New Results. May 9, 2018. DOI: 10.1101/318006. URL: https://www.biorxiv.org/content/10.1101/318006v1 (visited on 10/23/2023).

[33] J. W. S. Pringle. *Insect Flight*. Google-Books-ID: hPOsN4QExQMC. Cambridge University Press, Dec. 1957. 146 pp. ISBN: 978-0-521-05995-4.

[34] Tanvi Deora, Namrata Gundiah, and Sanjay P. Sane. "Mechanics of the thorax in flies". In: *The Journal of Experimental Biology* 220 (Pt 8 Apr. 15, 2017), pp. 1382–1395. ISSN: 1477-9145. DOI: 10.1242/jeb.128363.

[35] Werner Nachtigall and Donald M. Wilson. "Neuro-Muscular Control of Dipteran Flight". In: *Journal of Experimental Biology* 47.1 (Aug. 1, 1967), pp. 77–97. ISSN: 0022-0949. DOI: 10.1242/jeb.47.1.77. URL: https://doi.org/10.1242/jeb.47.1.77 (visited on 10/21/2022).

[36] Han S. J. Cheong et al. *Organization of an Ascending Circuit that Conveys Flight Motor State*. Pages: 2023.06.07.544074 Section: New Results. June 9, 2023. DOI: 10.1101/2023.06.07.544074. URL: https://www.biorxiv.org/content/10.1101/2023.06.07.544074v1 (visited on 10/12/2023).

[37] J. R. Trimarchi and A. M. Schneiderman. "The motor neurons innervating the direct flight muscles of Drosophila melanogaster are morphologically specialized". In: *The Journal of Comparative Neurology* 340.3 (Feb. 15, 1994), pp. 427–443. ISSN: 0021-9967. DOI: 10.1002/cne.903400311.

[38] Kazuo Ikeda and William D. Kaplan. "Neurophysiological Genetics in Drosophila melanogaster". In: *American Zoologist* 14.3 (1974), pp. 1055–1066. ISSN: 0003-1569. URL: https://www.jstor.org/stable/3881860 (visited on 03/17/2019).

[39] M. Schlurmann and K. Hausen. "Motoneurons of the flight power muscles of the blowfly Calliphora erythrocephala: Structures and mutual dye coupling". In: *Journal of Comparative Neurology* 500.3 (2007). _eprint: https://onlinelibrary.wiley.com/doi/pdf/10.1002/cn pp. 448–464. ISSN: 1096-9861. DOI: 10.1002/cne.21182. URL: https://onlinelibrary.wiley.com/doi/abs/10.1002/cne.21182 (visited on 12/03/2022).

[40] Silvan Hürkey et al. “Gap junctions desynchronize a neural circuit to stabilize insect flight”. In: *Nature* 618.7963 (June 2023). Number: 7963 Publisher: Nature Publishing Group, pp. 118–125. ISSN: 1476-4687. DOI: 10.1038/s41586-023-06099-0. URL: https://www.nature.com/articles/s41586-023-06099-0 (visited on 09/14/2023).

[41] D. G. King and R. J. Wyman. “Anatomy of the giant fibre pathway in Drosophila. I. Three thoracic components of the pathway”. In: *Journal of Neurocytology* 9.6 (Dec. 1980), pp. 753–770. ISSN: 0300-4864. DOI: 10.1007/BF01205017.

[42] Tyler Kennedy and Kendal Broadie. “Newly Identified Electrically Coupled Neurons Support Development of the Drosophila Giant Fiber Model Circuit”. In: *eNeuro* 5.6 (Dec. 2018), ENEURO.0346–18.2018. ISSN: 2373-2822. DOI: 10.1523/ENEURO.0346-18.2018.

[43] M A Tanouye and R J Wyman. “Motor outputs of giant nerve fiber in Drosophila.” In: *Journal of Neurophysiology* 44.2 (Aug. 1980). Publisher: American Physiological Society, pp. 405–421. ISSN: 0022-3077. DOI: 10.1152/jn.1980.44.2.405. URL: https://journals.physiology.org/doi/abs/10.1152/jn.1980.44.2.405 (visited on 10/20/2022).

[44] Catherine R. von Reyn et al. “A spike-timing mechanism for action selection”. In: *Nature Neuroscience* 17.7 (July 2014). Number: 7 Publisher: Nature Publishing Group, pp. 962–970. ISSN: 1546-1726. DOI: 10.1038/nn.3741. URL: https://www.nature.com/articles/nn.3741 (visited on 11/16/2022).

[45] Haluk Lacin et al. “Neurotransmitter identity is acquired in a lineage-restricted manner in the Drosophila CNS”. In: *eLife* 8 (Mar. 26, 2019). Ed. by K VijayRaghavan, Sonia Sen, and Matthias Landgraf. Publisher: eLife Sciences Publications, Ltd, e43701. ISSN: 2050-084X. DOI: 10.7554/eLife.43701. URL: https://doi.org/10.7554/eLife.43701 (visited on 10/21/2022).

[46] Gwyneth Card and Michael Dickinson. "Performance trade-offs in the flight initiation of Drosophila". In: *Journal of Experimental Biology* 211.3 (Feb. 1, 2008), pp. 341–353. ISSN: 0022-0949, 1477-9145. DOI: 10.1242/jeb.012682. URL: https://jeb.biologists.org/content/211/3/341 (visited on 07/07/2019).

[47] J. R. Trimarchi and A. M. Schneiderman. "Giant fiber activation of an intrinsic muscle in the mesothoracic leg of Drosophila melanogaster". In: *The Journal of Experimental Biology* 177 (Apr. 1993), pp. 149–167. ISSN: 0022-0949. DOI: 10.1242/jeb.177.1.149.

[48] Anthony W Azevedo et al. "A size principle for recruitment of Drosophila leg motor neurons". In: *eLife* 9 (June 3, 2020). Ed. by Ronald L Calabrese and Chris Q Doe. Publisher: eLife Sciences Publications, Ltd, e56754. ISSN: 2050-084X. DOI: 10.7554/eLife.56754. URL: https://doi.org/10.7554/eLife.56754 (visited on 11/09/2022).

[49] Steven J. Cook et al. "Whole-animal connectomes of both Caenorhabditis elegans sexes". In: *Nature* 571.7763 (July 2019). Number: 7763 Publisher: Nature Publishing Group, pp. 63–71. ISSN: 1476-4687. DOI: 10.1038/s41586-019-1352-7. URL: https://www.nature.com/articles/s41586-019-1352-7 (visited on 12/04/2022).

[50] Michael Winding et al. "The connectome of an insect brain". In: *Science* 379.6636 (Mar. 10, 2023). Publisher: American Association for the Advancement of Science, eadd9330. DOI: 10.1126/science.add9330. URL: https://www.science.org/doi/10.1126/science.add9330 (visited on 05/17/2023).

[51] H. S. J. Cheong et al. *Transforming descending input into behavior: The organization of premotor circuits in the Drosophila Male Adult Nerve Cord connectome*. Pages: 2023.06.07.543976 Section: New Results. Jan. 26, 2024. DOI: 10.1101/2023.06.07.543976. URL: https://www.biorxiv.org/content/10.1101/2023.06.07.543976v2 (visited on 02/15/2024).

[52] Claire Eschbach and Marta Zlatic. "Useful road maps: studying Drosophila larva's central nervous system with the help of connectomics". In: *Current Opinion in Neurobiology* 65 (Dec. 2020), pp. 129–137. ISSN: 1873-6882. DOI: 10.1016/j.conb.2020.09.008.

[53] Philipp Schlegel et al. *A consensus cell type atlas from multiple connectomes reveals principles of circuit stereotypy and variation*. Pages: 2023.06.27.546055 Section: New Results. June 27, 2023. DOI: 10.1101/2023.06.27.546055. URL: https://www.biorxiv.org/content/10.1101/2023.06.27.546055v1 (visited on 08/30/2023).

[54] Volker Hartenstein. "The Muscle Pattern of Drosophila". In: *Muscle Development in Drosophila*. Ed. by Helen Sink. Molecular Biology Intelligence Unit. New York, NY: Springer, 2006, pp. 8–27. ISBN: 978-0-387-32963-5. DOI: 10.1007/0-387-32963-3_2. URL: https://doi.org/10.1007/0-387-32963-3_2 (visited on 11/08/2022).

[55] Cornelia I. Bargmann and Eve Marder. "From the connectome to brain function". In: *Nature Methods* 10.6 (June 2013), pp. 483–490. ISSN: 1548-7105. DOI: 10.1038/nmeth.2451.

[56] Nils Eckstein et al. *Neurotransmitter Classification from Electron Microscopy Images at Synaptic Sites in Drosophila*. Pages: 2020.06.12.148775 Section: New Results. Sept. 2, 2020. DOI: 10.1101/2020.06.12.148775. URL: https://www.biorxiv.org/content/10.1101/2020.06.12.148775v2 (visited on 11/18/2022).

[57] Sweta Agrawal et al. "Central processing of leg proprioception in Drosophila". In: *eLife* 9 (Dec. 2, 2020). Ed. by Ronald L Calabrese, Eve Marder, and Terufumi Fujiwara. Publisher: eLife Sciences Publications, Ltd, e60299. ISSN: 2050-084X. DOI: 10.7554/eLife.60299. URL: https://doi.org/10.7554/eLife.60299 (visited on 11/16/2022).

[58] Chenghao Chen et al. "Functional architecture of neural circuits for leg proprioception in Drosophila". In: *Current Biology* 31.23 (Dec. 6, 2021), 5163–5175.e7. ISSN: 0960-

9822. DOI: 10.1016/j.cub.2021.09.035. URL: https://www.sciencedirect.com/science/article/pii/S0960982221012756 (visited on 11/16/2022).

[59] Clare E. Howard et al. "Serotonergic Modulation of Walking in Drosophila". In: *Current biology: CB* 29.24 (Dec. 16, 2019), 4218–4230.e8. ISSN: 1879-0445. DOI: 10.1016/j.cub.2019.10.042.

[60] Risa Kawai et al. "Motor cortex is required for learning but not for executing a motor skill". In: *Neuron* 86.3 (May 6, 2015), pp. 800–812. ISSN: 1097-4199. DOI: 10.1016/j.neuron.2015.03.024.

[61] Henrik Lindén et al. "Movement is governed by rotational neural dynamics in spinal motor networks". In: *Nature* 610.7932 (Oct. 2022). Number: 7932 Publisher: Nature Publishing Group, pp. 526–531. ISSN: 1476-4687. DOI: 10.1038/s41586-022-05293-w. URL: https://www.nature.com/articles/s41586-022-05293-w (visited on 12/03/2022).

[62] Britton A. Sauerbrei et al. "Cortical pattern generation during dexterous movement is input-driven". In: *Nature* 577.7790 (Jan. 2020). Number: 7790 Publisher: Nature Publishing Group, pp. 386–391. ISSN: 1476-4687. DOI: 10.1038/s41586-019-1869-9. URL: https://www.nature.com/articles/s41586-019-1869-9 (visited on 12/03/2022).

[63] Krishna V. Shenoy, Maneesh Sahani, and Mark M. Churchland. "Cortical control of arm movements: a dynamical systems perspective". In: *Annual Review of Neuroscience* 36 (July 8, 2013), pp. 337–359. ISSN: 1545-4126. DOI: 10.1146/annurev-neuro-062111-150509.

[64] Saurabh Vyas et al. "Computation Through Neural Population Dynamics". In: *Annual Review of Neuroscience* 43 (July 8, 2020), pp. 249–275. ISSN: 1545-4126. DOI: 10.1146/annurev-neuro-092619-094115.

[65] Michael H. Dickinson and Florian T. Muijres. "The aerodynamics and control of free flight manoeuvres in Drosophila". In: *Philosophical Transactions of the Royal Society B: Biological Sciences* 371.1704 (Sept. 26, 2016). Publisher: Royal Society, p. 20150388. DOI: 10.1098/rstb.2015.0388. URL: https://royalsocietypublishing.org/doi/10.1098/rstb.2015.0388 (visited on 04/10/2023).

[66] Florian Aymanns, Chin-Lin Chen, and Pavan Ramdya. "Descending neuron population dynamics during odor-evoked and spontaneous limb-dependent behaviors". In: *eLife* 11 (Oct. 26, 2022), e81527. ISSN: 2050-084X. DOI: 10.7554/eLife.81527.

[67] Shigehiro Namiki et al. "The functional organization of descending sensory-motor pathways in Drosophila". In: *eLife* 7 (June 26, 2018). Ed. by Kristin Scott, e34272. ISSN: 2050-084X. DOI: 10.7554/eLife.34272. URL: https://doi.org/10.7554/eLife.34272 (visited on 10/20/2019).

[68] Chin-Lin Chen et al. *Ascending neurons convey behavioral state to integrative sensory and action selection centers in the brain*. Pages: 2022.02.09.479566 Section: New Results. Feb. 9, 2022. DOI: 10.1101/2022.02.09.479566. URL: https://www.biorxiv.org/content/10.1101/2022.02.09.479566v1 (visited on 11/19/2022).

[69] Victor Lobato-Rios et al. "NeuroMechFly, a neuromechanical model of adult Drosophila melanogaster". In: *Nature Methods* 19.5 (May 2022). Number: 5 Publisher: Nature Publishing Group, pp. 620–627. ISSN: 1548-7105. DOI: 10.1038/s41592-022-01466-7. URL: https://www.nature.com/articles/s41592-022-01466-7 (visited on 10/21/2022).

[70] Sibo Wang-Chen et al. *NeuroMechFly 2.0, a framework for simulating embodied sensorimotor control in adult Drosophila*. Pages: 2023.09.18.556649 Section: New Results. Oct. 9, 2023. DOI: 10.1101/2023.09.18.556649. URL: https://www.biorxiv.org/content/10.1101/2023.09.18.556649v3 (visited on 10/12/2023).

[71] Chris J. Dallmann et al. “Mechanosensory Control of Locomotion in Animals and Robots: Moving Forward”. In: *Integrative and Comparative Biology* 63.2 (Aug. 23, 2023), pp. 450–463. ISSN: 1557-7023. DOI: 10.1093/icb/icad057.

[72] Brandon Mark et al. *A developmental framework linking neurogenesis and circuit formation in the Drosophila CNS*. eLife. Publisher: eLife Sciences Publications Limited. May 11, 2021. DOI: 10.7554/eLife.67510. URL: https://elifesciences.org/articles/67510 (visited on 11/18/2022).

[73] Aref Arzan Zarin et al. “A multilayer circuit architecture for the generation of distinct locomotor behaviors in Drosophila”. In: *eLife* 8 (Dec. 23, 2019). Ed. by Kristin Scott and Ronald L Calabrese. Publisher: eLife Sciences Publications, Ltd, e51781. ISSN: 2050-084X. DOI: 10.7554/eLife.51781. URL: https://doi.org/10.7554/eLife.51781 (visited on 04/22/2020).

[74] Sweta Agrawal and John C. Tuthill. “The two-body problem: Proprioception and motor control across the metamorphic divide”. In: *Current Opinion in Neurobiology* 74 (June 2022), p. 102546. ISSN: 1873-6882. DOI: 10.1016/j.conb.2022.102546.

[75] Ellie S. Heckscher et al. “Even-Skipped+ Interneurons Are Core Components of a Sensorimotor Circuit that Maintains Left-Right Symmetric Muscle Contraction Amplitude”. In: *Neuron* 88.2 (Oct. 21, 2015), pp. 314–329. ISSN: 0896-6273. DOI: 10.1016/j.neuron.2015.09.009. URL: https://www.sciencedirect.com/science/article/pii/S0896627315007667 (visited on 12/21/2023).

[76] Elizabeth Barsotti, Ana Correia, and Albert Cardona. “Neural architectures in the light of comparative connectomics”. In: *Current Opinion in Neurobiology* 71 (Dec. 2021), pp. 139–149. ISSN: 1873-6882. DOI: 10.1016/j.conb.2021.10.006.

[77] Kazuo Ikeda and J. H. Koenig. “Morphological identification of the motor neurons innervating the dorsal longitudinal flight muscle of Drosophila melanogaster”. In: *Journal of Comparative Neurology* 273.3 (1988). _eprint: https://onlinelibrary.wiley.com/doi/pdf/10.1002

pp. 436–444. ISSN: 1096-9861. DOI: 10.1002/cne.902730312. URL: https://onlinelibrary.wiley.com/doi/abs/10.1002/cne.902730312 (visited on 10/21/2022).

[78] Gerhard Heide. "Neural mechanisms of flight control in Diptera". In: *BIONA-report* 2 (1983), pp. 35–52.

[79] Jonathan P. Bacon and Nicholas J. Strausfeld. "The dipteran 'Giant fibre' pathway: neurons and signals". In: *Journal of Comparative Physiology A* 158.4 (July 1, 1986), pp. 529–548. ISSN: 1432-1351. DOI: 10.1007/BF00603798. URL: https://doi.org/10.1007/BF00603798 (visited on 12/05/2022).

[80] A. Miller. "The internal anatomy and histology of the imago of Drosophila melanogaster." In: *Biology of Drosophila.* (1950), pp. 420–534.

Chapter 3

SYNAPTIC ARCHITECTURE OF LEG AND WING PREMOTOR CONTROL NETWORKS IN *DROSOPHILA*

Ellen Lesser*, Anthony W. Azevedo*, Jasper S. Phelps, Leila Elabbady, Andrew Cook, Brandon Mark, Sumiya Kuroda, Anne Sustar, Anthony Moussa, Chris J. Dallmann, Sweta Agrawal, Su-Yee J. Lee, Brandon Pratt, Kyobi Skutt-Kakaria, Stephan Gerhard, Ran Lu, Nico Kemnitz, Kisuk Lee, Akhilesh Halageri, Manuel Castro, Dodam Ih, Jay Gager, Marwan Tammam, Sven Dorkenwald, Forrest Collman, Casey Schneider-Mizell, Derrick Brittain, Chris S. Jordan, H. Sebastian Seung, Thomas Macrina, Michael Dickinson, Wei-Chung Allen Lee, John C. Tuthill

3.0.1 Note

This chapter is closely adapted from a manuscript with the same title and authors, which has been resubmitted for review.

3.1 Abstract

Animal movement is controlled by motor neurons (MNs), which project out of the central nervous system to activate muscles. MN activity is coordinated by complex premotor networks that allow individual muscles to contribute to many different behaviors. Each MN innervates fibers within a single muscle, so coordination across MNs is performed by premotor circuits to drive robust yet adaptable motor output. MN activity is coordinated by specialized premotor circuitry that allows individual muscles to contribute to a range of different behaviors. The organization of these premotor circuits remains largely unknown. Here, we use comprehensive reconstruction of neuroanatomy and synaptic connectivity from

volumetric electron microscopy connectomics to analyze the wiring logic of premotor circuits controlling the *Drosophila* leg and wing. We find that both premotor networks cluster into modules that link MNs innervating muscles with related functions. Within most leg motor modules, the synaptic weights of each premotor neuron are proportional to the size of their target MNs, establishing a circuit basis for hierarchical MN recruitment. In contrast, wing premotor networks lack proportional synaptic connectivity, which may allow wing steering muscles to be recruited with different relative timing. By comparing the architecture of distinct limb motor control systems within the same animal, we identify common principles of premotor network organization and specializations that reflect the unique biomechanical constraints and evolutionary origins of leg and wing motor control.

3.2 Introduction

All motor behaviors, from simple postural reflexes to complex locomotor navigation, are produced by patterns of electrical activity in MNs, which extend axons from the central nervous system to excite muscles throughout the body[1]. A single MN and the muscle fibers it innervates comprise a motor unit. Animals achieve a remarkable diversity of behaviors by recruiting motor units in different combinations and sequences. Previous work has used analysis of limb biomechanics, movement kinematics, and electrophysiological recordings to identify these patterns of motor unit coordination;[2,3,4,5] however, the range of possible combinations of motor unit activations is ultimately constrained by the anatomy and connectivity of premotor neural circuits[6]. Thus, determining the wiring logic of premotor circuits can provide fundamental insight into how nervous systems coordinate motor units to accomplish diverse motor output.

Technical advances in reconstructing neurons and identifying synapses from volumetric electron microscopy (EM), or "connectomics", have recently made it possible to analyze synapse-resolution circuit diagrams. There are now connectomes for the nematode C. elegans[7,8] and the larval fruit fly,*Drosophila melanogaster*[9,10] which provide insight into premotor control of peristaltic locomotion[11,12]. In addition to multiple connectomes of the adult

fly brain[13,14], there also exist two EM volumes of the adult *Drosophila* ventral nerve cord (VNC), from a female (Female Adult Nerve Cord, FANC)[15] and male fly[16]. The fly VNC functions like the vertebrate spinal cord to sense and move the fly's legs and wings[17], making these connectome datasets the first in which it is possible to analyze limb premotor circuits. We recently combined reconstruction of leg and wing MN dendrites in the FANC dataset with genetic tools and x-ray holographic nanotomography to map the muscle targets of MN axons to the level of individual muscle fibers (**Figure 3.1a,b**)[18]. This high-resolution atlas of MN to muscle connectivity now makes it feasible to compare how premotor circuits are organized to control two evolutionarily distinct limbs, the leg and wing.

Flies use their legs to perform many behaviors, including locomotion, grooming, aggression, and courtship[19]. While walking, the position of the distal tip of the fly's leg is determined by seven mechanical degrees of freedom, specified by the biomechanics of the five joints within each leg. The most proximal joint (thorax-coxa) has three degrees of freedom, while the other joints have one[2]. Most leg joints are actuated by more than two muscles, e.g. two muscles in the femur contribute to tibia flexion and one antagonist muscle controls tibia extension. In total, the fly's front leg contains 18 muscles[20], collectively innervated by 69 MNs[18]. Most leg muscles are innervated by multiple MNs, i.e. they are composed of 2-8 motor units, with MNs innervating distinct fibers within the target muscle[18]. Unlike some other insect species, flies lack GABAergic inhibitory MNs[21,22]. In many animals, a motor pool refers to groups of motor units that are recruited together, and can include motor units in multiple muscles. The dynamic firing patterns of motor pools, including antagonist pools, then control joint torque by causing muscle contractions that act on complex, passive musculoskeletal biomechanics.

In many animals, from flies to humans, MNs within a motor pool typically fire in a stereotyped order, or recruitment hierarchy, which helps to smoothly increase muscle force in a graded manner[23,24,25,3,26,27,28]. Since the pioneering work of Henneman[29], it has been theorized that the MN recruitment hierarchy is established by correlations in physiological and neuromuscular properties that are collectively referred to as the size principle. The size

principle posits that if a common synaptic input excites a motor pool, MNs with the highest input resistance. i.e., small MNs that innervate slow-twitch fibers, will depolarize and fire first. As the strength of the common input increases, larger MNs that innervate fast-twitch fibers will then be recruited, establishing a recruitment order based on MN size[30]. The precise synaptic architecture of limb premotor circuits that is responsible for implementing the size principle has remained a mystery since the phenomenon was first described in cat leg muscles over 60 years ago[29]. Recent work in adult zebrafish has revealed that separate populations of interneurons synapse onto small/slow vs. large/fast MNs, calling into question the role of common input to a motor pool[31,32]. In addition, modern muscle recordings in primates demonstrate that the correlations in motor unit firing rates can flexibly change with the demands of the motor task, in contrast to the stereotyped recruitment order that inspired the size principle.

The fly wing is biomechanically and evolutionarily distinct from the leg[33,34], and wing MNs thus do not possess conventional MN recruitment hierarchies. Three separate groups of muscles with specialized physiological properties and functions control each wing[35,36]. One group of large muscles, called "indirect" because they do not directly attach to the wing hinge, span the thorax orthogonally, forming a pair of antagonist muscles that provide the power to flap the wings. The indirect muscles are innervated by 12 MNs per side and are asynchronous, stretch-activated muscles, so their contractions arise at the level of muscle biomechanics, rather than from neural input[37,38]. Another group of muscles, known as "tension" muscles, are thought to modify the stiffness of the thorax to modulate the power produced by the indirect muscles[39,40]. Forces from the resonant oscillations of the thorax are transmitted through the intricate linkages of the wing hinge to produce the trajectory of the wing stroke[41,42]. The third group of muscles are directly attached to cuticle thickenings, or sclerites, that make up the wing hinge[43,36,44,45]. The actions of these direct "steering" muscles create subtle deviations in the wing trajectory that modify aerodynamic forces for flight control and acrobatic maneuvers[46]. Each direct muscle is innervated by a single MN, so wing steering motor units are not organized into conventional motor pools. Although

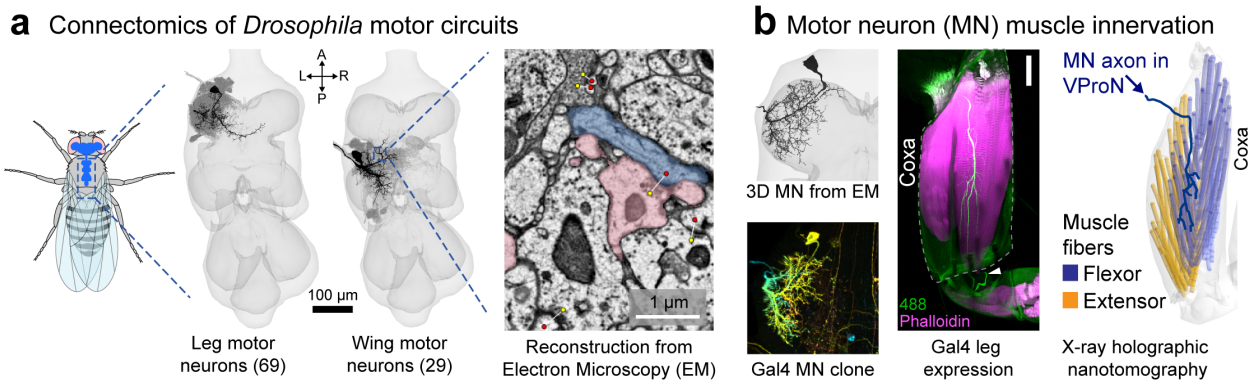

Figure 3.1: Reconstruction of identified motor neurons in *Drosophila*. **a,** Automated neuron segmentation and synapse prediction in a serial-section electron microscopy (EM) volume of an adult female VNC. The VNC contains the cell body and dendrites of MNs controlling the leg (left, N = 69) and the wing (right, N = 29). Axons extend out of the VNC to innervate muscles. Example EM image shows automated synapse predictions, with presynaptic sites labeled by yellow dots and postsynaptic sites by red. **b,** Identification of muscle targets of each leg MN[18]. Briefly, reconstructed EM neurons (top left) were compared with X-ray tomography of the leg (right) and light-microscope images of genetically identified MNs in the VNC (bottom left)[55] and in the leg (middle; GFP and cuticle autofluorescence in green, phalloidin in magenta, scale bar is 50 μm). Here, a clone of a trochanter flexor MN labeled by VT063626-Gal4[55], with axon expression in the trochanter flexor muscle in the coxa. The axon travels in the ventral prothoracic nerve. White arrowhead indicates a sensory axon in the prothoracic leg nerve, illustrating that not all Gal4 lines are specific for MNs.

past work has revealed mechanisms of flight motor control at the level of muscles and single MNs[47,48,49,50,51,52,35,53,54] comparatively little is known about wing premotor circuits within the VNC that coordinate MNs to control flight and other wing-related behaviors. Here, we use connectomics to comprehensively reconstruct premotor synaptic input to leg and wing MNs to compare similarities and differences in neural control of joints with distinct biomechanics.

3.3 Results

We reconstructed the anatomy and synaptic connectivity of all premotor neurons (preMNs) that synapse onto MNs that control either the left wing or the left front leg in the FANC dataset (**Figure 3.2a-b**)[18]. We focus here on the fly's front leg, which is specialized for

tactile exploration and possesses a greater range of motion than the middle and rear legs[56]. The resulting premotor connectome consists of 69 leg MNs that receive 212,190 synapses from 1,546 preMNs, and 29 wing and thorax MNs that receive 144,668 synapses from 1,784 preMNs. MNs have tortuous dendritic arbors and possess among the largest cell bodies in the *Drosophila* nervous system (**Figure 3.2c-d**). On average, each MN receives 3,641 input synapses from 188 preMNs (using a 3-synapse threshold; quantification for each MN in **Extended Data Figure S3.1a-h**) and each preMN synapses onto 6 MNs (7.2±7.4¬ for leg preMNs, 5.1±3.1 for wing preMNs).

In all limbed animals studied to date, measurements of MN size, such as soma volume, axon diameter, and dendritic surface area, have been found to correlate with the number and physiology of the muscle fibers it innervates and with the amount of force the motor unit produces[57,58,25,59,60,61,62,63]. When we reconstructed dendrites and somas of fly leg and wing MNs, we found that MN surface area and volume ranged over 40-fold (**Figure 3.2e-g**; **Extended Data Figure S3.1i-k**). This variation in MN size is consistent with the range in MN morphology in the cat[64,65]. Note, the somas of insect neurons do not typically receive synaptic input and thus may not serve the same important role in neuronal processing as they do in vertebrate neurons.

We found that the total number of MN input synapses is highly correlated with MN surface area, but that the relative densities are different for MNs that innervate different types of muscles. Leg MNs have a synapse density of ~ 0.45 synapses per μm^2 (**Figure 3.2e**; $r = 0.94$, $p < 10^{-33}$). This density is approximately 3 times more synapses per unit area than reported for cat MNs[66]. Consistent with the size principle, we found that each leg muscle is innervated by MNs of different sizes (**Extended Data Figure S3.1i**), so larger MNs receive proportionally more synapses. MNs that innervate direct and tension wing MNs have a similar density to leg MNs, ~ 0.41 synapses μm^{-2} (**Figure 3.2f**; $r = 0.90$, $p < 0.10^{-3}$, excluding the outlier b1, see Methods). Indirect MNs have a lower synapse density, with ~ 0.24 synapses μm^{-2} (**Figure 3.2g**; $r = 0.98$, $p < 10^{-7}$). In summary, our quantification of synaptic input to MNs identified strong correlations between MN size and

number of input synapses across both leg and wing MNs.

If MN recruitment were dictated entirely by the magnitude of premotor input, then these patterns of proportional connectivity would cause the largest, fastest MNs to be recruited first, at the bottom of the hierarchy. However, MNs controlling the fly tibia follow a conventional recruitment hierarchy during spontaneous movements, with the small, highly active MNs firing prior to the large MNs, which rarely spike[67]. Thus, the intrinsic electrical properties of the largest MNs must compensate for the higher number of input synapses to establish a recruitment hierarchy that follows the size principle.

Local neurons dominate synaptic input to both leg and wing MNs.

We next set out to dissect the sources of input to MNs and to compare the quantitative structure of synaptic connectivity for leg and wing premotor networks. We classified preMNs into five morphological classes: descending (from the brain), sensory, ascending (to the brain), intersegmental (from other VNC neuropils), and local neurons (**Figure 3.3a-c**). **Figure 3.3d-e** show the entire leg and wing premotor connectivity matrices: preMNs are rows, MNs are columns, and the color of each element indicates the number of synapses between the two cells. We sorted leg MNs from proximal to distal, according to the location of the muscle fibers they innervate[18]. For the wing, we ordered indirect wing MNs first, followed by tension MNs, and then direct MNs, sorted by the wing sclerite upon which they insert (**Figure 3.3e**). We sorted preMNs of each class by their top MN targets (per muscle), and then by total synapses onto MNs (the sum of each row).

We found that the predominant source of synaptic input to both leg and wing MNs is local VNC neurons (**Figure 3.3d-f**, **Extended Data Figure S3.1c-d**). Although previous work in the fly has focused on the contributions of descending neurons (DNs) to fly motor control[68,69,70,71,72]. we find that less than 10% of synapses to each leg and wing MN comes from DNs (mean = 9.1 ±4.2% st.dev. for leg MNs and 11.2 ±6.5% for wing MNs). Local preMNs, however, comprise 43% of all leg preMNs but 63.4±9% of synaptic input to each MN (**Extended Data Figure S3.1j**). These proportions suggest that most descending signals

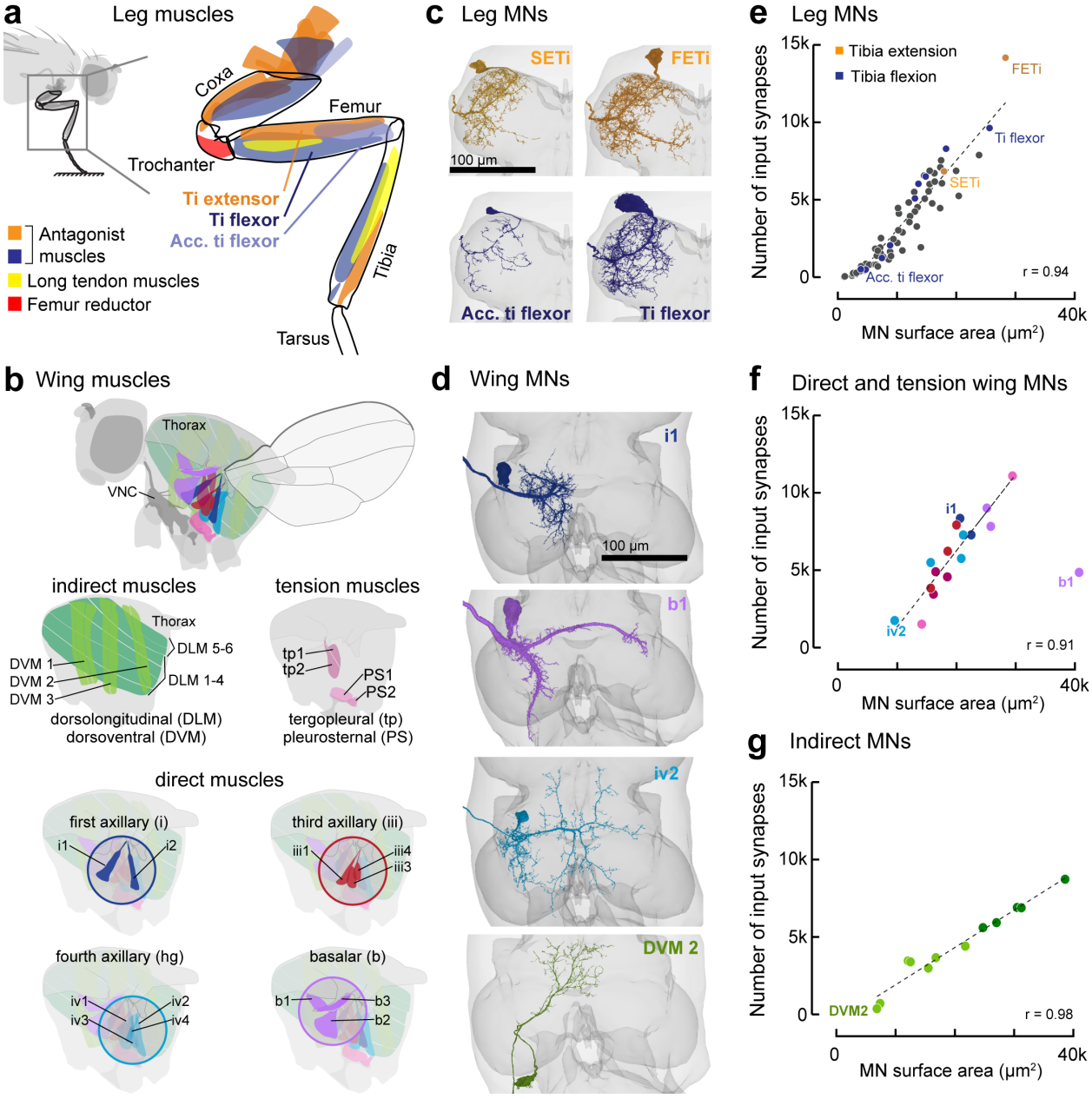

Figure 3.2: Reconstruction of synaptic inputs to identified leg and wing MNs in *Drosophila*. **a,** Schematic of the 18 muscles controlling the front leg. **d,** Flight musculature, separated according to muscle physiology and/or insertion anatomy. **e,** Reconstructed MNs that extend and flex the tibia. **f,** Reconstructed wing MNs. **g,** Leg MN input synapses scale linearly with surface area, such that synapse density is 0.45 synapses μm^{-2} ($r = 0.94$, $p < 10^{-33}$). **h,** Input synapses vs. surface area for direct and tension wing MNs (density = ~ 0.41 synapses μm^{-2} (**Figure 1h**; $r = 0.90$, $p < 0.10^{-3}$, excluding the outlier b1, see Methods) **i,** Input synapses vs surface area for indirect wing MNs (density=0.24 ± 0.02 synapses μm^{-2}, $r = 0.98, p < 10^{-7}$).

are routed through local premotor circuits, which then distribute the information to groups of MNs. We also observed input connectivity patterns that reflect specializations of specific MNs. For example, some wing steering MNs fire tonically during flight[52,35], at rates as high as wingbeat frequency[73] We found that the MNs to four tonic muscles were the only cells with more than 10% of synaptic input from sensory neurons (iii3=18.5%, b1=17.3%, b3=13.5%, i2=11%; **Extended Data Figure S3.1d**). This particular organization may reflect the importance of wingbeat-synchronous proprioceptive feedback in tuning the activation phase of these muscles[74], a feature that is known to modulate their wing stroke trajectory on a stroke-to-stroke basis[75].

In summary, we found quantitative similarities in the proportions of synapses to leg and wing MNs from different classes of preMNs. We next sought to understand how the structure of this premotor connectivity relates to the function of leg and wing muscles.

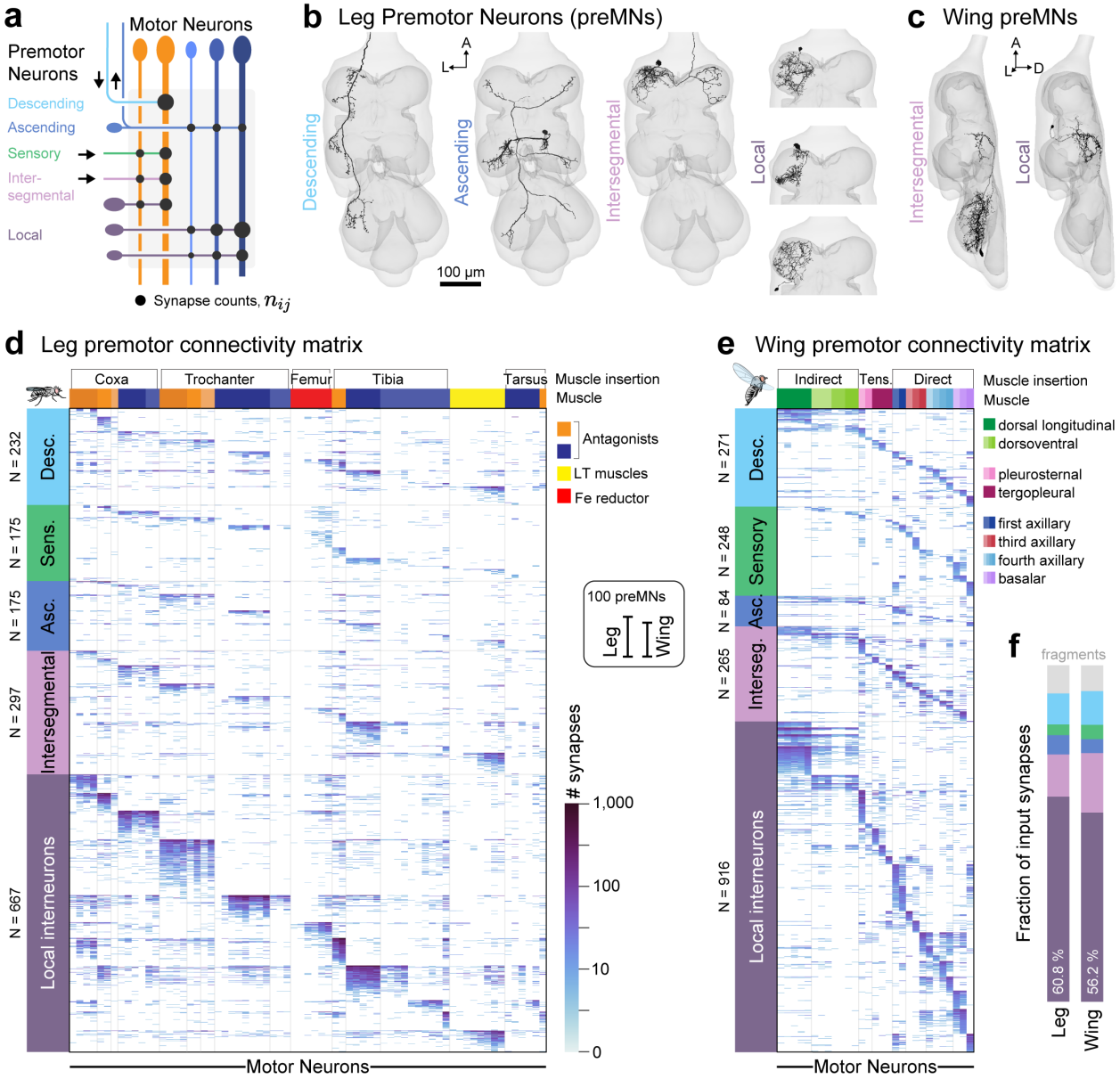

Figure 3.3: The majority of synaptic input to MNs is from local interneurons. **a,** Schematized premotor connectivity matrix. PreMNs (rows) are colored according to cell class. MNs (columns) are grouped by their distinct muscle targets (orange and blue). **b,** Examples of descending, ascending, intersegmental, and local leg preMNs. Intersegmental leg preMNs receive input from other neuromeres. **c,** Example intersegmental and local wing preMNs. Intersegmental wing preMNs receive input from leg neuromeres. **d,e** Premotor connectivity matrices for the left T1 leg (left) and left wing (right). The color of each element indicates the log10(n+1) of the number of synapses from each preMN (row) onto each MN (column). Note that the log scale makes differences appear smaller than they are. Gray vertical lines delineate muscle targets, from proximal to distal, indicated by color (top). PreMNs are ordered: 1) by cell class; 2) by MN targets; 3) by total synapses onto all MNs. Connectivity matrix only shows synapses from fully proofread neurons. **f,** Fraction of total synaptic input from each cell class onto leg or wing MNs. Fragments (8.3% for leg and 7.6% for wing) do not belong to any class, because they have not been attached to a primary neurite via proofreading.

Hierarchical clustering of MN input connectivity reveals patterns of common synaptic input

Common synaptic input to MNs within a motor pool has been proposed to underlie hierarchical MN recruitment by supporting graded production of muscle force to control a single joint[76,30]. On the other hand, common input to MNs that actuate neighboring or distant joints is thought to underlie coordinated firing patterns during complex multi-jointed movements, termed a muscle synergy[77,5]. Because we previously mapped the muscle innervation of each leg and wing MN from the FANC connectome[18], we were able to analyze the relationship between common premotor input to MNs and the identity of the muscles they control.

To quantify common input to MNs, we first compared pairs of MNs based on the number of synapses from preMNs (**Figure 3.3d, e**). We used cosine similarity, an established metric for comparing the similarity of vectors[78,79]. Cosine similarity is the dot product of the normalized inputs (L2-norm of the column vectors; **Figure 3.4a-d**). Normalization turns the columns into unit vectors in N-dimensional preMN space (N=1,546 leg preMNs or N=1,784 wing preMNs), which facilitates comparing MNs that vary in the total number of synapses they receive (**Figure 3.4b**). Values of high cosine similarity indicate that two MNs receive the same synaptic weights from the same preMNs, i.e. the same number of synapses in proportion to total synaptic input (**Figure 3.4b**), suggesting a high likelihood of co-activation or co-inhibition. Low similarity scores indicate either that two MNs share few synaptic partners or that the relative input weights from common preMNs are different enough to pull the column vectors in different directions (**Figure 3.4c**). The matrices of pairwise cosine similarity for leg MNs (**Figure 3.4e**) and wing MNs (**Figure 3.4f**) revealed distinct clusters of MNs with high cosine similarity, reaching extremely high values (more than 0.9) for some pairs.

To identify groups of MNs that share common premotor input, we performed unsupervised agglomerative clustering on the cosine similarity matrices (**Figure 3.4d-f**, see **Extended Data Figures S3.2, S3.3** for details of clustering procedures), so that MNs whose pairwise similarity is closer to 1 were closer together. This ordering allowed us to group

MNs according to the similarity of their premotor networks, irrespective of the muscles they innervate. We refer to each cluster as a "motor module", because MNs within each cluster are likely to be recruited together due to their common preMN input.

Leg MNs

Most leg motor modules contained MNs that innervate the same or mechanically linked muscles that attach to the same joint (**Figure 3.4e**). This organization is illustrated by the two modules that control the trochanter. The seven MNs that innervate the trochanter flexor muscle all cluster together, along with the MNs that innervate the accessory trochanter flexor, a separate muscle that actuates the same joint. The antagonist trochanter extensor module is composed of eight MNs that innervate three parts of the muscle with different origins and insertions on the same extensor tendon. The antagonist trochanter flexors and extensors have cosine similarity near zero, indicating they share few sources of input. The coxa muscles featured a different module organization, where the seven MNs innervating the four muscles that insert on its anterior aspect separate into two distinct modules. The coxa has three degrees-of-freedom, so the two promotor muscles (4 MNs) and the rotator and adductor muscles (3 MNs) are not strict synergists and thus may not share a common recruitment hierarchy, similar to the human shoulder (Wickham and Brown, 1998). The examples of the trochanter and coxa illustrate our general finding that the composition of most leg motor modules is consistent with the size principle model that MNs within a motor pool receive common input from preMNs. Clustering MNs by their preMN input also revealed some unexpected modules that indicate novel and specialized functions. First, the accessory tibia flexor MNs separate into three different clusters (**Figure 3.4e**). This finding is not necessarily inconsistent with the motor pool concept, as individual muscle fibers of the accessory tibia flexor muscle insert on the tibia through individual thin tendons, rather than inserting onto a single large tendon like the tibia flexor muscle[18]. Subdividing tibia modules may improve dexterity by allowing each muscle fiber some mechanical independence, as has been observed in the locust tibia[80,28]. Second, MNs that innervate tarsus control muscles

receive little common input. Instead, four of the six tarsus depressor MNs share common premotor input with each of the three clusters of tibia flexor modules, respectively. Thus, the most distal segments may be controlled by shared premotor input that produces co-contraction of tarsus and tibia muscles.

Wing MNs

Unsupervised agglomerative clustering of the wing premotor network revealed two subdivisions of wing MN modules that map onto the two anatomically and physiologically distinct muscle systems: indirect MNs and direct/tension MNs. Further, the MNs of the indirect muscles cluster into two groups, corresponding to the dorsolongitudinal muscles (DLMs, 5 MNs) and dorsoventral muscles (DVMs, 7 MNs). This organization is consistent with the antagonistic function of the DLMs and DVMs, which power the downstroke and upstroke, respectively. Notably, the two indirect modules also receive substantial shared input (similarity = 0.5 ±0.07). This similarity makes sense because the indirect muscles contract asynchronously from MN spikes and indirect MNs all spike at the same frequency during flight, though their timing is offset from each other[37,81,82]. Thus, while power MNs receive a high degree of common preMN input, these input patterns are unlikely to contribute to the establishment of a recruitment hierarchy.

Pairs of wing tension MNs, on the other hand, exhibit low similarity (**Figure 3.4f**, mean = 0.13 ±0.10), suggesting they do not receive substantial common input. These five MNs have large numbers of input synapses, on par with the largest leg MNs (Extended Data **Figure S3.1b**). However, tension MN synapses are largely from non-overlapping populations of preMNs. These distinct preMN populations may represent parallel premotor pathways for independent control. Interestingly, one tension MN, named "tpn" as it innervates both the tp1 and tp2 fibers of the tergopleural muscle[53], displayed higher similarity with two direct MNs than with other tension MNs.

Unlike most leg modules, we observed high similarity between MNs innervating direct (i.e., steering) muscles that attach on different sclerites within the wing hinge (**Figure 3.4f,**

g). Each direct muscle is innervated by a single MN and inserts on its sclerite at a different orientation to exert force in different directions. Each wing sclerite is equipped with at least one tonic muscle and one phasic muscle, which permits both constant trimming of the hinge mechanics as well as additional activation during rapid maneuvers[52]. Based on this organization, MNs controlling muscles attached to the same sclerite may need to be recruited independently, rather than all together. Consistent with this prediction, clustering delineated four distinct modules of direct MNs (plus the one tension MN) that receive common premotor input (**Figure 3.4f**, inset). The compositions of some of these modules are also supported by prior physiological recordings, such as anti-correlations between i1 and iii1 and correlations between b1 and b2 spiking within a wing stroke[49]. More recent work found correlations in muscle calcium signals that perfectly match this premotor module structure[35]. Thus, both neuromuscular recordings and clustering by preMN synaptic connectivity suggest that wing steering MNs form synergies that are coordinated by dedicated premotor pathways.

PreMNs preferentially synapse onto specific motor modules.

Agglomerative clustering revealed modularity of MNs due to shared preMN input (**Figure 3.4e, f**). We next sought to understand how preMN synaptic connectivity patterns give rise to this modular structure. Do all preMNs synapse predominantly onto a single module, or do some preMNs connect broadly across modules? For each preMN, we computed the "module weights", defined as the number of synapses a preMN makes in each module relative to its total number of synapses onto MNs. We defined "module preference" as the highest module weight of each preMN. The median module preference is 0.80 (interquartile range (iqr) =0.45) for leg preMNs and 0.90 (iqr=0.33) for wing preMNs. For leg modules that have clear antagonist modules, we found that the module weight for the antagonist module is low (mean of 0.012±0.001 (s.e.m.) vs. $0.026 < 10^{-4}$ for module weights for all non-preferred modules, $p < 10^{-6}$ Mann-Whitney U test). When we shuffled the preMN synapse counts, the median module preference decreased to 0.50 (**Figure 3.5a**), whereas the mean antagonist module weight increased almost 10-fold to 0.11±0.06 (s.e.m., N=10,000 shuffles).

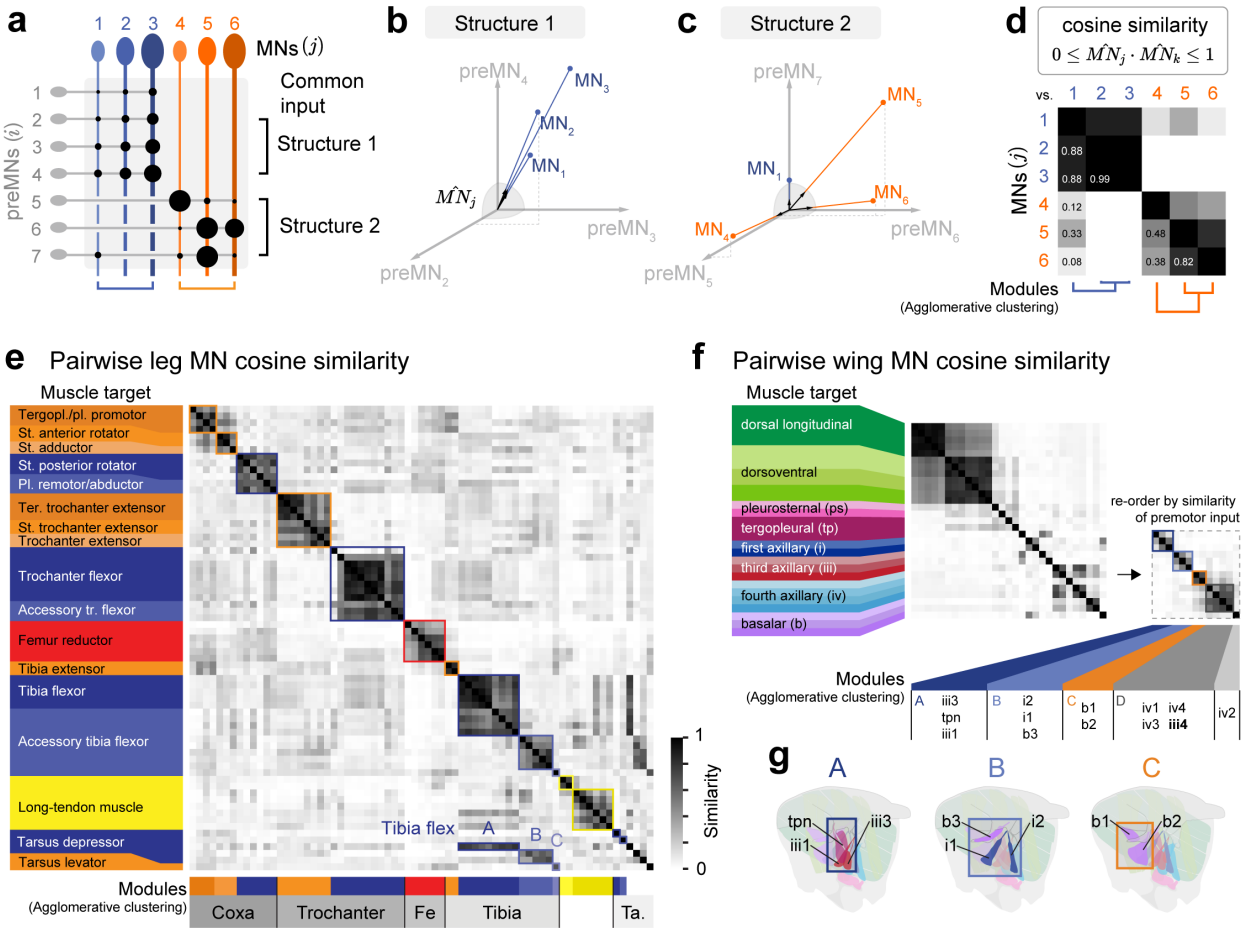

Figure 3.4: Motor neuron similarity based on common synaptic input. **a,** Schematic illustrating how cosine similarity depends on the structure of preMN input. Each MN can be thought of as a vector in a preMN space, with seven dimensions in this example. **b-c,** Cosine similarity is the dot product of the normalized column vectors in premotor space (black arrows) on the unit sphere (gray). **b,** If MNs (blue) receive the same normalized synaptic weights from the same preMNs, the pairwise similarity is near 1 (Structure 1). **c,** If MNs (orange) receive input from the same preMNs, but not the same weights, the cosine similarity will be non-zero, but less than 1 (Structure 2). **d,** Matrix of pairwise cosine similarity for MNs. Agglomerative clustering defines groups of MNs with high cosine similarity, which we call motor modules. **e,** Pairwise MN cosine similarity matrix for leg MNs. MNs are ordered as in **Figure 2**, from proximal to distal muscle targets. Muscle innervation of each MN is indicated at left. Motor modules are indicated below (see **Extended Data Figure S3.2a-f** for details). **f,** Pairwise similarity of wing MNs. Wing MNs are ordered by sclerite attachment as in **Figure 2**. Inset shows reordered direct steering MNs by module structure (defined in **Extended Data Figure S3.3a-d**). **g,** Steering modules are composed of muscles that attach to distinct sclerites.

The preference for a specific motor module thus varies across preMNs, but most leg and wing preMNs exhibit a preference for a specific motor module that is higher than would be expected from random wiring. Illustrating the strength of this preference, preMN synapses onto a preferred module account for 62.2% of synapses onto leg MNs and 75.7% of synapses onto wing MNs (**Extended Data Figure S3.4b, f**).

Even though preMNs tend to synapse on MNs in a single preferred module, this does not always result in high MN cosine similarity. For example, the cosine similarity of wing steering MNs is never as high as leg MNs (**Figure 3.5b**), even though wing preMNs have high module preference (**Figure 3.5a**). One way this could arise is depicted in **Figure 3.4c**: both network structures contain preMNs that preferentially target a single module, but Structure 2 results in lower cosine similarity because the synaptic weights of its preMN inputs are more variable across their MN targets. The cosine similarity of leg MNs is also lower if it is calculated using only the connections from intersegmental or descending preMNs (**Extended Data Figure S3.4c**). By contrast, for both leg and wing MNs, local preMN connectivity results in a similar distribution of cosine similarity for MNs in the same module (**Extended Data Figure S3.4d; Extended Data Figure S3.5e, g**). Together, this analysis suggests that the connectivity of local preMNs, as compared to other cell classes, is the primary driver of MN modularity. It also suggests that connectivity of local preMNs is structured differently for leg and wing motor systems, a hypothesis we explore next.

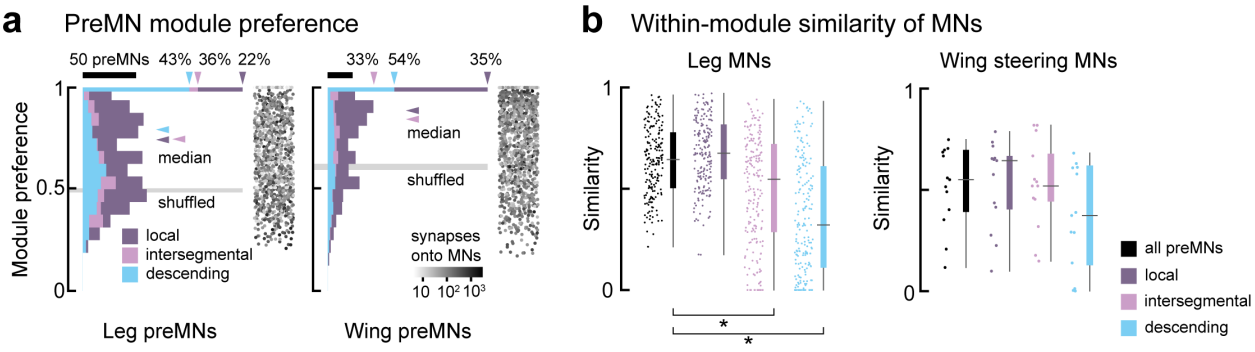

Figure 3.5: PreMNs preferentially target specific groups of MNs, forming motor modules. **a,** PreMN module preference (see Methods) for local (purple), intersegmental (pink), and descending (blue) leg preMNs, the three cell classes that account for most MN input. Vertical arrowheads indicate the fraction of preMNs that synapse onto a single module, i.e. module preference = 1. Horizontal arrowheads indicate the median module preference. Gray box is the range of median module preference when rows of the connectivity matrix are shuffled (N=104 shuffles). Gray dots show total number of MN synapses (log-scale) for individual preMNs. Module preference is not strongly correlated with total MN synapses (All leg preMNs: Pearson's r=-0.29, $p < 10^{-30}$; wing preMNs: r=-0.18, $p < 10^{-14}$). **b,** Pairwise similarity of MNs within modules, when considering all preMNs (black), or just a single class. Left: within-module leg MN similarity is lower when considering only intersegmental or descending preMNs ($p < 10^{-24}$, Kruskal-Wallis non-parametric one-way ANOVA. Conover's post-hoc pairwise test with Holm correction for multiple comparisons: * - $p < 10^{-6}$). Right: within-module similarity of wing MNs (excluding indirect and tension muscle MNs) is generally lower than for leg MNs.

The structure of local preMN input to motor modules reflects their unique biomechanics.

We next analyzed the structure of local preMN input within motor modules. We first focused on the tibia, where it is well established that MNs are hierarchically recruited (from slow/small to large/fast) in flies and other insects[67,57,83,28]. We quantified the structure of local preMN synaptic input onto MNs in their preferred module (**Figure 3.6a**). We defined the output weight, w_{ij}, as the synapse count from preMN, i, onto MN, j, divided by the sum of the synapses onto the entire motor module. We found that each preMN provides the same output weight onto all the MNs within the extensor (**Figure 3.6b**) as well as flexor modules (**Figure 3.6c**). Specifically, the preMN output weights onto each MN are proportional to the overall synaptic input to each MN. This is true regardless of the total number of preMN

synapses, which can range over 100-fold (**Figure 3.6b-c**, **Extended Data Figure S3.6a-c**). Shuffling the connections onto highly similar MNs lowered the mean cosine similarity, showing that the pattern of proportional synaptic weights is a key factor that determines MN input similarity (**Extended Data Figure S3.6d-g**). We observed this pattern in all leg motor modules with more than one MN.

When we plotted the preMN synaptic weights onto wing steering modules, we found a different, non-proportional structure (**Figure 3.6d-g**). Specifically, preMNs that contact each MN in a wing steering module do not tend to distribute their synapses in proportion to overall synaptic input. Even steering Module C, which contains only the b1 and b2 MNs, is characterized by wider variance of weights (**Figure 3.6g**) when compared with the pair of tibia extensor MNs (**Figure 3.6b**). In this case, the smaller b2 MN receives a greater proportion of input from the majority of common local preMNs. To explore how the structure of preMN synaptic weights compares to a random connectivity scheme, we computed the average cosine similarity of MNs when synapse counts are shuffled within the module (**Figure 3.7a**). For most modules, shuffling lowered the mean cosine similarity, consistent with most modules having a proportional connectivity structure. By contrast, if the synapse counts for wing steering modules A or D were shuffled, the resulting average cosine similarity was almost always higher, suggesting that these connectivity patterns are not random (**Figure 3.7a**).

In summary, the strength of connections from local preMNs to leg motor modules is proportional to total MN input, while local preMN input to wing steering motor modules is not. This difference explains why modules controlling the wing steering muscles have lower within-module similarity than leg modules (**Figure 3.7b**). The difference in preMN connectivity structure in wing modules may reflect specialized motor control strategies for the leg and wing, which possess distinct biomechanics (**Figure 3.7b, c**). Tibia flexor MNs in the same module act together to control flexion torque, but produce force per spike that ranges over three orders of magnitude[67]. By contrast, the muscles that form each wing steering module have different origin and insertion points. Non-proportional patterns of preMN

connectivity may allow wing steering MNs to be recruited in different combinations, or with different relative timing. Prior electrophysiological[47,73,84] and biomechanical[75] studies posit that the action of direct wing MNs are regulated not just by firing frequency, but also by firing phase within the wingbeat cycle, a mechanism that allows a single motor neuron to regulate wing motion with great precision. The connectivity of wing preMNs may provide a basis for flexibly tuning the recruitment order of MNs within a module, whereas the proportional connectivity of leg preMNs provides a basis for stereotyped but fine-scale control of joint force production.

The precision of proportional preMN connectivity onto leg MNs is striking, especially given the fact that leg MN dendrites are spatially intermingled within the leg neuropil[18]. During development, each preMN must find its target module and establish the appropriate number of synapses in proportion to MN size (**Extended Data Figure S3.6a-c**)[85]. To investigate what preMN properties determine motor modules, we next identified premotor local and intersegmental preMNs according to their developmental identity.

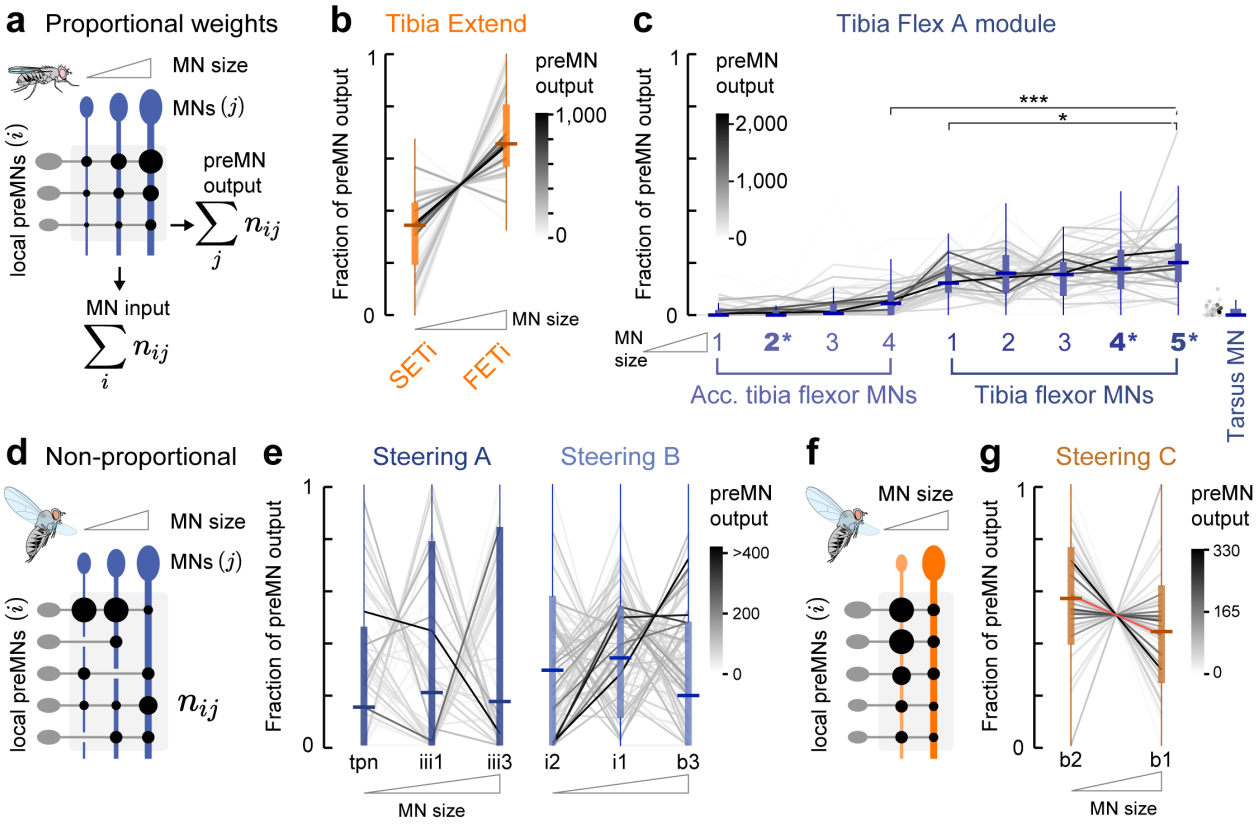

Figure 3.6: Local preMN connectivity differs between leg and wing steering motor modules. a, Illustration of proportional connectivity of module-preferring preMNs in leg modules. PreMN output is defined as the sum of a preMN's synapses onto MNs in the module. **b,** Proportional connection weights from local preMNs that prefer the Tibia Extensor module onto the Slow (SETi) and Fast (FETi) tibia extensor MNs. Line hue indicates total number of synapses onto the module. **c,** Proportional connection weights from local preMNs that prefer the Tibia Flex A module onto the Tibia Flex A module. The module is composed of four accessory tibia flexor MNs, the five tibia flexor MNs, and the synergist tarsus MN. Tibia MNs are ordered by surface area. Asterisks (*) indicate MNs previously characterized using electrophysiology[67]. The fraction of preMN output onto the largest MN is significantly larger than onto smaller MNs (p¡10-4,, Kruskal-Wallis non-parametric one-way ANOVA. Conover's post-hoc pairwise test with Holm correction for multiple comparisons: *** - p¡10-28, * - p=0.012). **d,** Wing steering motor modules lack proportional connectivity. **e,** Local preMN connections onto wing Steering Modules A and B. **f,** Local preMNs make more synapses onto the smaller b2 MN than the larger b1 MN. **g,** Same as **e** for Steering Module C.

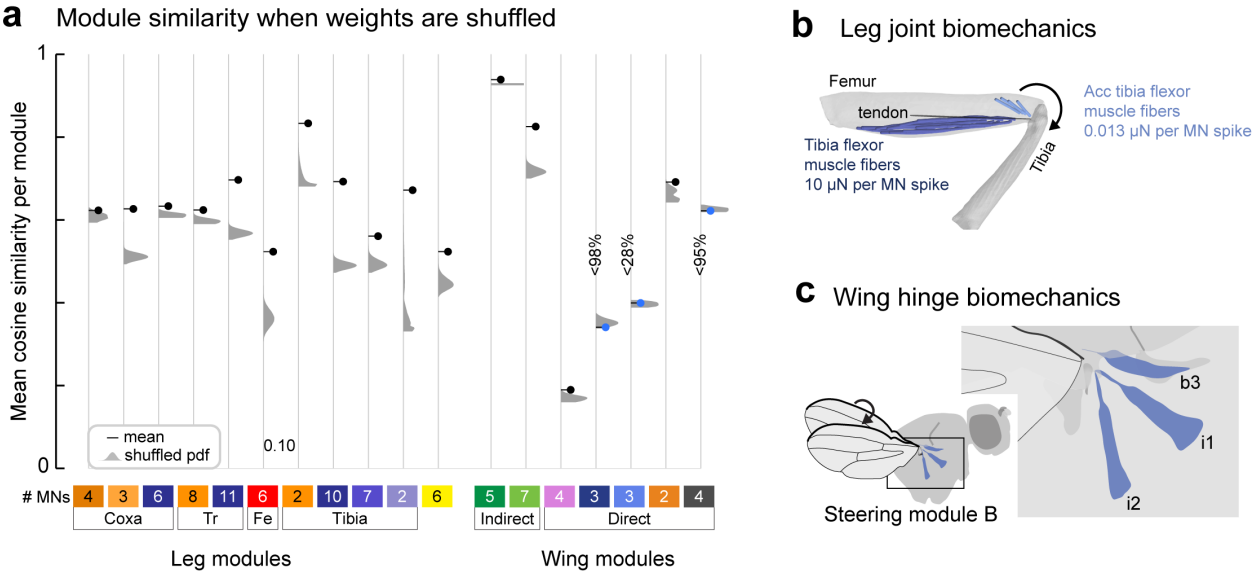

Figure 3.7: Connectivity structure and biomechanics. **a,** Average cosine similarity (black dots) compared to the average cosine similarity when synapse counts from local preMNs onto their preferred module are shuffled (gray probabilities density function (PDF), N=10,000 shuffles). The measured mean is larger than 99% of the PDF in all cases except for coxa promotors (left, larger than 98.3%), steering module B (62%), and steering modules A and D (larger than only 2% and 5% of shuffles, respectively). **b,** MNs in the Tibia Flex A module work together to produce torque on the tibia. Measurements of tibia force produced by single spikes in the 2* and 5* MNs from Azevedo et al., 2020. **c,** Schematic of muscles innervated by wing steering module B. Each muscle has a different origin and attachment to the wing hinge, suggesting co-contraction of muscles can have variable biomechanical effects.

PreMNs with diverse developmental lineages contact each motor module.

The neurons that make up the *Drosophila* nervous system develop from less than 40 stem cell hemilineages[86]. Neurons within a hemilineage tend to enter the neuropil through common primary neurite tracts, and develop diverse but identifiable morphologies[87,88,89]. We identified the hemilineage of local and intersegmental preMNs by comparing stereotyped morphological features to hemilineage-specific genetic driver lines[90,91]. We also validated our hemilineage identification against a parallel effort in the male VNC connectome (**Figure 3.8a** and **Extended Data Figure S3.7**)[88]. We found that some hemilineages contain preMNs that predominantly synapse on either leg or wing MNs (**Figure 3.8b**). Notably, many different motor modules are targeted by individual local and intersegmental preMNs that that develop from the same hemilineage. Conversely, each motor module also receives synaptic input from preMNs from multiple different hemilineages. In other words, our results demonstrate that a preMN's preference for a particular module is not strictly determined by its developmental origin.

The majority of *Drosophila* neurons release one of three primary neurotransmitters:[92,93] acetylcholine, GABA, or glutamate. In the fly central nervous system (CNS), acetylcholine is typically excitatory, acting via nicotinic acetylcholine receptors (nAChR), while GABA is typically inhibitory, acting via $GABA_A$ receptors[92,94,95]. Glutamate is excitatory at the fly neuromuscular junction, acting on ionotropic glutamate receptors (GluRs), but can be inhibitory in the CNS, acting on the glutamate-gated chloride channel, GluCl[96]. GluCl is the most highly expressed glutamate receptor in MNs, although they also express lower levels of GluRIA and GluRIB[92].

Most VNC neurons within a hemilineage release the same primary neurotransmitter[87], although exceptions may exist[88]. We therefore inferred the neurotransmitter of each local and intersegmental preMNs with an identifiable hemilineage (1830 of 2115 = 86% of neurons; 89.9% of synapses). We found that each MN receives a consistent ratio of input from preMNs with different putative neurotransmitters, and that this mix differs across leg and wing

systems, with leg MNs receiving more input from putative glutamatergic preMNs (**Figure 3.9a**). The consistency of this ratio is striking, considering both that leg and wing MNs differ up to 40-fold in size and total synaptic input, and that preMNs develop from different lineages and vary up to 100-fold in output synapses.

Finally, we asked whether local leg preMNs with different putative neurotransmitter identities form different patterns of connectivity with MNs. We found that the module preference value is lower for cholinergic preMNs than for GABAergic or glutamatergic preMNs (**Figure 3.9b**), indicating that cholinergic preMNs tend to make more synapses onto MNs in non-preferred modules. We then investigated the specificity of these connections outside the preferred module. As described above, the module weight for the antagonist MN is extremely low. For example, the local preMNs that synapse onto trochanter flexor MNs do not synapse on the trochanter extensor MNs and vice versa. Instead, cholinergic leg preMNs tend to synapse onto their preferred module and a second module that controls a different joint, establishing a potential motor synergy. Furthermore, when that secondary module itself has an antagonist, preMNs avoid synapsing onto the antagonist (**Figure 3.9c**). For instance, if a preMN preferentially synapses on MNs in the Tibia Flex A module as well as trochanter flexor MNs (synergist), then it does not synapse on trochanter extensor MNs (antagonist of the synergist, **Figure 3.9d**). Glutamatergic and GABAergic preMNs follow this pattern as well (**Figure 3.9c, d**). Thus, local leg preMNs make stereotyped synaptic connections within their preferred leg modules (**Figure 3.6b, c**), and form precise connectivity patterns across modules.

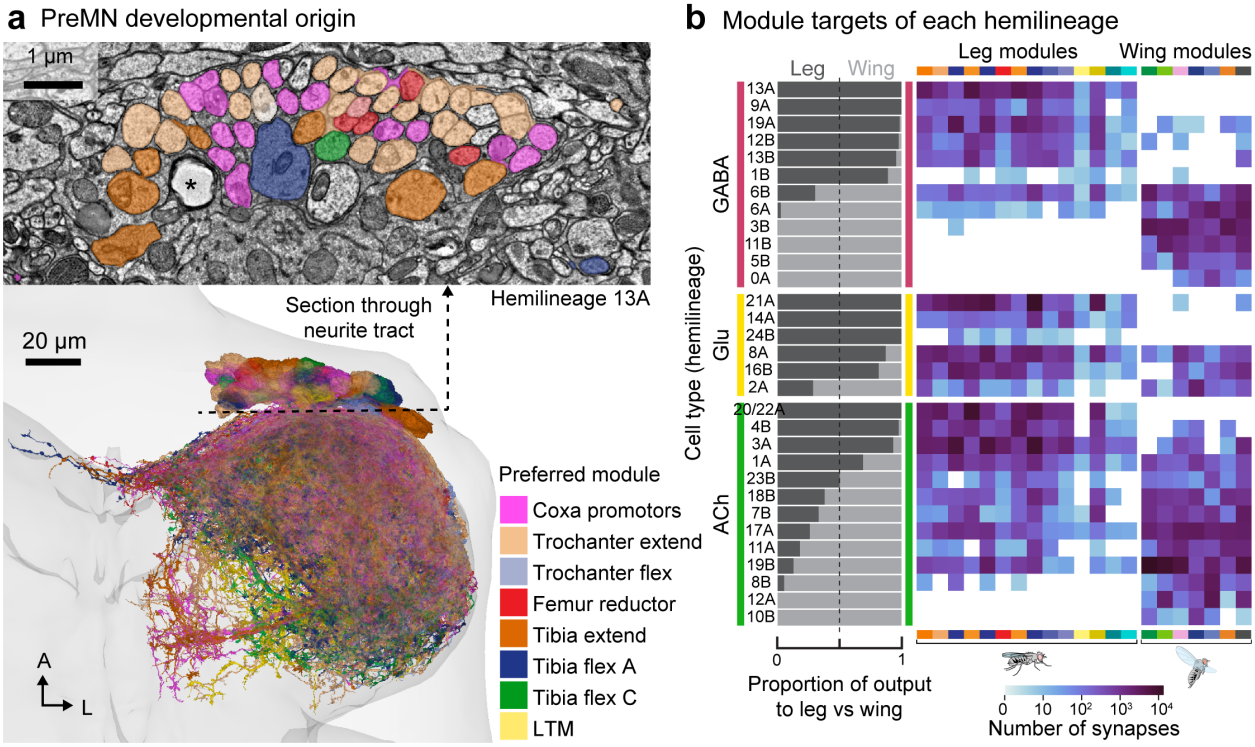

Figure 3.8: PreMNs with diverse developmental lineages contact each motor module. **a,** PreMNs from hemilineage 13A (GABAergic), colored according to their preferred leg motor module. **b,** Left: proportion of the total synapses from all local and intersegmental preMNs in each hemilineage onto leg MNs vs. wing MNs. Right: total synapses onto MNs in each leg or wing module.

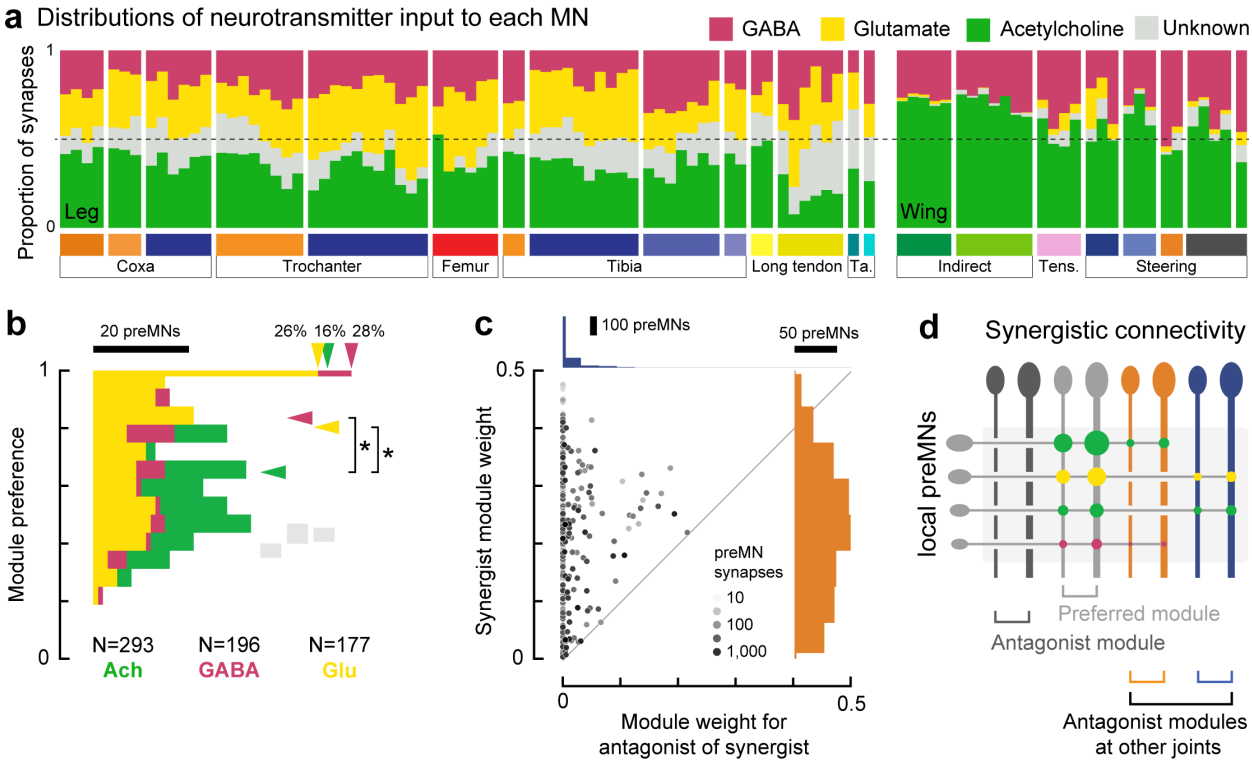

Figure 3.9: Cholinergic preMNs contact other modules more frequently than other preMNs. **a,** Proportion of synaptic input to MNs from cholinergic (green), glutamatergic (yellow), GABAergic (pink), and unidentified (light gray), hemilineages. Only local and intersegmental preMNs are included in this analysis (see Methods). **b,** Module preference of local preMNs, by hemilineage neurotransmitter. Horizontal arrows indicate the median module preference (p=0.0013, Kruskal-Wallis non-parametric one-way ANOVA. Conover's post-hoc pairwise test with Holm correction for multiple comparisons: * - p=0.002). Gray rectangles indicate the range of medians when preMN connections are shuffled. Vertical arrows show the percentage of neurons that target a single module. **c,** Module weights for synergist module (y-axis, orange histogram), vs. the antagonist of the synergist module (x-axis, blue histogram) (See Methods). Dot hues indicate total synapses onto all MNs. **d,** Schematic of preMNs targeting synergist module while avoiding antagonist modules.

3.4 Discussion

Using connectomics, we reconstructed and analyzed the structure of premotor neural circuits that control the fly leg and wing. Our analyses suggest that local VNC interneurons play a central role in integrating descending motor commands with proprioceptive feedback to coordinate MN activity[97,98]. The connectome is only a static anatomical wiring diagram, but the structure of premotor circuits leads to innumerable testable hypotheses for future research, such as specialized functions of motor modules and mechanisms of neural circuit development. Our analyses also reveal an unexpected level of complexity in the *Drosophila* motor system. We found that a typical fly MN receives thousands of synapses from hundreds of presynaptic preMNs. This number is on par with the scale of synaptic integration in pyramidal cells of the rodent cortex[99], but ten times fewer synapses than cat MNs (16,000 - 140,000)[65,66,100], and an order of magnitude more than larval zebrafish MNs[101]. Vertebrates also exhibit variation in synapse size[102], which have not been observed in insects. Thus, synapse count is thought to be a reasonable estimate of synaptic weight in *Drosophila*[103].

Motor output from the VNC is modular

Our analysis of premotor connectivity showed that leg and wing MNs cluster into motor modules formed by patterns of synaptic input from common presynaptic partners. These modules are largely shaped by the synaptic weights of local preMNs. Most modules contain MNs that share clear biomechanical functions. For example, leg modules contain MNs that innervate either the same muscle, or multiple muscles with origins and tendon insertion points that create torque in the same direction[18,20,104]. The leg module structure is consistent with the organization of canonical motor pools in other species, such as the gastrocnemius and soleus extensor muscles in vertebrates[61,63]. The module structure of the wing motor system is different. One pair of modules are composed of the MNs that innervate the large, asynchronous indirect power muscles that contract the thorax. Other modules are composed of 2-4 synchronous direct wing MNs that control multiple sclerites of the wing hinge for

steering. The structure of these steering modules suggests how groups of muscles act via the wing hinge to create subtle 3D deviations in wing trajectory. Some modules align with experimental results and theoretical predictions from past literature[49,52,35,53,54], while others offer new predictions. For example, we predict that steering module "B", which contains MNs i1, i2, and b3, is recruited to unilaterally decrease wing stroke amplitude. This prediction is consistent with EMG recordings correlating i1 muscle activity with ipsilateral turns[50], but remains to be tested using causal perturbations.

We found that most preMNs have a strong module preference, in that they make biased synaptic connections onto MNs within the same module. PreMNs within the same developmental lineage also have strong preferences for different modules, consistent with past work in larval *Drosophila*[105]. A proposed mechanism for wiring precision between preMNs and MNs is that the stereotyped dendritic morphology of MNs that innervate the same muscle allows sequentially born preMNs to find anatomically similar MNs[106,107,108,109,105]. In the adult fly, however, the dendrites of MNs in different motor modules are highly intermingled within the neuropil[18,110]. This lack of spatial topography suggests that spatial location alone is not sufficient for ensuring the wiring precision between preMNs and MNs that we observe in the connectome. Overall, our analyses raise a number of intriguing developmental questions which cannot be answered using connectomics alone, such as what molecular signals cause preMNs from the same hemilineage to target different postsynaptic MNs.

Architecture of premotor networks to generate module activity, the neural input to biomechanical systems.

The premotor connectivity matrices for wing and leg MNs provided an opportunity to compare how neural circuits are structured to control musculoskeletal systems with distinct biomechanical challenges. Shared presynaptic input provides a mechanism to control correlations in the firing rates of functionally related MNs. If we define module activity as the vector, $r(t)$, of firing rates, $r(t)$, of the MNs in a module[3], then firing rate correlations constrain $r(t)$, relative to a system in which MNs are independently driven[30]. Conceptu-

ally, correlated firing rates reduce the information entropy of $r(t)$, i.e., some module activity states cannot occur[111]. We propose that preMN input, particularly input from local preMNs, may be structured so that the entropy of the module activity matches the biomechanical constraints of the target musculoskeletal elements.

At one extreme, the MNs in the two flight power modules receive nearly the same synaptic weights from shared presynaptic partners. During flight, DLM and DVM MNs all spike at around 6 Hertz[112,82]. At the same time, the instantaneous firing rates of DLMs are desynchronized in a pattern called a "splay state", such that the DLMs spike one at a time in a regular, repeated pattern, due to gap junction coupling between MNs[81]. Although their timing is offset, the DLM MNs always spike once within each splay state cycle, which controls the calcium levels in the asynchronously contracting power muscles[113]. Our results suggest that the strong similarity of premotor input to all indirect MNs drives the low frequency central pattern generator that governs the frequency, but not the relative spike timing, of the musculoskeletal flight oscillator.

At the other extreme, clustering the cosine similarity of direct wing MNs revealed modules that arise from preMNs that form variable, non-proportional synaptic weights onto the 2-4 MNs in each steering module. In contrast to the indirect muscles, the timing of steering muscle activation is not thought to arise from a central pattern generator[49]. We propose that such patterns allow preMNs to vary the correlations between the MN firing rates, allowing r(t) to range throughout module activity space. We further hypothesize that the advantage of shared synaptic input—relative to independent input to each MN—is the ability to control the precise timing of MN spikes and steering muscle contractions. If each steering muscle has unique effects on the wing's trajectory[35], and these effects depend on the phase of firing within the wingstroke[49,75], then it would be advantageous for preMNs to finely control spike timing while taking advantage of the full module activity space.

Finally, the structure of synaptic input to leg modules creates correlations in MN firing rates in the form of a recruitment hierarchy, consistent with long-standing predictions of the size principle[30,114]. Leg modules arise from the connectivity of excitatory and inhibitory local

preMNs that make one-to-all connections onto leg MNs, suggesting that all MNs within a module are collectively excited or inhibited by changes in the activity of each preMN. Each preMN tends to make more synapses onto larger MNs, in proportion to the total synaptic input to that MN. The structure we found is fundamentally different from the connectivity of premotor circuits that control MN recruitment and swimming speed in adult zebrafish, where dedicated pools of V2a premotor neurons synapse onto either slow or fast MNs[31,32]. This pattern of roughly equal synaptic weights highlights the need for a reciprocal gradient of excitability to ensure that leg MNs are recruited in the correct order. Patterns of voltage- and ligand-gated ion channel expression likely complement the electrotonic properties of MN morphology to create nonlinear excitable membranes that enforce the rank order of recruitment[115,116]. This result also provides a cautionary tale when interpreting connectomes: without knowledge of MN activity in behaving flies[67,28], we would have predicted that MNs that receive the most synaptic input are the most active, when in fact they are rarely recruited.

Past work argues that constraining module activity with a recruitment hierarchy simplifies the problem of how the nervous system controls motor units with a range of neuromuscular properties[6]. However, violations of the recruitment hierarchy have been observed in many species, particularly during rapid, oscillating movements[67,117,118,119]. Recent work in primates demonstrated flexible relationships between MN firing rates that changed with the demands of a motor task[3]. Integration of common preMN inputs may also vary across MNs of different sizes, thus influencing the trajectory of the module activity. MNs with large dendritic fields, high conductances, and faster time constants may precisely integrate rapidly oscillating excitatory and inhibitory inputs, whereas smaller neurons may be both more sensitive to inhibition and slower to depolarize[120]. We found that many intersegmental and descending neurons target specific motor modules, but with less proportional structure than local preMNs. These pathways may evoke flexible correlations in MN firing rates, as they do in primates[3]. Thus, we propose that the leg premotor network balances two seemingly opposed demands, reducing the dimensionality of local control within motor modules

while maintaining the capacity to flexibly recruit MNs within a module to achieve specific motor tasks[121].

3.5 Acknowledgements

This work was supported by a Searle Scholar Award, a Klingenstein-Simons Fellowship, a Pew Biomedical Scholar Award, a McKnight Scholar Award, a Sloan Research Fellowship, the New York Stem Cell Foundation, and a UW Innovation Award to JCT; a Genise Goldenson Award to WAL; NIH U19NS104655 to JCT and MD; NIH R01MH117808 to JCT, WAL, and HSS. JCT is a New York Stem Cell Foundation – Robertson Investigator. We thank Jim Truman, David Shepherd, and Elizabeth Marin for assistance with hemilineage identification. We thank Greg Jefferis and Gwyneth Card for helpful discussions, and for their lab's contributions to proofreading in the FANC dataset, particularly Katharina Eichler, Paul Brooks and Gregory Jefferis for sharing comprehensive proofreading and annotation of DNs in the FANC dataset. We thank members of the Tuthill and Dickinson Labs, Sama Ahmed, Bing Brunton, and Jim Truman for comments on the manuscript.

3.6 Methods

Reconstruction of premotor neurons (preMN) anatomy and connectivity

The automated segmentation of the Female Adult Nerve Cord electron microscopy dataset[15], as well as the identification and reconstruction of leg and wing motor neurons (MNs), was described in a companion paper[18]. To manually correct the automated segmentation of premotor neurons (preMNs), we used Google's collaborative Neuroglancer interface[122]. We identified all objects in the automated segmentation that were predicted to synapse onto MNs. As a metric of both the quality of the segmentation and the speed of manual proofreading, initially 20% of the pre-synapses were associated with objects that had a soma. We proofread segments until more than 90% of all input to front left leg and left wing MNs was associated with either a cell body, or an identified descending or sensory process. The

remaining inputs were categorized as fragment segments (**Extended Data Figure S3.1**). We deemed a neuron as "proofread" once its cell body was attached, its full backbone reconstructed, and it had as many branches as could be confidently attached.

Motor neuron volume and surface area were calculated using the statistics of the level 2 cache, which is the graph of "level 2 chunks" in the hierarchy of the PyChunkedGraph data structure[123,99]. Note, the surface area and volume measurements we report do not include the portions of MNs beyond which their axons were cut in the nerve. The computed level 2 cache maintains a representative central point in space, the volume, and the surface area for each level 2 chunk and these statistics are updated when new chunks are created due to proofreading edits. We used the Connectome Annotation Versioning Engine (CAVE) to annotate neurons and keep track of their identities through iterations of proofreading and materializations[124]. Somatic segmentations of all motor neurons (downloaded at 68.8 x 68.8 x 45 nm resolution) were cleaned using a heuristic cleaning procedure that removed missing slices of data and incorrectly merged fragments. This procedure has been explained in detail elsewhere[125]. Briefly, a radius of 15 microns surrounding each soma's center of mass was cut out from the dense segmentation and converted into a binary mask. Subsequent binary dilation in 3D was performed, followed by filling of all holes, and then binary erosion. The resulting binary mask was meshed using marching cubes and connected component analysis was run on the result. For each cell, the somatic surface area and volume measurements were calculated based on the cleaned meshed 15 micron cutout.

Analysis of MNs controlling the front left leg and the left wing

We described the identification of the muscle targets of the front leg and wing MNs in a separate study[18], summarized in **Figure 3.1b**. The leg muscles are named according to the literature[20,104].

We focused on the front (prothoracic) leg because 1) we have measured the physiology and neuromechanical properties of MNs innervating the front tibia flexor[67], 2) the high resolution of our CT volume of the front leg allowed us to count axons entering specific muscles, and 3)

T1 contains 69 MNs compared to 62 or 63 for T2 and T3, so we tackled the most challenging task first. We focused on the left T1 because it was better preserved than the right T1[18].

We analyzed the left wing because the left wing nerve was more intact than the right wing nerve[18]. The MNs in both nerves are intact and fully reconstructed, but the sensory domain of the right wing nerve is damaged.

Definition of cell classes

We classified all premotor neurons (preMNs) into five groups. Descending neurons had a process in the neck connective and no cell body in the VNC. Ascending neurons had a process in the neck connective and a cell body in the VNC. Sensory neurons had processes entering the VNC from peripheral nerves and no cell body in the VNC. The rest of the neurons were fully contained within the VNC. Leg preMNs were classified as local if all their input synapses were within a bounding box containing the left T1 neuromere, and as intersegmental if they had input synapses outside the bounding box. The bounding box, in pixels, was x = [3000 , 38000], y = [90483, 123190], and z = [980, 3858]. Wing preMNs were classified as intersegmental if they had input synapses in any of the six leg neuropils or the abdominal neuropil (e.g., wing preMNs were considered local if they received input from the contralateral wing neuromere, haltere neuromeres, or neck neuromere). We did not split the wing neuropil into right and left sides because some wing MNs cross the midline. All preMNs were manually checked to make sure they were in the correct categories.

In total, we found 271,145 synapses onto leg MNs. We ignored synapses that came from segmented objects that made less than 3 synapses onto MNs, to focus on connections that are less likely to be affected by noise in the synapse detection algorithm[18], leaving 232,534 synapses (86%). We found 212,190 synapses from the preMN classes above. We also found the following synapses onto leg MNs from sources that fall outside these five cell classes: 4 synapses onto MNs from a neuron with a soma in the VNC and a process in the sensory part of the leg nerve that is not a motor neuron;[15] 407 synapses from poorly segmented objects with annotations points in the leg nerve that appear to be merges with glia; and 19,349

synapses from fragments. Finally, we also found 584 output synapses from 37 MNs onto other MNs. Upon inspection, these apparent synapses were all noise; many were at Golgi membranes in the soma, most were dark spots in dendrites, none would have been visually identified as output presynapses with vesicles.

Definition of motor modules

We previously identified the muscle targets of MNs using anatomical features alone[18], which we summarize in **Figure 3.1b**. Here, we used the premotor connectivity matrix to cluster MNs according to shared presynaptic partners (**Figure 3.4**), agnostic to muscle innervation. For both leg and wing MNs, we calculated the matrix of pairwise cosine similarity of columns of the connectivity matrix (**Extended Data Figure S3.2, S3.3**) using the cosine similarity function from the sklearn.metrics module of the sklearn python package[126]. We then used the AgglomerativeClustering routine from the sklearn python package to merge clusters based on the Ward linkage distance, i.e. minimizing the variance of the merged clusters. The threshold for defining specific clusters differs between the leg and wing data because of differences in network structure and scale.

We chose the cosine similarity measure because it normalizes for total input to each MN, which is the dominant source of variation across MNs. It does not otherwise modify connection weights, thus preserving the quantitative structure of the common input, which we argue is the most salient feature of MN input after normalizing for total input. Cosine similarity is a commonly used technique, including in the connectomics literature, to compare sparse feature vectors, such as the synapse counts across all possible inputs[78]. Alternative similarity measures like the Jaccard index binarize the connection weights[79], and network measures like weighted stochastic block models[8] assume probability distributions for connections and weights.

As an alternative to agglomerative clustering, we used the UMAP algorithm to plot the normalized column vectors of the connectivity matrix (L2-norm) on a low dimensional manifold, e.g. from N=1,546-D for the leg matrix to 2-D (**Extended Data Figure S3.2e**)[127].

To test the robustness of clustering, we compared the distributions of cosine similarity for MNs that clustered together (in-cluster) vs. for MNs in different clusters (out-of-cluster). We quantified the overlap between these distributions using the area-under-the-curve (AUC) metric, as we show in **Extended Data Figure S3.4d**. The AUC was calculated using the scipy.stats.mannwhitneyu function and dividing by number of comparisons[128]. For leg MNs, the AUC for the assigned clusters is 0.9974, which captures the fact that only a few out-of-cluster comparisons are larger than some in-cluster comparisons. Then, we tested how the AUC changed if each MN was removed from its computed cluster. An increase in the AUC would indicate a better separation between the in-cluster vs. out-of-cluster distributions. The AUC only increased when two small MNs were individually removed from their assigned clusters: the small femur reductor MN that receives a scant 19 total synapses (AUC = 0.9976), and a long-tendon muscle MN that bears enough similarity to the two small long-tendon muscle MNs (dip-alpha positive)[129] that removing it from the assigned cluster increased the AUC (0.99785). Thus, except for these two interpretable edge cases, the agglomerative clustering led to the largest difference (largest AUC) between the in- vs. out-cluster distributions of cosine similarity. While we observed a similar overall trend for steering MNs, the AUC was maximized when individual tension MNs were removed from that cluster. This finding corroborates our characterization of tension MNs as bearing little similarity to one another. This gave us confidence that we were not overlooking better ways of clustering, in terms of maximizing cosine similarity within clusters.

Finally, we adopt the synonym "module" to refer to these clusters, based on our finding that most clusters include MNs that innervate muscles with synergistic anatomy, according to our previous identifications. See Supplemental Table 1 for links to view MNs grouped by modules in Neuroglancer, an online tool for viewing connectomics datasets.

Module weight, preferred module, and module preference

We define a module weight as the number synapses that a preMN makes onto the 1-10 MNs in a module, divided by the total number of synapses onto MNs, expressed as a fraction.

Thus, each preMN has a module weight for each module, and also likely synapses onto neurons other than MNs. For example, say a preMN makes 100 synapses onto wing MNs, 80 of which are onto different DLM MNs and 20 of which are onto various DVMs. The preMN would have a module weight of 0.8 for the DLM module, 0.2 for the DVM module, and a module weight of 0 for other modules. We define the module preference as the max over module weight, onto the "preferred module". Overall, in the leg connectivity matrix, 62.2% of synapses are from preMNs onto their preferred module, and 75.7% for the wing connectivity matrix.

In the Results, we report the module weight for antagonist modules. We considered three groups of antagonist modules: coxa promotor and coxa remotor/adductor modules vs. coxa posterior, trochanter extend vs. trochanter flex, and tibia extend vs. tibia flex A. Together, these modules receive 75% of the synapses from preMNs. We did not include Tibia flex B or C modules because we are uncertain about their role or function. MNs in Tibia flex B and C modules receive more input from preMNs that target other modules, compared to other similarly sized MNs (**Extended Data Figure S3.4b**).

To analyze the structure of preMN synapses onto non-preferred modules (**Figure 3.9c**), we found the second highest module weight (after the module preference) for each preMN, which we refer to as a secondary module. If the secondary module had an antagonist, we then compared the module weight for those two modules (see "Module weight, preferred module, and module preference").

See Supplemental Table 2 for links to view entire premotor populations that prefer specific modules in Neuroglancer.

Hypothesis testing by shuffling synapse counts

We compared our measurements to null models by computing the same metric when we shuffled the synapse counts in the connectivity matrix, using N=10,000 shuffles. Shuffling the synapse counts preserves both the total number of synapses and the distribution of synapses in a connection,[130] but does not preserve information about synapse location. We

did not consider randomized connectivity that preserved the total number of synapses but broke apart connections, such as Erdös-Rényi networks or Watts-Strogatz networks[131].

To test whether high cosine similarity (max=0.96, median=0.07) arose stochastically, we computed the maximum and median cosine similarity when we shuffled all synapse counts (max=0.61, median=0.02), just the rows of each column (max=0.54, median=0.03), or just the columns of each row (max=0.82, median=0.09). We conclude that shuffling which preMNs a MN receives input from (columns) lowers the overall distribution of cosine similarity. By contrast shuffling the synapse counts that each preMN makes onto MNs (rows) never results in the observed high cosine similarity, but it can produce a median cosine similarity comparable to the unshuffled distribution. However, if we fixed the leg modules and shuffled each row, the AUC of the distributions of in-module vs. out-of-module cosine similarity ranged from 0.44 to 0.56, compared to 0.9974 (above, and **Extended Data Figure S3.4d**).

To test whether high module preference arises stochastically (**Figure 3.5a**), we shuffled the rows of each column, i.e. the synapse counts that each preMN makes onto MNs. Over N=10,000 shuffles, the median module preference ranged from 0.48 to 0.50, compared to 0.80 for the unshuffled leg MN adjacency matrix. The analogous range is plotted for wing preMNs.

For leg preMNs that contact a module that has an antagonist, the mean module weight for the antagonist module is 0.012, and 84% of preMNs avoid the antagonist altogether. When the preMN synapse counts are shuffled, only 30% of preMNs avoid the antagonist and the mean module weight increases to 0.11.

In **Figure 3.9c**, we performed the same comparisons but grouped local preMNs that were predicted to use the same neurotransmitters.

In **Figure 3.7a**, we compared the mean cosine similarity within each module to the shuffled connectivity. Here, we only shuffled the synapse counts that a preMN makes onto the MNs in its preferred module. The probability density function (PDF) of mean cosine similarity for each shuffled matrix was computed by interpolating the cumulative density function (CDF) of mean cosine similarity using linear interpolation from the scipy python

package[128], and differentiating the CDF.

Finally, to test whether proportional connectivity of local preMNs drives high similarity between MNs (**Extended Data Figure S3.6e**), we considered only the connections from preMNs onto the MNs with the highest similarity, which were the largest MNs in each module. This narrowly tests how often we observe such high MN similarity if we break the tendency of each preMN to make proportionally more synapses onto the largest MNs.

Identification of premotor hemilineages

The assignment of premotor neurons into hemilineages was based on a suite of evidence, the foundation of which are hemilineage-specific split-Gal4 lines created by Jim Truman, Haluk Lacin, and David Shepherd, which they have experimentally validated, both in prior work[91,87,132] and in manuscripts that are still in preparation. These split-Gal4 lines identified anatomical hallmarks, namely the neurite bundle through which each cell enters the neuropil, that have allowed us and others to determine hemilineage identity. We also consulted closely with our colleagues working in the male VNC connectome (MANC), particularly Lisa Marin and Greg Jefferis, to ensure continuity of hemilineage identifications across FANC and MANC and to resolve any edge cases. Since the submission of our paper, the MANC group has released a preprint describing the identification of VNC hemilineages[88]. That effort included the deployment of a convolutional neural network (CNN) that predicts the neurotransmitter at a synapse from the EM images[133]. The CNN predicted that over 80% of neurons in each hemilineage express the same transmitter, and the same transmitter predicted from the split-Gal4 lines[88]. One exception, hemilineage 09B, was predicted to produce both cholinergic and glutamatergic neurons in nearly equal measure, but we identified no 09B neurons as preMNs.

Groups of VNC preMNs were first identified by the entry of their primary neurite into the neuropil. Primary neurite groups that bundled together were then identified as known hemilineages based on light microscopy images of sparse GAL4 lines, and cell body position along the dorsal-ventral axis[90,91,87,88,134]. Of the 2,115 local and intersegmental preMNs for each limb, 1,830 were matched to a hemilineage (**Extended Data Figure S3.7**), which

accounted for 89.9% of the VNC input to left front leg and left wing MNs.

See Supplemental Table 3 for links to view entire premotor populations of each hemilineage in Neuroglancer.

Software and data availability

Data presented in the paper was analyzed from the CAVE materialization version 840 (v840). Annotated connectivity matrices (**Figure S3.3**) are available as python Pandas data frames (https://pandas.pydata.org/) at the git-hub repository for this paper, `https://github.com/tuthill-lab/Lesser_Azevedo_2023`. Also available at the repository are scripts to recreate the analyses and figures in the paper, as well as scripts to recreate the connectivity matrices, for users authorized to interact with the CAVEclient. Links to public preMN and MN segmentations are available throughout the text, as well as in Supplemental Tables 1-3. All analysis was performed in Python 3.9 using custom code, making extensive use of CAVEclient (`https://github.com/seung-lab/CAVEclient`;[124] and CloudVolume to interact with data infrastructure, and libraries Matplotlib, Numpy, Pandas, Scikit-learn, Scipy, stats-models and VTK for general computation, machine learning and data visualization. Additional code is available at `https://github.com/htem/FANC_auto_recon`, providing additional tutorials, documentation for interacting with FANC, and instructions for joining the FANC community.

3.7 Supplementary materials

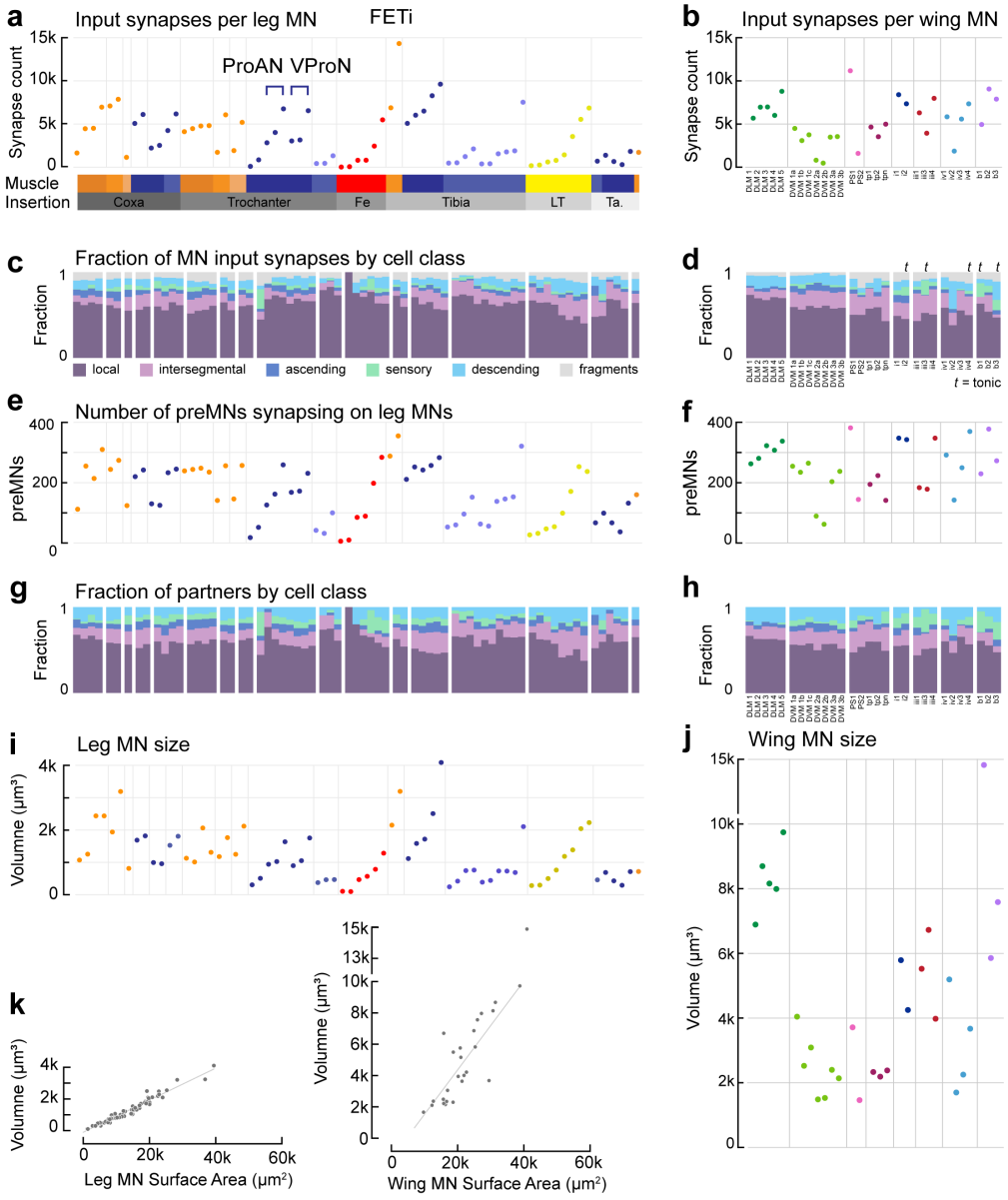

Figure S3.1: Detailed properties of individual leg and wing MNs. **a,** Number of input synapses on each leg MN. MNs are ordered by the muscle they innervate, from proximal coxa muscles in the thorax to distal tarsus muscles located in the tibia. **b,** Number of input synapses on each wing MN. Indirect MNs are shown first, direct MNs are ordered according to sclerite. **c,** Fraction of synapses on each leg MN broken down by cell class (see Methods). **d,** Fraction of synapses on each wing MN broken down by cell class. **e,** Number of preMNs presynaptic to each leg MN. **f,** Number of preMNs presynaptic to each wing MN. **g, h,** Fraction of presynaptic partners from each cell class. Presynaptic partners include proofread neurons only, so fragments are not included. **i, j,** MN volume. **k,** MN volume vs. surface area for leg MNs (left) and wing MNs (right). Wing MNs tend to have thicker neurites, explaining the steeper relationship. The thick b1 wing steering MN is the outlier.

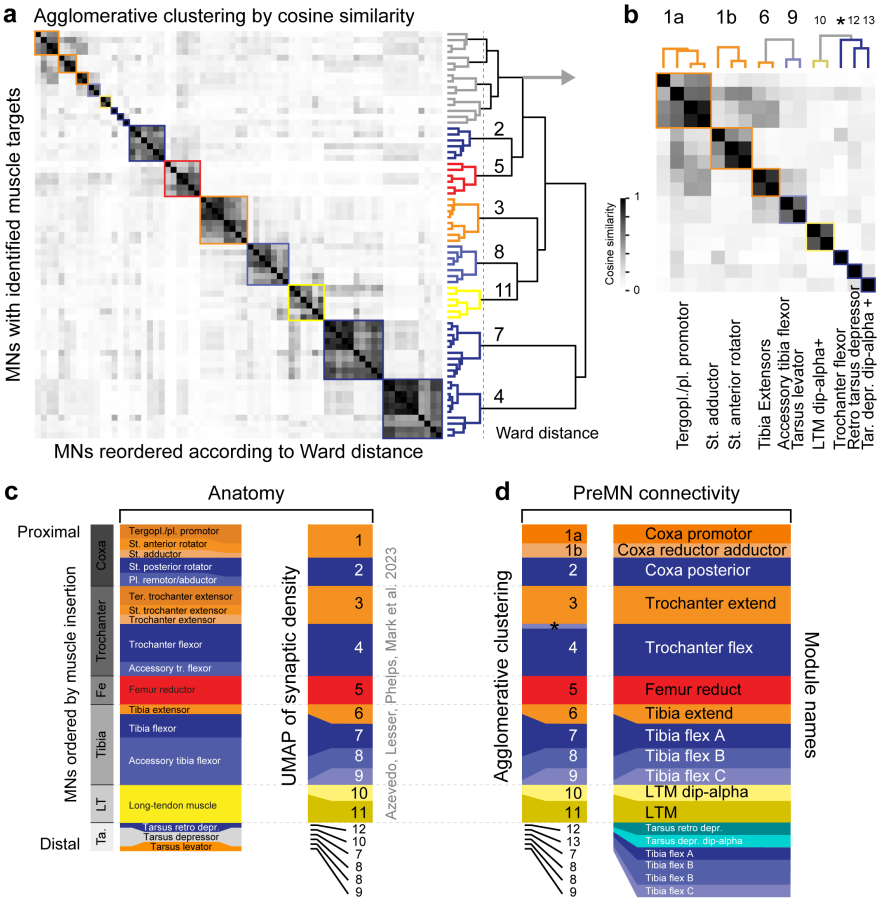

Figure S3.2: Agglomerative clustering of leg MNs according to premotor connectivity. **a,** Hierarchical clustering of MNs based on the cosine similarity of the columns of the premotor connectivity matrix (**Figure 3.3d**). The scipy.cluster AgglomerativeClustering algorithm minimizes the sum of squared distances in each cluster (Ward, scikit-learn). The algorithm identifies seven clear clusters numbered according to the proximal-to-distal origins and insertion points of the innervated muscles (right). **b,** Magnification of seven additional clusters at the top left of the similarity matrix. The muscle targets of MNs in each cluster are indicated below. We remain uncertain about which of four MNs innervate the tergopleural vs. the pleural promotor muscles that insert on the anterior aspect of the coxa (cluster 1a). **c,** In Azevedo et al. 2022, we identified the muscle targets of each MN by comparing anatomical criteria (left). We performed UMAP clustering of the density of input synapses in 3D onto each MN, as an independent, quantitative verification of our anatomical assignments (right). This analysis revealed surprising features that are corroborated by analyzing preMN connectivity here. Specifically, accessory tibia flexor MNs split into 3 distinct clusters, clusters 7, 8, and 9, where the four accessory tibia flexors in cluster 7 clustered with the five main tibia flexor MNs. Additionally, four of the six tarsus MNs clustered with the same groups, one in cluster 7, two in cluster 8, and 1 in cluster 9 (see numbers at bottom). A fifth tarsus MN, the retro depressor MN, clustered on its own (cluster 12). The final tarsus MN clustered with the small LTM MNs in cluster 10; all three are known to express dip-alpha[129]. **d,** Clusters based on premotor connectivity from **a** and **b**. The differences from the UMAP of synapse density include: promotor MNs of the coxa (cluster 1a) clustered separately from the adductor and rotator MNs (cluster 1b); the tarsus depressor MN (cluster 13) clustered separately from the two dip-alpha-positive LTM MNs (cluster 10); a small MN clustered in a separate cluster labeled with an asterisk (*), depicted in f. Names for each module are given on the right.

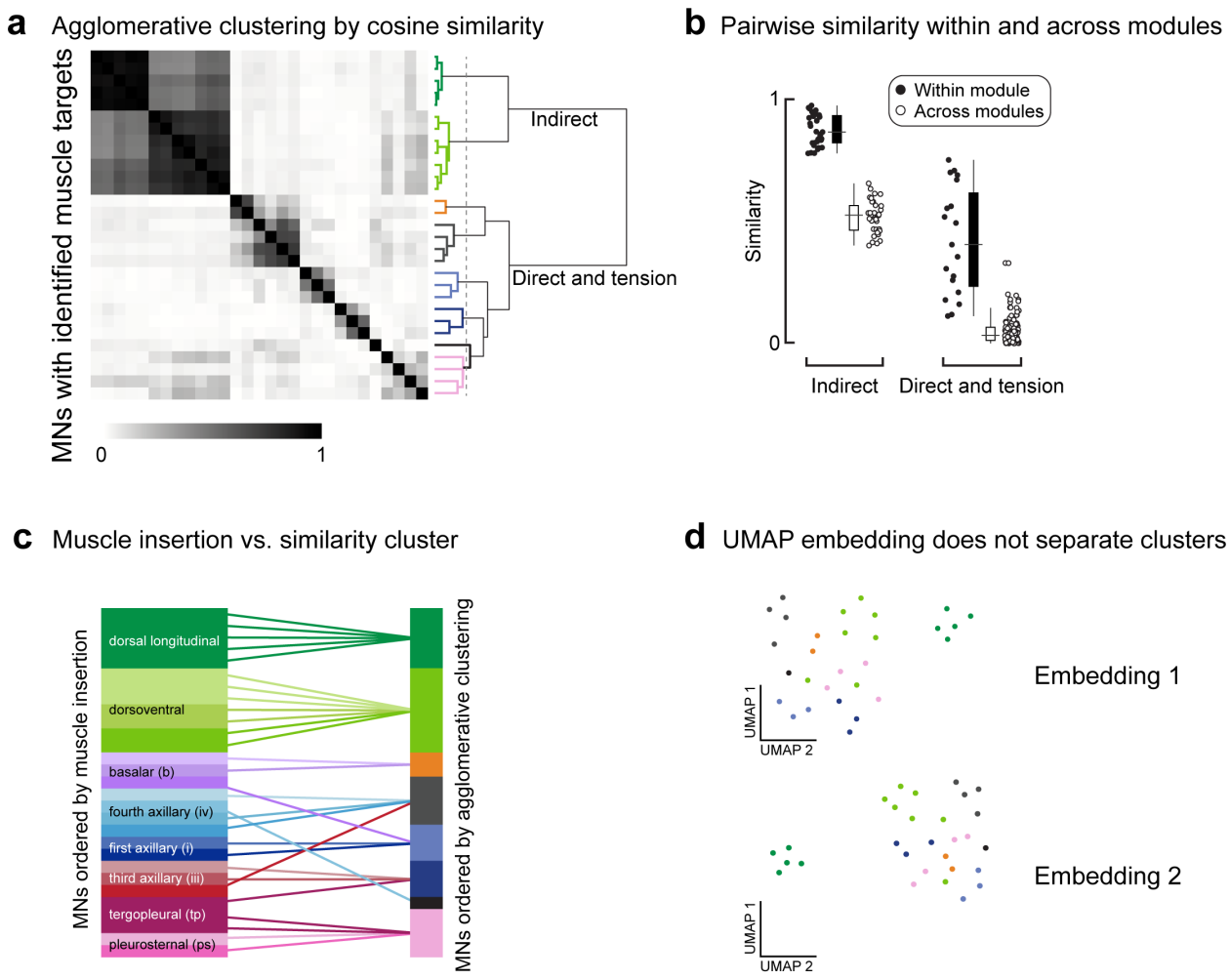

Figure S3.3: Similarity of wing MNs creates separable modules through agglomerative clustering. **a,** Cosine similarity matrix for all wing MNs. Axes are symmetric, each row/column is an MN. (Right) The agglomerative clustering dendrogram along with the threshold at which clusters are separable. Colored branches on the dendrogram depict different modules, not muscles. **b,** Similarity scores for each pair of wing MNs. Indirect MNs are separated from direct and tension MNs to better show the distribution of similarity scores of direct and tension MNs. **c,** Schematic showing how ordering by anatomy (left) relates to agglomerative clustering by cosine similarity (right). **d,** UMAP does not separate the wing MNs by connectivity, possibly because their synaptic input weights are not stereotyped (or proportional) from preMNs. Data points are colored post-hoc according to the agglomerative clustering results.

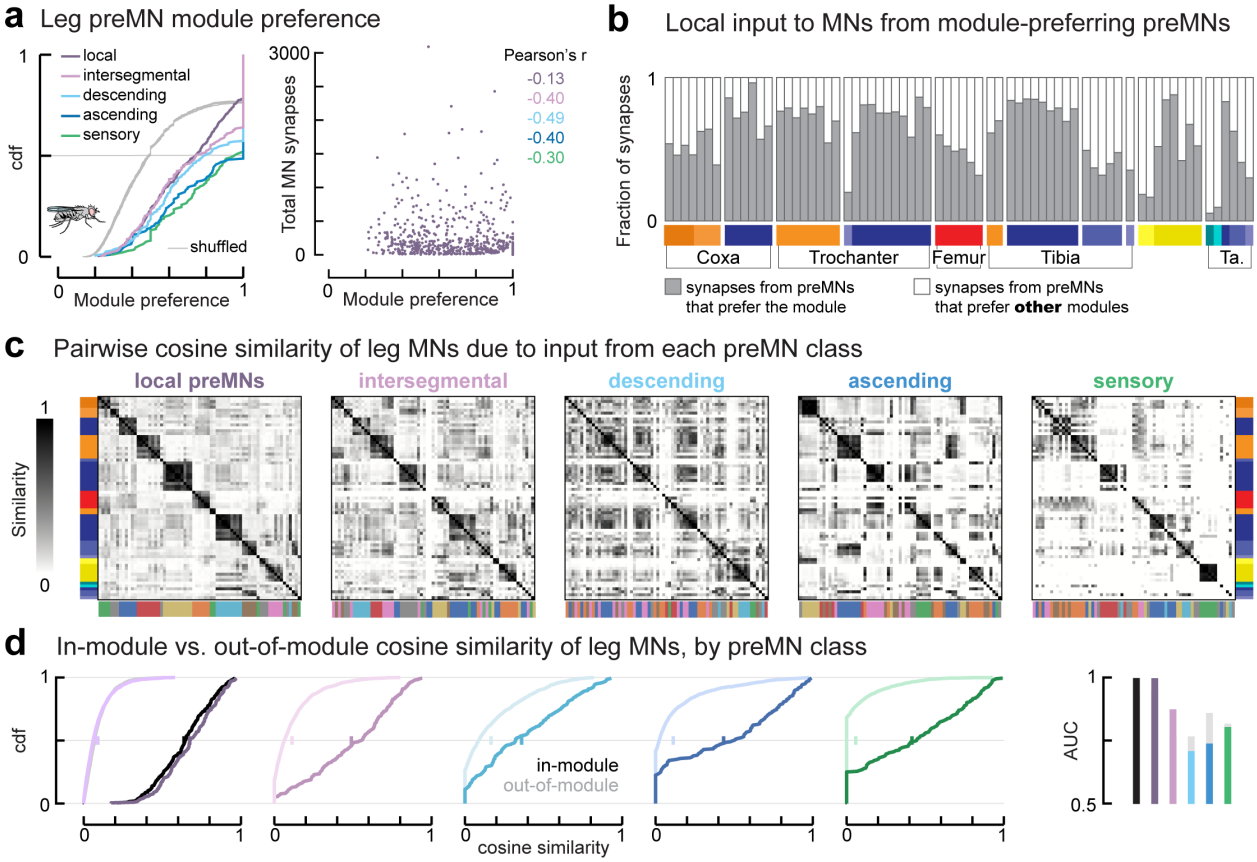

Figure S3.4: Local PreMNs drive MN cosine similarity and modularity, for wing and leg systems. **a,** Cumulative density functions (CDFs) of module preference for individual preMNs targeting leg MNs, separated by preMN cell class. Gray indicates ten overlaid example CDFs randomly selected from shuffling the columns of each row of the connectivity matrix. Right, Total MN synapses (y-axis) vs. module preference of local preMNs. Pearson's r for each cell class is shown, p¡10-13. PreMNs with fewer MN synapses have a slight tendency to contact a single module. **b,** Fraction of MN input synapses (each bar) from local preMNs that prefer that MN's module (gray) vs. prefer a different module (white). **c,** Cosine similarity matrices for leg MNs, calculated using synapses from preMNs of each cell class. Modules found in **Extended Data Figure S3.2** are shown at left and right. Below each matrix is a color bar indicating clusters found by performing the same agglomerative clustering algorithm on the matrix above. Only local preMN connectivity gives the same clusters as using all preMNs. **d,** CDFs of pairwise similarity of MNs within modules defined in **Extended Data Figure S3.2** (dark lines) vs. across modules (light colors). Right, the area under the curve (AUC) measures the overlap of the CDFs, with 0.5 indicating similar CDFs, and 1 indicating complete separation (see Methods). Gray bars show the improvement in the AUC if the clusters shown below the similarity matrices in **c** are used instead. Together, these analyses show that local neurons are responsible for the modularity of MNs. Other classes of preMNs tend to prefer a single module but can make select synapses across modules.
d, CDFs of pairwise similarity of MNs within modules defined in **Extended Data Figure S3.2** (dark lines) vs. across modules (light colors). Right, the area under the curve (AUC) measures the overlap of the CDFs, with 0.5 indicating similar CDFs, and 1 indicating complete separation (see Methods). Gray bars show the improvement in the AUC if the clusters shown below the similarity matrices in **c** are used instead. Together, these analyses show that local neurons are responsible for the modularity of MNs. Other classes of preMNs tend to prefer a single module but make select synapses across modules.

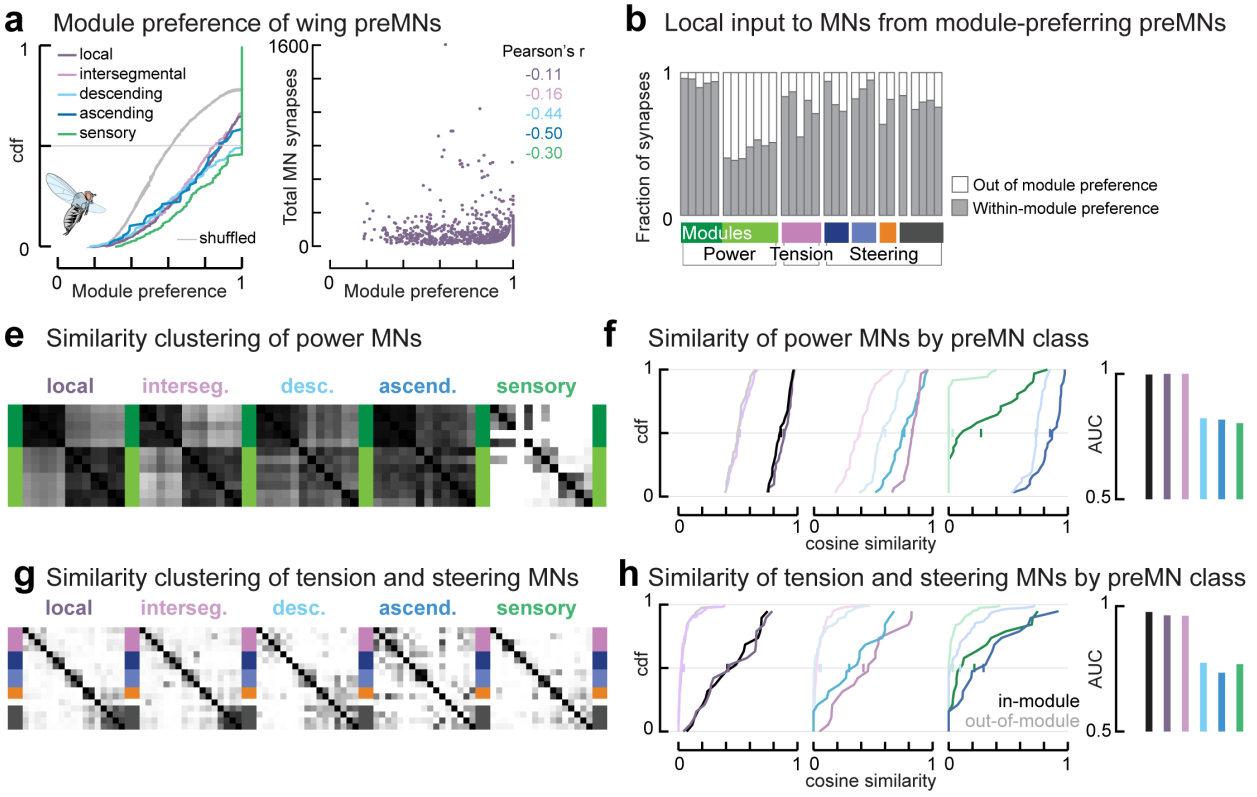

Figure S3.5: Local PreMNs drive MN cosine similarity and modularity, for wing and leg systems. a, Cumulative density functions (CDFs) of module preference for individual preMNs targeting wing MNs, separated by preMN cell class. Gray indicates ten overlaid example CDFs randomly selected from shuffling the columns of each row of the connectivity matrix. Right, Total MN synapses (y-axis) vs. module preference of local preMNs. Pearson's r for each cell class is shown, p¡10-13. PreMNs with fewer MN synapses have a slight tendency to contact a single module. **b,** Fraction of MN input synapses (each bar) from local preMNs that prefer that MN's module (gray) vs. prefer a different module (white). **c,** Cosine similarity matrices for indirect (power) MNs, calculated using synapses from preMNs of each cell class. Indirect muscles are divided into two modules: dorsal longitudinal muscles (DLMs, dark green) and dorso-ventral muscles (DVMs, light green). They share common input from all cell classes except sensory axons, from which they receive few synapses. **d,** Pairwise similarity of indirect MNs within modules, based on connectivity of each cell class. **e,** Similarity matrices for tension and direct (steering) MNs. **f,** Pairwise similarity of indirect MNs within (dark line) vs. across (light) modules, for each preMN cell class. Colors are indicated in a.

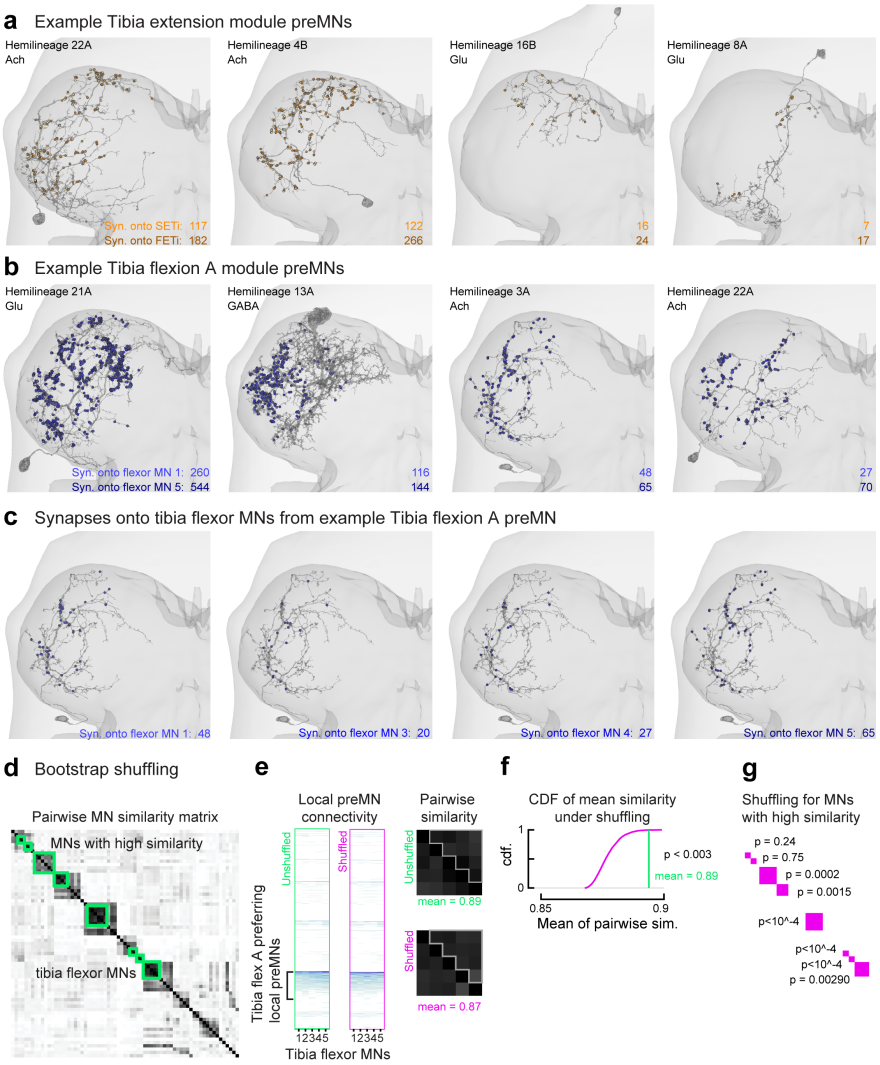

Figure S3.6: Example leg preMNs, their synapses onto motor modules, and impact of proportional connectivity on MN similarity. **a,** The location of synapses (spheres) from example preMNs that preferentially synapse onto the SETi (light orange) and FETi (dark orange) tibia extensor MNs. **b,** Example preMNs that preferentially synapse onto the five tibia flexor MNs in the Tibia flex A module (different shades of blue spheres). **c,** A single example preMN from **b**, showing the locations of synapses onto four of the five tibia flexor MNs in the module. The preMN makes more synapses onto the largest neuron, with extra synapses distributed throughout the processes. **d,** Bootstrap shuffling of module connectivity (see Methods for details). This analysis is similar to **Figure 3.5a**, but for only the largest neurons with the highest similarity (green squares), where high MN similarity reflects proportional preMN weights onto each MN in the module, as in **a-c**. **e,** Left, the unshuffled synapse counts from all local preMNs onto the Tibia Flex A MNs; middle, the same matrix with example shuffled synapse counts from the module-targeting preMNs; right, the resulting MN similarity matrices, highlighting the pairwise similarities in the upper triangle. **f,** The cumulative probability density function (cdf) of the mean pairwise MN similarity for N=10,000 shuffling repeats, compared to the actual mean. The actual mean is larger than 99.7% of the shuffled instances. **g,** The bootstrap p-value for the regions of high MN similarity. The high p-values indicate pairs of neurons with small differences in their total synaptic input, such that shuffling the proportional synapses does not disrupt a large difference like exists for the FETi and SETi in **a**

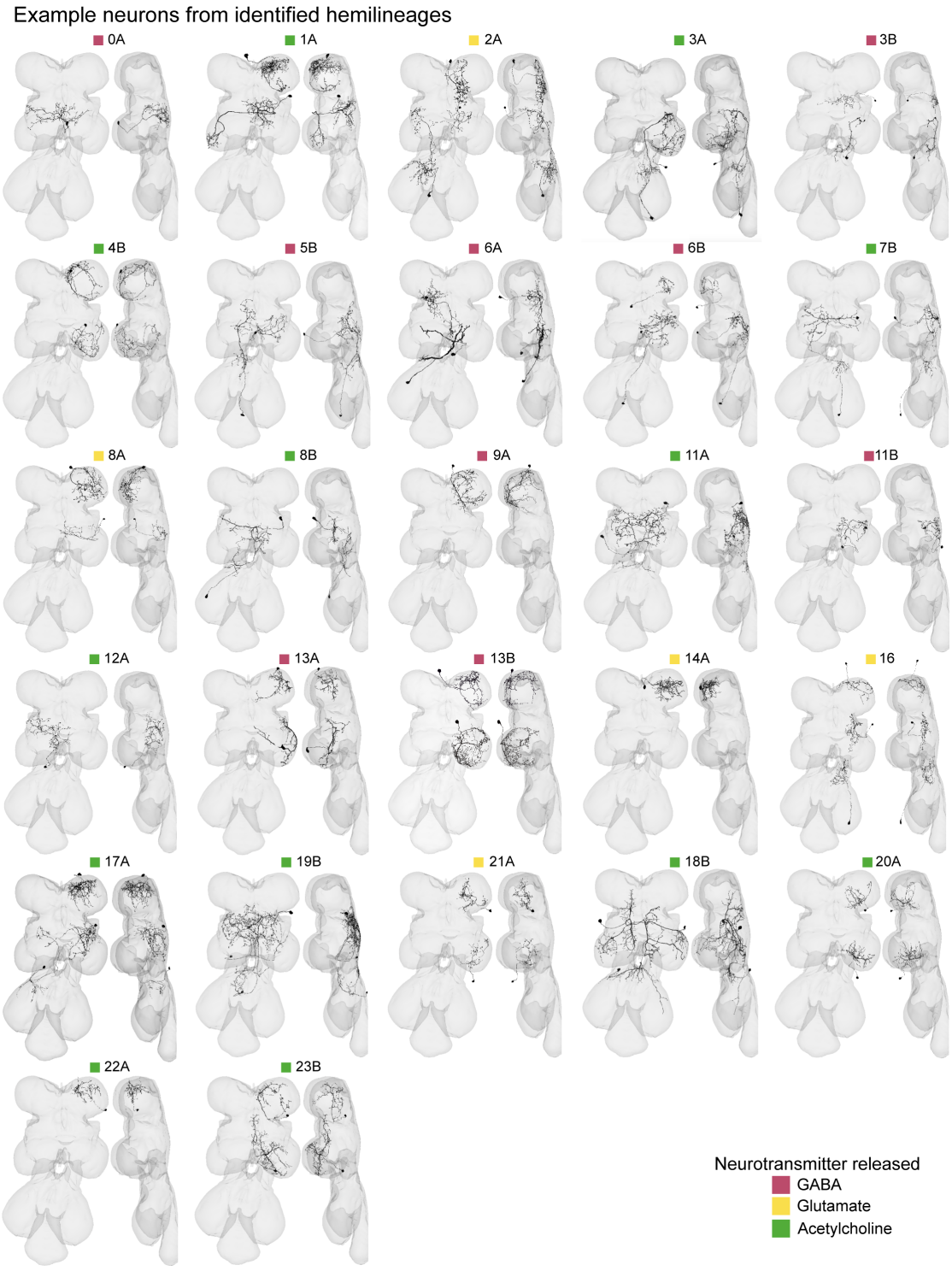

Figure S3.7: Example neurons from each premotor hemilineage. Example preMNs from each premotor hemilineage. See Supplemental Table 3 for links to view entire premotor populations of each hemilineage in Neuroglancer, an online tool for viewing connectomics datasets.

Leg	Coxa promotion
	Coxa reductor adductor
	Coxa posterior
	Trochanter extend
	Trochanter flex
	Femur reduct
	Tibia extend
	Tibia flex A Tibia flex B
	Tibia flex C
	LTM dip-alpha
	LTM
	Tarsus retro depressor
	Tarsus depressor dip-alpha
Wing	Dorsal longitudinal
	Dorsoventral
	Tension
	Steering A
	Steering B
	Steering C
	Steering D
	hg2

Table 3.1: Links to motor modules in Neuroglancer. The second column contains clickable links to view the motor neurons that make up each motor module.

Preferred Module (Leg)	**Desc.**	**Sensory**	**Asc.**	**Interseg.**	**Local**
Coxa promotion	link	link	link	link	link
Coxa reductor adductor	link	link	link	link	link
Coxa posterior	link	link	link	link	link
Trochanter extend	link	link	link	link	link
Trochanter flex	link	link	link	link	link
Femur reduct	link	link	link	link	link
Tibia extend	link	link	link	link	link
Tibia flex A	link	link	link	link	link
Tibia flex B	link	link	link	link	link
Tibia flex C	link	link	link	link	link
LTM dip-alpha	link	link	link	link	link
LTM	link	link	link	link	link
Tarsus depressor retro depressor	link	link	link	link	link
Tarsus depressor dip-alpha	link	link	link	link	link
Preferred Module (Wing)					
DLM	link	link	link	link	link
DVM	link	link	link	link	link
Tension	link	link	link	link	link
Steering A	link	link	link	link	link
Steering B	link	link	link	link	link
Steering C	link	link	link	link	link
Steering D	link	link	link	link	link
iv2	link	link	link	link	link

Table 3.2: Links to premotor modules in Neuroglancer. The "link" text contains clickable links to view all premotor neurons in this chapter, organized by the motor module that they devote the most synapses to and their cell class.

GABA	13A 9A 19A 12B 13B 1B 6B 6A 3B 11B 5B 0A
Glu	21A 14A 24B 8A 16 2A
ACh	20 22A 4B 3A 1A 23B 18B 7B 17A 11A 19B 8B 12A 10B

Table 3.3: Links to hemilineages in Neuroglancer. The second columns contains clickable links to the local and intersegmental premotor neurons whose hemilineage could be identified.

References

[1] Charles Scott Sherrington. *The integrative action of the nervous system*. Yale paperbound ; Y-35. New Haven: Yale University Press, 1906.

[2] Victor Lobato-Rios et al. "NeuroMechFly, a neuromechanical model of adult Drosophila melanogaster". In: *Nature Methods* 19.5 (May 2022). Number: 5 Publisher: Nature Publishing Group, pp. 620–627. ISSN: 1548-7105. DOI: 10.1038/s41592-022-01466-7. URL: https://www.nature.com/articles/s41592-022-01466-7 (visited on 10/21/2022).

[3] Najja J. Marshall et al. "Flexible neural control of motor units". In: *Nature Neuroscience* 25.11 (Nov. 2022). Number: 11 Publisher: Nature Publishing Group, pp. 1492–1504. ISSN: 1546-1726. DOI: 10.1038/s41593-022-01165-8. URL: https://www.nature.com/articles/s41593-022-01165-8 (visited on 11/14/2022).

[4] Lena H. Ting and Jane M. Macpherson. "A Limited Set of Muscle Synergies for Force Control During a Postural Task". In: *Journal of Neurophysiology* 93.1 (Jan. 2005). Publisher: American Physiological Society, pp. 609–613. ISSN: 0022-3077. DOI: 10.1152/jn.00681.2004. URL: https://journals.physiology.org/doi/full/10.1152/jn.00681.2004 (visited on 04/10/2023).

[5] Matthew C Tresch et al. "Coordination and localization in spinal motor systems". In: *Brain Research Reviews*. The Segerfalk symposium on Principles of Spinal Cord Function, Plasticity and Repair 40.1 (Oct. 1, 2002), pp. 66–79. ISSN: 0165-0173. DOI: 10.1016/S0165-0173(02)00189-3. URL: https://www.sciencedirect.com/science/article/pii/S0165017302001893 (visited on 01/13/2023).

[6] Emma F. Hodson-Tole and James M. Wakeling. "Motor unit recruitment for dynamic tasks: current understanding and future directions". In: *Journal of Comparative Physiology B* 179.1 (Jan. 1, 2009), pp. 57–66. ISSN: 1432-136X. DOI: 10.1007/s00360-

008-0289-1. URL: https://doi.org/10.1007/s00360-008-0289-1 (visited on 04/10/2023).

[7] Steven J. Cook et al. "Whole-animal connectomes of both Caenorhabditis elegans sexes". In: *Nature* 571.7763 (July 2019). Number: 7763 Publisher: Nature Publishing Group, pp. 63–71. ISSN: 1476-4687. DOI: 10.1038/s41586-019-1352-7. URL: https://www.nature.com/articles/s41586-019-1352-7 (visited on 12/04/2022).

[8] Daniel Witvliet et al. "Connectomes across development reveal principles of brain maturation". In: *Nature* 596.7871 (Aug. 2021). Number: 7871 Publisher: Nature Publishing Group, pp. 257–261. ISSN: 1476-4687. DOI: 10.1038/s41586-021-03778-8. URL: https://www.nature.com/articles/s41586-021-03778-8 (visited on 12/14/2023).

[9] Tomoko Ohyama et al. "A multilevel multimodal circuit enhances action selection in Drosophila". In: *Nature* 520.7549 (Apr. 2015). Number: 7549 Publisher: Nature Publishing Group, pp. 633–639. ISSN: 1476-4687. DOI: 10.1038/nature14297. URL: https://www.nature.com/articles/nature14297 (visited on 11/18/2022).

[10] Michael Winding et al. "The connectome of an insect brain". In: *Science* 379.6636 (Mar. 10, 2023). Publisher: American Association for the Advancement of Science, eadd9330. DOI: 10.1126/science.add9330. URL: https://www.science.org/doi/10.1126/science.add9330 (visited on 05/17/2023).

[11] Quan Wen et al. "Proprioceptive Coupling within Motor Neurons Drives C. elegans Forward Locomotion". In: *Neuron* 76.4 (Nov. 21, 2012), pp. 750–761. ISSN: 0896-6273. DOI: 10.1016/j.neuron.2012.08.039. URL: https://www.sciencedirect.com/science/article/pii/S0896627312008057 (visited on 05/17/2023).

[12] Aref Arzan Zarin et al. "A multilayer circuit architecture for the generation of distinct locomotor behaviors in Drosophila". In: *eLife* 8 (Dec. 23, 2019). Ed. by Kristin Scott and Ronald L Calabrese. Publisher: eLife Sciences Publications, Ltd, e51781. ISSN:

2050-084X. DOI: 10.7554/eLife.51781. URL: https://doi.org/10.7554/eLife.51781 (visited on 04/22/2020).

[13] Louis K Scheffer et al. "A connectome and analysis of the adult Drosophila central brain". In: *eLife* 9 (Sept. 3, 2020). Ed. by Eve Marder et al. Publisher: eLife Sciences Publications, Ltd, e57443. ISSN: 2050-084X. DOI: 10.7554/eLife.57443. URL: https://doi.org/10.7554/eLife.57443 (visited on 10/15/2023).

[14] Zhihao Zheng et al. "A Complete Electron Microscopy Volume of the Brain of Adult Drosophila melanogaster". In: *Cell* 174.3 (July 26, 2018), 730–743.e22. ISSN: 0092-8674. DOI: 10.1016/j.cell.2018.06.019. URL: http://www.sciencedirect.com/science/article/pii/S0092867418307876 (visited on 07/09/2019).

[15] Jasper S. Phelps et al. "Reconstruction of motor control circuits in adult Drosophila using automated transmission electron microscopy". In: *Cell* 184.3 (Feb. 2021), 759–774.e18. ISSN: 00928674. DOI: 10.1016/j.cell.2020.12.013. URL: https://linkinghub.elsevier.com/retrieve/pii/S0092867420316834 (visited on 12/22/2023).

[16] Shin-ya Takemura et al. *A Connectome of the Male Drosophila Ventral Nerve Cord*. Pages: 2023.06.05.543757 Section: New Results. June 6, 2023. DOI: 10.1101/2023.06.05.543757. URL: https://www.biorxiv.org/content/10.1101/2023.06.05.543757v1 (visited on 02/14/2024).

[17] Robert Court et al. "A Systematic Nomenclature for the Drosophila Ventral Nerve Cord". In: *Neuron* 107.6 (Sept. 23, 2020), 1071–1079.e2. ISSN: 1097-4199. DOI: 10.1016/j.neuron.2020.08.005.

[18] Anthony Azevedo et al. *Tools for comprehensive reconstruction and analysis of Drosophila motor circuits*. Pages: 2022.12.15.520299 Section: New Results. Dec. 15, 2022. DOI: 10.1101/2022.12.15.520299. URL: https://www.biorxiv.org/content/10.1101/2022.12.15.520299v1 (visited on 12/12/2023).

[19] John C. Tuthill and Rachel I. Wilson. "Mechanosensation and Adaptive Motor Control in Insects". In: *Current biology: CB* 26.20 (Oct. 24, 2016), R1022–R1038. ISSN: 1879-0445. DOI: 10.1016/j.cub.2016.06.070.

[20] A. Miller. "The internal anatomy and histology of the imago of Drosophila melanogaster." In: *Biology of Drosophila.* (1950), pp. 420–534.

[21] A. Schmid, A. Chiba, and C. Q. Doe. "Clonal analysis of Drosophila embryonic neuroblasts: neural cell types, axon projections and muscle targets". In: *Development (Cambridge, England)* 126.21 (Nov. 1999), pp. 4653–4689. ISSN: 0950-1991.

[22] J. L. Witten and J. W. Truman. "Distribution of GABA-like immunoreactive neurons in insects suggests lineage homology". In: *Journal of Comparative Neurology* 398.4 (1998), pp. 515–528. ISSN: 1096-9861. DOI: 10.1002/(SICI)1096-9861(19980907)398:4<515::AID-CNE4>3.0.CO;2-5. URL: https://onlinelibrary.wiley.com/doi/abs/10.1002/%28SICI%291096-9861%2819980907%29398%3A4%3C515%3A%3AAID-CNE4%3E3.0.CO%3B2-5 (visited on 07/26/2019).

[23] Jens Peter Gabriel et al. "Control of flexor motoneuron activity during single leg walking of the stick insect on an electronically controlled treadwheel". In: *Journal of Neurobiology* 56.3 (2003), pp. 237–251. ISSN: 1097-4695. DOI: 10.1002/neu.10237. URL: https://onlinelibrary.wiley.com/doi/abs/10.1002/neu.10237 (visited on 05/22/2019).

[24] Elwood Henneman, George Somjen, and David O. Carpenter. "Functional significance of cell size in spinal motoneurons". In: *Journal of Neurophysiology* 28.3 (May 1, 1965), pp. 560–580. ISSN: 0022-3077. DOI: 10.1152/jn.1965.28.3.560. URL: https://www.physiology.org/doi/abs/10.1152/jn.1965.28.3.560 (visited on 06/17/2019).

[25] A. A. V. Hill and D. Cattaert. "Recruitment in a heterogeneous population of motor neurons that innervates the depressor muscle of the crayfish walking leg muscle". In: *Journal of Experimental Biology* 211.4 (Feb. 15, 2008), pp. 613–629. ISSN: 0022-0949,

1477-9145. DOI: 10.1242/jeb.006270. URL: http://jeb.biologists.org/cgi/doi/10.1242/jeb.006270 (visited on 03/12/2019).

[26] David L. McLean and Kimberly J. Dougherty. "Peeling back the layers of locomotor control in the spinal cord". In: *Current Opinion in Neurobiology* 33 (Aug. 2015), pp. 63–70. ISSN: 1873-6882. DOI: 10.1016/j.conb.2015.03.001.

[27] H. S. Milner-Brown, R. B. Stein, and R. Yemm. "The orderly recruitment of human motor units during voluntary isometric contractions". In: *The Journal of Physiology* 230.2 (Apr. 1973), pp. 359–370. ISSN: 0022-3751. DOI: 10.1113/jphysiol.1973.sp010192.

[28] K. Sasaki and M. Burrows. "Innervation pattern of a pool of nine excitatory motor neurons in the flexor tibiae muscle of a locust hind leg". In: *Journal of experimental biology* 201.12 (1998), pp. 1885–1893. URL: http://jeb.biologists.org/content/201/12/1885.short (visited on 03/28/2017).

[29] Elwood Henneman. "Relation between Size of Neurons and Their Susceptibility to Discharge". In: *Science* 126.3287 (Dec. 27, 1957), pp. 1345–1347. ISSN: 0036-8075, 1095-9203. DOI: 10.1126/science.126.3287.1345. URL: https://science.sciencemag.org/content/126/3287/1345 (visited on 05/22/2019).

[30] E Henneman et al. "Rank order of motoneurons within a pool: law of combination." In: *Journal of Neurophysiology* 37.6 (Nov. 1974), pp. 1338–1349. ISSN: 0022-3077, 1522-1598. DOI: 10.1152/jn.1974.37.6.1338. URL: https://www.physiology.org/doi/10.1152/jn.1974.37.6.1338 (visited on 02/04/2024).

[31] Irene Pallucchi et al. "Molecular blueprints for spinal circuit modules controlling locomotor speed in zebrafish". In: *Nature Neuroscience* 27.1 (Jan. 2024). Number: 1 Publisher: Nature Publishing Group, pp. 78–89. ISSN: 1546-1726. DOI: 10.1038/s41593-023-01479-1. URL: https://www.nature.com/articles/s41593-023-01479-1 (visited on 02/17/2024).

[32] Jianren Song et al. "Multiple Rhythm-Generating Circuits Act in Tandem with Pacemaker Properties to Control the Start and Speed of Locomotion". In: *Neuron* 0.0 (Jan. 22, 2020). ISSN: 0896-6273. DOI: 10.1016/j.neuron.2019.12.030. URL: http://www.cell.com/neuron/abstract/S0896-6273(19)31096-7 (visited on 01/28/2020).

[33] David Grimaldi and Michael S. Engel. *Evolution of the Insects*. Google-Books-ID: Ql6Jl6wKb88C. Cambridge University Press, May 16, 2005. 790 pp. ISBN: 978-0-521-82149-0.

[34] Thomas Hörnschemeyer. "Phylogenetic significance of the wing-base of the Holometabola (Insecta)". In: *Zoologica Scripta* 31.1 (2002). _eprint: https://onlinelibrary.wiley.com/doi/pdf/10.1046/j.0300-3256.2001.00086.x, pp. 17–29. ISSN: 1463-6409. DOI: 10.1046/j.0300-3256.2001.00086.x. URL: https://onlinelibrary.wiley.com/doi/abs/10.1046/j.0300-3256.2001.00086.x (visited on 05/16/2023).

[35] Johan M. Melis, Igor Siwanowicz, and Michael H. Dickinson. *Machine learning reveals the control mechanics of an insect wing hinge*. Pages: 2023.06.29.547116 Section: New Results. Feb. 2, 2024. DOI: 10.1101/2023.06.29.547116. URL: https://www.biorxiv.org/content/10.1101/2023.06.29.547116v3 (visited on 02/14/2024).

[36] J. A. Miyan and A. W. Ewing. "How Diptera move their wings: a re-examination of the wing base articulation and muscle systems concerned with flight". In: *Philosophical Transactions of the Royal Society of London. B, Biological Sciences* 311.1150 (Nov. 19, 1985). Publisher: Royal Society, pp. 271–302. DOI: 10.1098/rstb.1985.0154. URL: https://royalsocietypublishing.org/doi/10.1098/rstb.1985.0154 (visited on 10/19/2022).

[37] J. C. Coggshall. "Neurons associated with the dorsal longtitudinal flight muscles of Drosophilla melanogaster". In: *The Journal of Comparative Neurology* 177.4 (Feb. 15, 1978), pp. 707–720. ISSN: 0021-9967. DOI: 10.1002/cne.901770410.

[38] J. W. S. Pringle. "The excitation and contraction of the flight muscles of insects". In: *The Journal of Physiology* 108.2 (1949). _eprint: https://onlinelibrary.wiley.com/doi/pdf/10.1113/jp pp. 226–232. ISSN: 1469-7793. DOI: 10.1113/jphysiol.1949.sp004326. URL: https://onlinelibrary.wiley.com/doi/abs/10.1113/jphysiol.1949.sp004326 (visited on 04/10/2023).

[39] Werner Nachtigall and Donald M. Wilson. "Neuro-Muscular Control of Dipteran Flight". In: *Journal of Experimental Biology* 47.1 (Aug. 1, 1967), pp. 77–97. ISSN: 0022-0949. DOI: 10.1242/jeb.47.1.77. URL: https://doi.org/10.1242/jeb.47.1.77 (visited on 10/21/2022).

[40] J. W. S. Pringle. *Insect Flight*. Google-Books-ID: hPOsN4QExQMC. Cambridge University Press, Dec. 1957. 146 pp. ISBN: 978-0-521-05995-4.

[41] F. O. Lehmann and M. H. Dickinson. "The production of elevated flight force compromises manoeuvrability in the fruit fly Drosophila melanogaster". In: *The Journal of Experimental Biology* 204 (Pt 4 Feb. 2001), pp. 627–635. ISSN: 0022-0949. DOI: 10.1242/jeb.204.4.627.

[42] F. O. Lehmann and M. H. Dickinson. "The changes in power requirements and muscle efficiency during elevated force production in the fruit fly Drosophila melanogaster". In: *The Journal of Experimental Biology* 200 (Pt 7 Apr. 1997), pp. 1133–1143. ISSN: 0022-0949. DOI: 10.1242/jeb.200.7.1133.

[43] Edward G. Boettiger and Edwin Furshpan. "The mechanics of flight movements in diptera". In: *The Biological Bulletin* 102.3 (June 1952). Publisher: The University of Chicago Press, pp. 200–211. ISSN: 0006-3185. DOI: 10.2307/1538368. URL: https://www.journals.uchicago.edu/doi/abs/10.2307/1538368 (visited on 05/16/2023).

[44] J. R. Trimarchi and A. M. Schneiderman. "The motor neurons innervating the direct flight muscles of Drosophila melanogaster are morphologically specialized". In: *The Journal of Comparative Neurology* 340.3 (Feb. 15, 1994), pp. 427–443. ISSN: 0021-9967. DOI: 10.1002/cne.903400311.

[45] Carroll M. Williams and Muriel Voter Williams. "The flight muscles of Drosophila repleta". In: *Journal of Morphology* 72.3 (1943). _eprint: https://onlinelibrary.wiley.com/doi/pdf/10.10 pp. 589–599. ISSN: 1097-4687. DOI: 10.1002/jmor.1050720308. URL: https://onlinelibrary.wiley.com/doi/abs/10.1002/jmor.1050720308 (visited on 05/16/2023).

[46] Michael H Dickinson and Michael S Tu. "The Function of Dipteran Flight Muscle". In: *Comparative Biochemistry and Physiology Part A: Physiology* 116.3 (Mar. 1, 1997), pp. 223–238. ISSN: 0300-9629. DOI: 10.1016/S0300-9629(96)00162-4. URL: https://www.sciencedirect.com/science/article/pii/S0300962996001624 (visited on 02/14/2024).

[47] C. N. Balint and M. H. Dickinson. "The correlation between wing kinematics and steering muscle activity in the blowfly Calliphora vicina". In: *The Journal of Experimental Biology* 204 (Pt 24 Dec. 2001), pp. 4213–4226. ISSN: 0022-0949. DOI: 10.1242/jeb.204.24.4213.

[48] M. H. Dickinson, F. O. Lehmann, and K. G. Götz. "The active control of wing rotation by Drosophila". In: *The Journal of Experimental Biology* 182 (Sept. 1993), pp. 173–189. ISSN: 0022-0949. DOI: 10.1242/jeb.182.1.173.

[49] Gerhard Heide. "Neural mechanisms of flight control in Diptera". In: *BIONA-report* 2 (1983), pp. 35–52.

[50] Gerhard Heide. "Properties of a motor output system involved in the optomotor response in flies". In: *Biological Cybernetics* 20.2 (Oct. 1, 1975), pp. 99–112. ISSN: 1432-0770. DOI: 10.1007/BF00327047. URL: https://doi.org/10.1007/BF00327047 (visited on 01/13/2023).

[51] Fritz-Olaf Lehmann and Jan Bartussek. "Neural control and precision of flight muscle activation in Drosophila". In: *Journal of Comparative Physiology. A, Neuroethology, Sensory, Neural, and Behavioral Physiology* 203.1 (2017). Publisher: Springer, p. 1.

DOI: 10.1007/s00359-016-1133-9. URL: https://www.ncbi.nlm.nih.gov/pmc/articles/PMC5263198/ (visited on 10/21/2022).

[52] Theodore Lindsay, Anne Sustar, and Michael Dickinson. "The Function and Organization of the Motor System Controlling Flight Maneuvers in Flies". In: *Current biology: CB* 27.3 (Feb. 6, 2017), pp. 345–358. ISSN: 1879-0445. DOI: 10.1016/j.cub.2016.12.018.

[53] Angela O'Sullivan et al. "Multifunctional Wing Motor Control of Song and Flight". In: *Current biology: CB* 28.17 (Sept. 10, 2018), 2705–2717.e4. ISSN: 1879-0445. DOI: 10.1016/j.cub.2018.06.038.

[54] Samuel C. Whitehead et al. "Neuromuscular embodiment of feedback control elements in Drosophila flight". In: *Science Advances* 8.50 (Dec. 14, 2022). Publisher: American Association for the Advancement of Science, eabo7461. DOI: 10.1126/sciadv.abo7461. URL: https://www.science.org/doi/10.1126/sciadv.abo7461 (visited on 01/13/2023).

[55] Geoffrey W Meissner et al. "A searchable image resource of Drosophila GAL4 driver expression patterns with single neuron resolution". In: *eLife* 12 (Feb. 23, 2023). Ed. by Ilona C Grunwald Kadow and Claude Desplan. Publisher: eLife Sciences Publications, Ltd, e80660. ISSN: 2050-084X. DOI: 10.7554/eLife.80660. URL: https://doi.org/10.7554/eLife.80660 (visited on 02/19/2024).

[56] Martyna Grabowska et al. "Quadrupedal gaits in hexapod animals – inter-leg coordination in free-walking adult stick insects". In: *Journal of Experimental Biology* 215.24 (Dec. 15, 2012), pp. 4255–4266. ISSN: 0022-0949. DOI: 10.1242/jeb.073643. URL: https://doi.org/10.1242/jeb.073643 (visited on 11/16/2023).

[57] Malcolm Burrows. *The Neurobiology of an Insect Brain*. Oxford, New York: Oxford University Press, Sept. 26, 1996. 698 pp. ISBN: 978-0-19-852344-4.

[58] Staffan Cullheim. "Relations between cell body size, axon diameter and axon conduction velocity of cat sciatic α-motoneurons stained with horseradish peroxidase". In: *Neuroscience Letters* 8.1 (Apr. 1, 1978), pp. 17–20. ISSN: 0304-3940. DOI: 10.1016/0304-3940(78)90090-3. URL: https://www.sciencedirect.com/science/article/pii/0304394078900903 (visited on 05/10/2023).

[59] Graham Hoyle. *Muscles and Their Neural Control*. Google-Books-ID: cJbwAAAAMAAJ. Wiley, 1983. 712 pp. ISBN: 978-0-471-87709-7.

[60] Daniel Kernell. *The Motoneurone and its Muscle Fibres*. Oxford University Press, Aug. 17, 2006. ISBN: 978-0-19-172389-6. URL: http://www.oxfordscholarship.com.offcampus.lib.washington.edu/view/10.1093/acprof:oso/9780198526551.001.0001/acprof-9780198526551 (visited on 01/16/2019).

[61] A. M. Mcphedran, R. B. Wuerker, and E. Henneman. "Properties of motor units in a homogeneous red muscle (soleus) of the cat". In: *Journal of Neurophysiology* 28 (Jan. 1965), pp. 71–84. ISSN: 0022-3077. DOI: 10.1152/jn.1965.28.1.71.

[62] A. W. Monster and H. Chan. "Isometric force production by motor units of extensor digitorum communis muscle in man". In: *Journal of Neurophysiology* 40.6 (Nov. 1, 1977), pp. 1432–1443. ISSN: 0022-3077. DOI: 10.1152/jn.1977.40.6.1432. URL: https://www.physiology.org/doi/abs/10.1152/jn.1977.40.6.1432 (visited on 10/17/2019).

[63] Raymond B. Wuerker, Alexander M. McPhedran, and Elwood Henneman. "Properties of motor units in a heterogeneous pale muscle (m. gastrocnemius) of the cat". In: *Journal of Neurophysiology* 28.1 (Jan. 1, 1965), pp. 85–99. ISSN: 0022-3077. DOI: 10.1152/jn.1965.28.1.85. URL: https://www.physiology.org/doi/abs/10.1152/jn.1965.28.1.85 (visited on 06/17/2019).

[64] S. Cullheim et al. "Membrane area and dendritic structure in type-identified triceps surae alpha motoneurons". In: *Journal of Comparative Neurology* 255.1 (1987). _eprint: https://onlinelibrary.wiley.com/doi/pdf/10.1002/cne.902550106, pp. 68–81.

ISSN: 1096-9861. DOI: 10.1002/cne.902550106. URL: https://onlinelibrary.wiley.com/doi/abs/10.1002/cne.902550106 (visited on 05/10/2023).

[65] D Kernell and B Zwaagstra. "Size and remoteness: two relatively independent parameters of dendrites, as studied for spinal motoneurones of the cat." In: *The Journal of Physiology* 413.1 (1989). _eprint: https://onlinelibrary.wiley.com/doi/pdf/10.1113/jphysiol.1989.sp0 pp. 233–254. ISSN: 1469-7793. DOI: 10.1113/jphysiol.1989.sp017651. URL: https://onlinelibrary.wiley.com/doi/abs/10.1113/jphysiol.1989.sp017651 (visited on 05/10/2023).

[66] G. Örnung et al. "Distribution of glutamate-, glycine- and GABA-immunoreactive nerve terminals on dendrites in the cat spinal motor nucleus". In: *Experimental Brain Research* 118.4 (Feb. 1, 1998), pp. 517–532. ISSN: 1432-1106. DOI: 10.1007/s002210050308. URL: https://doi.org/10.1007/s002210050308 (visited on 05/10/2023).

[67] Anthony W Azevedo et al. "A size principle for recruitment of Drosophila leg motor neurons". In: *eLife* 9 (June 3, 2020). Ed. by Ronald L Calabrese and Chris Q Doe. Publisher: eLife Sciences Publications, Ltd, e56754. ISSN: 2050-084X. DOI: 10.7554/eLife.56754. URL: https://doi.org/10.7554/eLife.56754 (visited on 11/09/2022).

[68] Salil S. Bidaye et al. "Neuronal Control of Drosophila Walking Direction". In: *Science* 344.6179 (Apr. 4, 2014). Publisher: American Association for the Advancement of Science, pp. 97–101. DOI: 10.1126/science.1249964. URL: https://www.science.org/doi/full/10.1126/science.1249964 (visited on 05/16/2023).

[69] H. S. J. Cheong et al. *Transforming descending input into behavior: The organization of premotor circuits in the Drosophila Male Adult Nerve Cord connectome*. Pages: 2023.06.07.543976 Section: New Results. Jan. 26, 2024. DOI: 10.1101/2023.06.07.543976. URL: https://www.biorxiv.org/content/10.1101/2023.06.07.543976v2 (visited on 02/15/2024).

[70] Kai Feng et al. “Distributed control of motor circuits for backward walking in Drosophila”. In: *Nature Communications* 11.1 (Dec. 2, 2020), p. 6166. ISSN: 2041-1723. DOI: 10.1038/s41467-020-19936-x.

[71] Shigehiro Namiki et al. “The functional organization of descending sensory-motor pathways in Drosophila”. In: *eLife* 7 (June 26, 2018). Ed. by Kristin Scott, e34272. ISSN: 2050-084X. DOI: 10.7554/eLife.34272. URL: https://doi.org/10.7554/eLife.34272 (visited on 10/20/2019).

[72] Bettina Schnell, Ivo Ros, and Michael H. Dickinson. “A descending neuron correlated with the rapid steering maneuvers of flying Drosophila”. In: *Current biology : CB* 27.8 (Apr. 24, 2017), pp. 1200–1205. ISSN: 0960-9822. DOI: 10.1016/j.cub.2017.03.004. URL: https://www.ncbi.nlm.nih.gov/pmc/articles/PMC6309624/ (visited on 01/13/2023).

[73] G. Heide and K. G. Götz. “Optomotor control of course and altitude in Drosophila melanogaster is correlated with distinct activities of at least three pairs of flight steering muscles”. In: *The Journal of Experimental Biology* 199 (Pt 8 Aug. 1996), pp. 1711–1726. ISSN: 0022-0949. DOI: 10.1242/jeb.199.8.1711.

[74] A. Fayyazuddin and M. H. Dickinson. “Convergent mechanosensory input structures the firing phase of a steering motor neuron in the blowfly, Calliphora”. In: *Journal of Neurophysiology* 82.4 (Oct. 1999), pp. 1916–1926. ISSN: 0022-3077. DOI: 10.1152/jn.1999.82.4.1916.

[75] Michael S. Tu and Michael H. Dickinson. “Modulation of Negative Work Output from a Steering Muscle of the Blowfly Calliphora Vicina”. In: *Journal of Experimental Biology* 192.1 (July 1, 1994), pp. 207–224. ISSN: 0022-0949. DOI: 10.1242/jeb.192.1.207. URL: https://doi.org/10.1242/jeb.192.1.207 (visited on 05/16/2023).

[76] C. J. De Luca and Z. Erim. “Common drive of motor units in regulation of muscle force”. In: *Trends in Neurosciences* 17.7 (July 1994), pp. 299–305. ISSN: 0166-2236. DOI: 10.1016/0166-2236(94)90064-7.

[77] Lena H Ting and J Lucas McKay. "Neuromechanics of muscle synergies for posture and movement". In: *Current Opinion in Neurobiology*. Motor systems / Neurobiology of behaviour 17.6 (Dec. 1, 2007), pp. 622–628. ISSN: 0959-4388. DOI: 10.1016/j.conb.2008.01.002. URL: https://www.sciencedirect.com/science/article/pii/S0959438808000044 (visited on 10/21/2022).

[78] Feng Li et al. "The connectome of the adult Drosophila mushroom body provides insights into function". In: *eLife* 9 (Dec. 14, 2020), e62576. ISSN: 2050-084X. DOI: 10.7554/eLife.62576.

[79] Arie Matsliah et al. *Neuronal "parts list" and wiring diagram for a visual system*. Pages: 2023.10.12.562119 Section: New Results. Dec. 4, 2023. DOI: 10.1101/2023.10.12.562119. URL: https://www.biorxiv.org/content/10.1101/2023.10.12.562119v2 (visited on 12/22/2023).

[80] Graham Hoyle. "The anatomy and innervation of locust skeletal muscle". In: *Proceedings of the Royal Society of London. Series B - Biological Sciences* 143.911 (Jan. 27, 1955), pp. 281–292. ISSN: 2053-9193. DOI: 10.1098/rspb.1955.0011. URL: http://www.royalsocietypublishing.org/doi/10.1098/rspb.1955.0011 (visited on 07/19/2019).

[81] Silvan Hürkey et al. "Gap junctions desynchronize a neural circuit to stabilize insect flight". In: *Nature* 618.7963 (June 2023). Number: 7963 Publisher: Nature Publishing Group, pp. 118–125. ISSN: 1476-4687. DOI: 10.1038/s41586-023-06099-0. URL: https://www.nature.com/articles/s41586-023-06099-0 (visited on 09/14/2023).

[82] J. H. Koenig and Kazuo Ikeda. "Reciprocal excitation between identified flight motor neurons inDrosophila and its effect on pattern generation". In: *Journal of comparative physiology* 150.3 (Sept. 1, 1983), pp. 305–317. ISSN: 1432-1351. DOI: 10.1007/BF00605020. URL: https://doi.org/10.1007/BF00605020 (visited on 12/03/2022).

[83] Philip L. Newland and Yasuhiro Kondoh. "Dynamics of Neurons Controlling Movements of a Locust Hind Leg II. Flexor Tibiae Motor Neurons". In: *Journal of Neurophysiology* 77.4 (Apr. 1997), pp. 1731–1746. ISSN: 0022-3077, 1522-1598. DOI: 10.1152/jn.1997.77.4.1731. URL: http://www.physiology.org/doi/10.1152/jn.1997.77.4.1731 (visited on 07/08/2019).

[84] M. S. Tu and M. H. Dickinson. "The control of wing kinematics by two steering muscles of the blowfly (Calliphora vicina)". In: *Journal of Comparative Physiology A* 178.6 (June 1, 1996), pp. 813–830. ISSN: 1432-1351. DOI: 10.1007/BF00225830. URL: https://doi.org/10.1007/BF00225830 (visited on 05/16/2023).

[85] L M Mendell and E Henneman. "Terminals of single Ia fibers: location, density, and distribution within a pool of 300 homonymous motoneurons." In: *Journal of Neurophysiology* 34.1 (Jan. 1971). Publisher: American Physiological Society, pp. 171–187. ISSN: 0022-3077. DOI: 10.1152/jn.1971.34.1.171. URL: https://journals.physiology.org/doi/abs/10.1152/jn.1971.34.1.171 (visited on 04/30/2023).

[86] David Shepherd et al. "Developmental organization of central neurons in the adult Drosophila ventral nervous system". In: *The Journal of Comparative Neurology* (Mar. 28, 2019). ISSN: 1096-9861. DOI: 10.1002/cne.24690.

[87] Haluk Lacin et al. "Neurotransmitter identity is acquired in a lineage-restricted manner in the Drosophila CNS". In: *eLife* 8 (Mar. 26, 2019). Ed. by K VijayRaghavan, Sonia Sen, and Matthias Landgraf. Publisher: eLife Sciences Publications, Ltd, e43701. ISSN: 2050-084X. DOI: 10.7554/eLife.43701. URL: https://doi.org/10.7554/eLife.43701 (visited on 10/21/2022).

[88] Elizabeth C. Marin et al. *Systematic annotation of a complete adult male Drosophila nerve cord connectome reveals principles of functional organisation.* Pages: 2023.06.05.543407 Section: New Results. June 6, 2023. DOI: 10.1101/2023.06.05.543407. URL: https://www.biorxiv.org/content/10.1101/2023.06.05.543407v1 (visited on 08/30/2023).

[89] James W. Truman et al. “Developmental architecture of adult-specific lineages in the ventral CNS of Drosophila”. In: *Development* 131.20 (Oct. 15, 2004), pp. 5167–5184. ISSN: 0950-1991. DOI: 10.1242/dev.01371. URL: https://doi.org/10.1242/dev.01371 (visited on 11/08/2022).

[90] Robin Harris. “Form and function of the secondary hemilineages in the adult Drosophila thoracic nervous system”. ISBN: 9781267696748. PhD thesis. United States – Washington: University of Washington, 2012. 183 pp. URL: https://www.proquest.com/docview/1143510156/abstract/648C45B8548A4090PQ/1 (visited on 10/21/2022).

[91] Robin M Harris et al. “Neuron hemilineages provide the functional ground plan for the Drosophila ventral nervous system”. In: *eLife* 4 (July 20, 2015). Ed. by Leslie C Griffith. Publisher: eLife Sciences Publications, Ltd, e04493. ISSN: 2050-084X. DOI: 10.7554/eLife.04493. URL: https://doi.org/10.7554/eLife.04493 (visited on 10/21/2022).

[92] Aaron M Allen et al. “A single-cell transcriptomic atlas of the adult Drosophila ventral nerve cord”. In: *eLife* 9 (Apr. 21, 2020). Ed. by Richard S Mann, K VijayRaghavan, and Peter A Sims. Publisher: eLife Sciences Publications, Ltd, e54074. ISSN: 2050-084X. DOI: 10.7554/eLife.54074. URL: https://doi.org/10.7554/eLife.54074 (visited on 06/01/2023).

[93] Hongjie Li et al. “Fly Cell Atlas: A single-nucleus transcriptomic atlas of the adult fruit fly”. In: *Science* (Mar. 4, 2022). Publisher: American Association for the Advancement of Science. DOI: 10.1126/science.abk2432. URL: https://www.science.org/doi/10.1126/science.abk2432 (visited on 10/21/2022).

[94] Swetha B. M. Gowda et al. “GABAergic inhibition of leg motoneurons is required for normal walking behavior in freely moving Drosophila”. In: *Proceedings of the National Academy of Sciences* 115.9 (Feb. 27, 2018), E2115–E2124. ISSN: 0027-8424, 1091-6490. DOI: 10.1073/pnas.1713869115. URL: https://www.pnas.org/content/115/9/E2115 (visited on 07/09/2019).

[95] Kristin Lees et al. "Actions of Agonists, Fipronil and Ivermectin on the Predominant In Vivo Splice and Edit Variant (RDLbd, I/V) of the Drosophila GABA Receptor Expressed in Xenopus laevis Oocytes". In: *PLOS ONE* 9.5 (May 13, 2014). Publisher: Public Library of Science, e97468. ISSN: 1932-6203. DOI: 10.1371/journal.pone.0097468. URL: https://journals.plos.org/plosone/article?id=10.1371/journal.pone.0097468 (visited on 02/05/2024).

[96] Wendy W. Liu and Rachel I. Wilson. "Glutamate is an inhibitory neurotransmitter in the Drosophila olfactory system". In: *Proceedings of the National Academy of Sciences* (May 31, 2013). Publisher: National Academy of Sciences Section: Biological Sciences. ISSN: 0027-8424, 1091-6490. DOI: 10.1073/pnas.1220560110. URL: https://www.pnas.org/content/early/2013/05/30/1220560110 (visited on 11/01/2021).

[97] H. L. Atwood and C. A. G. Wiersma. "Command Interneurons in the Crayfish Central Nervous System". In: *Journal of Experimental Biology* 46.2 (Apr. 1967). Number: 2 Publisher: Company of Biologists, pp. 249–261. ISSN: 0022-0949. URL: https://resolver.caltech.edu/CaltechAUTHORS:20120815-091637081 (visited on 05/18/2023).

[98] Emanuel Todorov, Weiwei Li, and Xiuchuan Pan. "From task parameters to motor synergies: A hierarchical framework for approximately-optimal control of redundant manipulators". In: *Journal of robotic systems* 22.11 (Nov. 2005), pp. 691–710. ISSN: 0741-2223. DOI: 10.1002/rob.20093. URL: https://www.ncbi.nlm.nih.gov/pmc/articles/PMC1945248/ (visited on 05/16/2023).

[99] Casey M. Schneider-Mizell et al. *Cell-type-specific inhibitory circuitry from a connectomic census of mouse visual cortex*. Pages: 2023.01.23.525290 Section: New Results. Feb. 14, 2023. DOI: 10.1101/2023.01.23.525290. URL: https://www.biorxiv.org/content/10.1101/2023.01.23.525290v2 (visited on 04/10/2023).

[100] B. Ulfhake and S. Cullheim. "Postnatal development of cat hind limb motoneurons. III: Changes in size of motoneurons supplying the triceps surae muscle". In: *The*

Journal of Comparative Neurology 278.1 (Dec. 1, 1988), pp. 103–120. ISSN: 0021-9967. DOI: 10.1002/cne.902780107.

[101] Fabian N. Svara et al. "Volume EM Reconstruction of Spinal Cord Reveals Wiring Specificity in Speed-Related Motor Circuits". In: *Cell Reports* 23.10 (June 5, 2018), pp. 2942–2954. ISSN: 2211-1247. DOI: 10.1016/j.celrep.2018.05.023. URL: https://www.sciencedirect.com/science/article/pii/S2211124718307563 (visited on 02/13/2024).

[102] Simone Holler et al. "Structure and function of a neocortical synapse". In: *Nature* 591.7848 (Mar. 2021). Number: 7848 Publisher: Nature Publishing Group, pp. 111–116. ISSN: 1476-4687. DOI: 10.1038/s41586-020-03134-2. URL: https://www.nature.com/articles/s41586-020-03134-2 (visited on 02/19/2024).

[103] Christopher L. Barnes, Daniel Bonnéry, and Albert Cardona. "Synaptic counts approximate synaptic contact area in Drosophila". In: *PLOS ONE* 17.4 (Apr. 4, 2022). Publisher: Public Library of Science, e0266064. ISSN: 1932-6203. DOI: 10.1371/journal.pone.0266064. URL: https://journals.plos.org/plosone/article?id=10.1371/journal.pone.0266064 (visited on 02/27/2024).

[104] Cédric Soler et al. "Coordinated development of muscles and tendons of the Drosophila leg". In: *Development* 131.24 (Dec. 15, 2004), pp. 6041–6051. ISSN: 0950-1991. DOI: 10.1242/dev.01527. URL: https://doi.org/10.1242/dev.01527 (visited on 12/05/2022).

[105] Brandon Mark et al. *A developmental framework linking neurogenesis and circuit formation in the Drosophila CNS*. eLife. Publisher: eLife Sciences Publications Limited. May 11, 2021. DOI: 10.7554/eLife.67510. URL: https://elifesciences.org/articles/67510 (visited on 11/18/2022).

[106] M. Baek and R. S. Mann. "Lineage and Birth Date Specify Motor Neuron Targeting and Dendritic Architecture in Adult Drosophila". In: *Journal of Neuroscience* 29.21 (May 27, 2009), pp. 6904–6916. ISSN: 0270-6474, 1529-2401. DOI: 10.1523/

JNEUROSCI.1585-09.2009. URL: http://www.jneurosci.org/cgi/doi/10.1523/JNEUROSCI.1585-09.2009 (visited on 05/18/2017).

[107] D.J. Brierley et al. "Developmental origins and architecture of Drosophila leg motoneurons". In: *The Journal of Comparative Neurology* 520.8 (June 1, 2012), pp. 1629–1649. ISSN: 1096-9861. DOI: 10.1002/cne.23003. URL: http://onlinelibrary.wiley.com/doi/10.1002/cne.23003/abstract (visited on 05/18/2017).

[108] Jonathan Enriquez et al. "Specification of individual adult motor neuron morphologies by combinatorial transcription factor codes". In: *Neuron* 86.4 (May 20, 2015), pp. 955–970. ISSN: 1097-4199. DOI: 10.1016/j.neuron.2015.04.011.

[109] Wenyue Guan et al. "Post-transcriptional regulation of transcription factor codes in immature neurons drives neuronal diversity". In: *Cell Reports* 39.13 (June 28, 2022). Publisher: Elsevier. ISSN: 2211-1247. DOI: 10.1016/j.celrep.2022.110992. URL: https://www.cell.com/cell-reports/abstract/S2211-1247(22)00778-1 (visited on 10/21/2022).

[110] Nikolaos Balaskas et al. "Positional Strategies for Connection Specificity and Synaptic Organization in Spinal Sensory-Motor Circuits". In: *Neuron* 102.6 (June 19, 2019), 1143–1156.e4. ISSN: 0896-6273. DOI: 10.1016/j.neuron.2019.04.008. URL: https://www.sciencedirect.com/science/article/pii/S0896627319303435 (visited on 03/02/2023).

[111] Thomas M. Cover and Joy A. Thomas. *Elements of Information Theory*. Google-Books-ID: VWq5GG6ycxMC. John Wiley & Sons, Nov. 28, 2012. 771 pp. ISBN: 978-1-118-58577-1.

[112] E. S. Harcombe and R. J. Wyman. "Output pattern generation by Drosophila flight motoneurons". In: *Journal of Neurophysiology* 40.5 (Sept. 1977). Publisher: American Physiological Society, pp. 1066–1077. ISSN: 0022-3077. DOI: 10.1152/jn.1977.40.5.1066. URL: https://journals.physiology.org/doi/abs/10.1152/jn.1977.40.5.1066 (visited on 12/03/2022).

[113] Shefa Gordon and Michael H. Dickinson. "Role of calcium in the regulation of mechanical power in insect flight". In: *Proceedings of the National Academy of Sciences* 103.11 (Mar. 14, 2006), pp. 4311–4315. ISSN: 0027-8424, 1091-6490. DOI: 10.1073/pnas.0510109103. URL: https://pnas.org/doi/full/10.1073/pnas.0510109103 (visited on 02/14/2024).

[114] Elwood Henneman, George Somjen, and David O. Carpenter. "Excitability and inhibitibility of motoneurons of different sizes". In: *Journal of Neurophysiology* 28.3 (May 1, 1965), pp. 599–620. ISSN: 0022-3077. DOI: 10.1152/jn.1965.28.3.599. URL: https://www.physiology.org/doi/abs/10.1152/jn.1965.28.3.599 (visited on 06/17/2019).

[115] Marc D. Binder et al. "Does orderly recruitment of motoneurons depend on the existence of different types of motor units?" In: *Neuroscience Letters* 36.1 (Mar. 28, 1983), pp. 55–58. ISSN: 0304-3940. DOI: 10.1016/0304-3940(83)90485-8. URL: http://www.sciencedirect.com/science/article/pii/0304394083904858 (visited on 07/10/2019).

[116] Marc D. Binder, Randall K. Powers, and C. J. Heckman. "Nonlinear Input-Output Functions of Motoneurons". In: *Physiology (Bethesda, Md.)* 35.1 (Jan. 1, 2020), pp. 31–39. ISSN: 1548-9221. DOI: 10.1152/physiol.00026.2019.

[117] John E. Desmedt and E. Godaux. "Spinal Motoneuron Recruitment in Man: Rank Deordering with Direction but not with Speed of Voluntary Movement". In: *Science* 214.4523 (1981), pp. 933–936. ISSN: 0036-8075. URL: https://www.jstor.org/stable/1686338 (visited on 06/17/2019).

[118] Evdokia Menelaou, Sandeep Kishore, and David L McLean. "Mixed synapses reconcile violations of the size principle in zebrafish spinal cord". In: *eLife* 11 (Sept. 27, 2022). Ed. by Markus Meister et al. Publisher: eLife Sciences Publications, Ltd, e64063. ISSN: 2050-084X. DOI: 10.7554/eLife.64063. URL: https://doi.org/10.7554/eLife.64063 (visited on 01/14/2023).

[119] J. L. Smith et al. “Rapid ankle extension during paw shakes: selective recruitment of fast ankle extensors”. In: *Journal of Neurophysiology* 43.3 (Mar. 1, 1980), pp. 612–620. ISSN: 0022-3077. DOI: 10.1152/jn.1980.43.3.612. URL: https://www.physiology.org/doi/abs/10.1152/jn.1980.43.3.612 (visited on 06/17/2019).

[120] Wilfrid Rall. “Branching dendritic trees and motoneuron membrane resistivity”. In: *Experimental Neurology* 1.5 (Nov. 1, 1959), pp. 491–527. ISSN: 0014-4886. DOI: 10.1016/0014-4886(59)90046-9. URL: https://www.sciencedirect.com/science/article/pii/0014488659900469 (visited on 05/15/2023).

[121] François Hug et al. “Common synaptic input, synergies and size principle: Control of spinal motor neurons for movement generation”. In: *The Journal of Physiology* 601.1 (2023). _eprint: https://onlinelibrary.wiley.com/doi/pdf/10.1113/JP283698, pp. 11–20. ISSN: 1469-7793. DOI: 10.1113/JP283698. URL: https://onlinelibrary.wiley.com/doi/abs/10.1113/JP283698 (visited on 01/13/2023).

[122] Jeremy Maitin-Shepard et al. *google/neuroglancer:* Oct. 16, 2021. DOI: 10.5281/zenodo.5573294. URL: https://zenodo.org/record/5573294 (visited on 09/12/2022).

[123] Sven Dorkenwald et al. “FlyWire: online community for whole-brain connectomics”. In: *Nature Methods* 19.1 (Jan. 2022), pp. 119–128. ISSN: 1548-7105. DOI: 10.1038/s41592-021-01330-0.

[124] Sven Dorkenwald et al. *CAVE: Connectome Annotation Versioning Engine*. Pages: 2023.07.26.550598 Section: New Results. July 28, 2023. DOI: 10.1101/2023.07.26.550598. URL: https://www.biorxiv.org/content/10.1101/2023.07.26.550598v1 (visited on 10/16/2023).

[125] Leila Elabbady et al. *Perisomatic Features Enable Efficient and Dataset Wide Cell-Type Classifications Across Large-Scale Electron Microscopy Volumes*. Pages: 2022.07.20.499976 Section: New Results. Jan. 13, 2024. DOI: 10.1101/2022.07.20.499976. URL: https://www.biorxiv.org/content/10.1101/2022.07.20.499976v2 (visited on 01/30/2024).

[126] Fabian Pedregosa et al. "Scikit-learn: Machine Learning in Python". In: *Journal of Machine Learning Research* 12.85 (2011), pp. 2825–2830. ISSN: 1533-7928. URL: http://jmlr.org/papers/v12/pedregosa11a.html (visited on 02/19/2024).

[127] Leland McInnes, John Healy, and James Melville. *UMAP: Uniform Manifold Approximation and Projection for Dimension Reduction*. Sept. 17, 2020. DOI: 10.48550/arXiv.1802.03426. arXiv: 1802.03426[cs,stat]. URL: http://arxiv.org/abs/1802.03426 (visited on 10/19/2023).

[128] Pauli Virtanen et al. "SciPy 1.0: fundamental algorithms for scientific computing in Python". In: *Nature Methods* 17.3 (Mar. 2020). Number: 3 Publisher: Nature Publishing Group, pp. 261–272. ISSN: 1548-7105. DOI: 10.1038/s41592-019-0686-2. URL: https://www.nature.com/articles/s41592-019-0686-2 (visited on 02/05/2024).

[129] Lalanti Venkatasubramanian et al. "Stereotyped terminal axon branching of leg motor neurons mediated by IgSF proteins DIP-α and Dpr10". In: *eLife* 8 (Feb. 4, 2019). ISSN: 2050-084X. DOI: 10.7554/eLife.42692.

[130] Christopher W. Lynn, Caroline M. Holmes, and Stephanie E. Palmer. "Heavy-tailed neuronal connectivity arises from Hebbian self-organization". In: *Nature Physics* (Jan. 17, 2024). Publisher: Nature Publishing Group, pp. 1–8. ISSN: 1745-2481. DOI: 10.1038/s41567-023-02332-9. URL: https://www.nature.com/articles/s41567-023-02332-9 (visited on 02/02/2024).

[131] Alex Fornito, Andrew Zalesky, and Edward Bullmore. *Fundamentals of Brain Network Analysis*. Google-Books-ID: j9aDoAEACAAJ. Elsevier Science, Mar. 29, 2016. 494 pp. ISBN: 978-0-12-407908-3.

[132] Haluk Lacin and James W. Truman. "Lineage mapping identifies molecular and architectural similarities between the larval and adult Drosophila central nervous system". In: *eLife* 5 (Mar. 15, 2016), e13399. ISSN: 2050-084X. DOI: 10.7554/eLife.13399.

[133] Nils Eckstein et al. *Neurotransmitter Classification from Electron Microscopy Images at Synaptic Sites in Drosophila*. Pages: 2020.06.12.148775 Section: New Results. Sept. 2, 2020. DOI: 10.1101/2020.06.12.148775. URL: https://www.biorxiv.org/content/10.1101/2020.06.12.148775v2 (visited on 11/18/2022).

[134] Geoffrey W. Meissner et al. *An image resource of subdivided Drosophila GAL4-driver expression patterns for neuron-level searches*. Company: Cold Spring Harbor Laboratory Distributor: Cold Spring Harbor Laboratory Label: Cold Spring Harbor Laboratory Section: New Results Type: article. May 30, 2020, p. 2020.05.29.080473. DOI: 10.1101/2020.05.29.080473. URL: https://www.biorxiv.org/content/10.1101/2020.05.29.080473v1 (visited on 10/27/2021).

Chapter 4

CONNECTIVITY AND MORPHOLOGY OF IDENTIFIED WING SENSORY NEURONS

4.1 Abstract

Sensory neurons bridge the nervous system and the body. Their cell bodies reside along the body, and they have a long axon that enters the central nervous system through a nerve to synapse onto other neurons. The *Drosophila* wing has hundreds of sensory neurons, and some of them play a role in setting the precise phase of muscle spiking during flight[1,2]. The advent of synapse-level connectomes has made the mapping of sensorimotor circuits possible, but only if the inputs and output of the system are identified, e.g. the sensory structures that afferent axons come from and the muscles that efferent axons innervate. Here, we reconstruct sensory axons from a *Drosophila* wing and map them to peripheral sensory structures using genetic tools and light microscopy. We focus on sensory structures whose central projection morphology has not previously been shown, including both wing chordotonal organs, the tegula campaniform sensilla and hair plate, as well as a cluster of previously unidentified sensory neurons at the wing hinge. These identities can guide future work on the neuronal networks that integrate sensory information from the wing.

4.2 Introduction

A fly's wing is both extremely delicate and massively powerful. Wings sweep through the air to keep the animal aloft and they buzz to get the attention of a mate. But wings don't just move, they also sense the world through multiple modalities. Some sensory neurons on the wing are equipped to sense odors, pheromones, or the presence of particles or mites (bristle sensilla), and others sense the wing itself and its interaction with the environment[3].

These neurons, called proprioceptors for their self-sensing capabilities, are equipped with mehcanotransduction channels[4] and are structured so that they may sense how the wing twists and bends. Technical limitations make functional studies of wing sensors difficult, so what we know about wing sensory encoding is from quiescent preps. Axons in the wing nerve are sensitive to vibration[5], and the single campaniform sensilla that are sensitive to wing deformation and can be either slow- or fast-adapting[6,7]. Proprioceptive sensory neurons are of particular interest for their role during flight, as they operate on a faster timescale than vision, and are therefore able to provide the feedback necessary for stabilizing flight[8]. During flight, the dynamic conformation of the highly-folded wing hinge causes the wing to move[9], so the timing of wing hinge muscle activation within each phase determines the magnitude and direction of force produced[10]. The sensorimotor neural circuits that coordinate this responsive agility illustrate a feat of evolution, and recent advances in tools offer an opportunity to increase our understanding about the anatomy and synaptic connectivity of these circuits.

Connectomics is a quickly accelerating field concerned with mapping, quantifying, and analyzing neural circuits by reconstructing neurons and synapses and offers new opportunities for understanding circuit bases of behaviors[11]. To map these networks, electron microscopy images of the nervous system at synapse-level resolution are stitched together into a 3D image volume. Shapes are then segmented according to borders (e.g. cell membranes) and synapses are predicted according to identifiable features such as vesicles and postsynaptic densities. In addition to informing network matrices of the nervous system, the high-resolution image volumes also offer an opportunity to investigate morphology and ultrastructure of different components of the nervous system. In this study we use the densely reconstructed 3D volume of a Female Adult Nerve Cord (FANC, pronounced "fancy")[12] to characterize and make testable predictions about the morphology, ultrastructure, and connectivity of wing sensory neurons.

In reconstructing the wing sensory axons, we discovered a greater diversity of axon morphologies than has previously been reported in literature. This discrepancy is likely due to the resolution of connectomics, which allows for the identification of each sensory neuron as a

single segment. In contrast, previous studies on wing sensory neurons either show the central projections of sensory neurons as a group by filling the entire nerve with dye[13] or detail a subpopulation of single axons[14]. Notably, this study showed that the single axons from the same campaniform sensilla across flies can have slightly different morphologies. Although some of the smaller branches are different, the primary backbone of the neuron remains the same across flies e.g. if the primary backbone of one descends to the haltere neuropil, the same is true across flies. As more connectomes are collected and analyzed, variation in morphology vs. variation in synaptic partners will be an important question to address.

In this study, we reconstruct all of the proprioceptive (e.g. non-bristle) sensory axons from the wing and map many of the axon morphologies to the peripheral structure from which they originate. Some of these mappings revealed surprising results, including novel peripheral sensory neurons, such as neurons that innervate a hair plate on the tegula as well as a cluster of neurons around a sclerite of the wing hinge. The relationships between peripheral structures, axon morphologies, and synaptic partners provide testable predictions for the future, such as the stabilizing role during flight of strong direct sensory input from tegula campaniform sensilla to the wing steering motor neuron b1. More precise mapping of axons to fields of campaniform sensilla is ongoing; here we identify wing sensory neurons that innervate the tegula sensors, the radial chordotonal organ, and the base of the parascutal shelf.

4.3 Results

Matching central axons to peripheral sensory neurons

Sensory neurons bring information from outside of the central nervous system into the central nervous system (**Figure 4.1A**). What this information is and how it is processed depends on the ion channel expression of the sensory neuron, its morphology, its location, and what neurons it forms synapses with. The fly wing is home to a variety of sensory neurons (**Figure 4.1B**). Other than the neurons that innervate bristles along the anterior edge of the wing,

the most common sensory cell on the wing are campaniform sensilla. These structures consist of a single neuron with a dendrite that contacts a cuticular cap, or dome, on the surface of the animal and are sensitive to deformations of the dome[15,16]. Campaniform sensilla can be found alone or in groups, or "fields" of domes of similar size and orientation[17,18]. There are also two chordotonal organs on the wing[19]. Chordotonal organs are clusters of neurons with attachment "cap" cells that anchor them to an internal structure, such as a tendon[20]. In the wing, they are anchored to the inner cuticle wall of the tegula and the inner wall of the radial vein. Finally, the fly wing also has a single hair plate, a row of short stubby hairs close together. These sensory neurons are found all over the wing, but they are concentrated proximally (**Figure 4.1C**).

Recent advances in algorithmic tools for image alignment, segmentation, and analysis have yielded large datasets: 3D volumes of the ventral nerve cord (VNC) at synapse-level resolution with individual segmented neurons and predicted synapse locations[21,22]. One drawback of these techniques is that the imaged tissue is from a dissected preparation, so neurons that enter or exit through nerves are cut off. These neurons are the inputs and outputs of the central nervous system, so understanding their identities is crucial to interpreting circuitry of the central nervous system. One such electron microscopy (EM) dataset comprises the entire VNC of a female adult fly (FANC; **Figure 4.2A**; also see **Methods**)[21,12]. We reconstructed all 490 afferents in the left wing nerve (anterior dorsomedial nerve, ADMN), 126 of which were not bristle afferents, which are identifiable from their very-ventral axons. Some of these axon morphologies can be found in past literature detailing wing sensory neurons filled from the periphery[23,24,14,13], but many did not resemble any prior illustrations or images.

To interpret the sensory inputs from the wing, it is necessary to know what type of sensory neuron the axon originates from and its location on the wing. In order to map central projections in FANC to identified sensory neurons, we found sparse GAL4 lines in the FlyLight collection[25] that labeled axon morphologies that looked like reconstructed axons from FANC, crossed these lines to a fluorescent reporter, then imaged the wing and wing hinge to see where there was expression (**Figure 4.2B**, also see **Methods**). Most sensory

neurons were identifiable based on their structure and location according to literature.

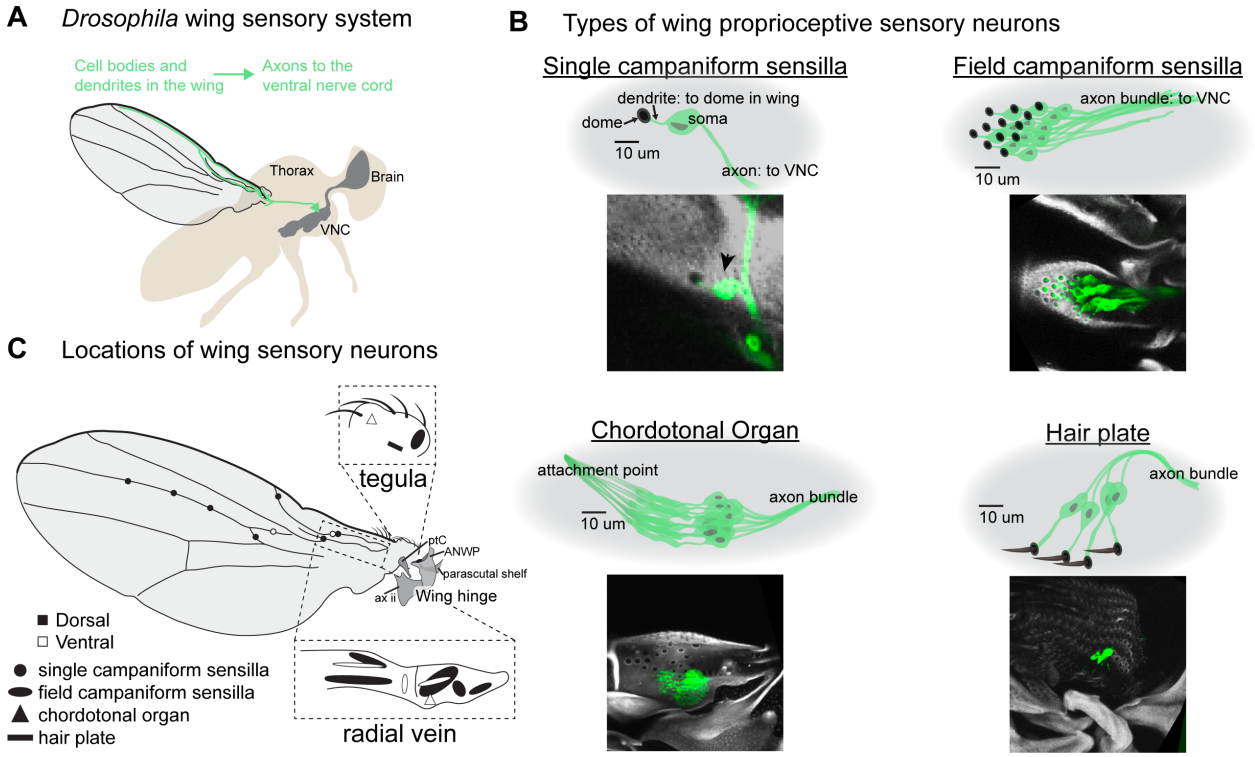

Figure 4.1: *Drosophila* wing sensory neurons. (A) The cell bodies and dendrites of sensory neurons are in the periphery of the animal, at the wing and wing hinge, and their axons travel to the ventral nerve cord. Before entering the nerve cord, they fasciculate together and enter through the Anterior Dorsomedial Nerve (ADMN). **(B)** Proprioceptors on the wing include campaniform sensilla, either single domes or fields of similar domes, chordotonal organs, and a hair plate. Each campaniform sensilla dome is innervated by a single sensory neuron, as is each hair in a hair plate. The chordotonal organ is made up of a group of sensory neurons with supporting cells that attach them to the inside of a vein or cuticle. **(C)** The wing is richly innervated with sensory neurons, with most being concentrated along the radial vein at the on the tegula.

Comprehensive reconstructions of wing axons

All segments in the left ADMN were reconstructed, including sensory neurons, motor neurons, and other efferent neurons. Segments were considered sensory if they did not attach to a cell body in the VNC. Postsynaptic partners of sensory neurons were reconstructed until 70% of the output was accounted for. Sensory axons made direct synapses onto motor neurons,

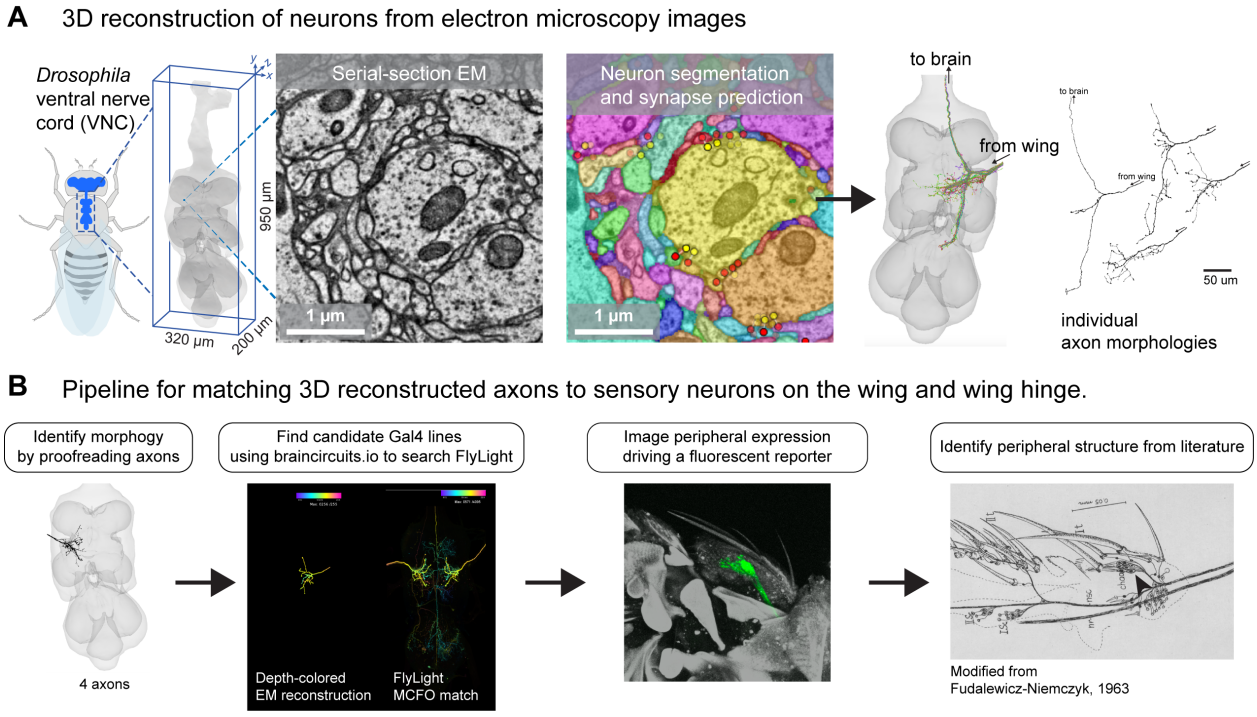

Figure 4.2: Tools for identifying *Drosophila* wing sensory neurons. (A) Each sensory axon in the wing nerve was reconstructed to show its full morphology in the ventral nerve cord as well as to analyze its connectivity. More information on each of these steps in Methods. **(B)** Pipeline for matching 3D reconstructed axons to sensory neurons on the wing and wing hinge. Driver lines were identified by their sparse expression in the wing nerve, then crossed to a membrane-bound GFP, imaged with a confocal microscope, and then compared with the literature for identification.

premotor neurons, post-sensory neurons (e.g. non-premotor interneurons), and other sensory neurons (**Figure 4.3A**). To define groups of sensory axons, we compared their postsynaptic connectivity using a pairwise measure of cosine similarity, where a score of one indicates that the two axons contact the same partners with the same proportion of synapses. The axons were then ordered via agglomerative clustering, which revealed six "coarse" groups that was further split into twenty sub-groups (**Figure 4.3B**). Although connectivity is not a perfect descriptor of morphology, in most cases similarity of postsynaptic partners mapped well with morphology (**Figure 2D**).

Direct sensory connections onto motor neurons can be a circuit mechanism for rapid

feedback-driven movement. We found that many of the sensory axons synapsed directly onto motor neurons that innervate muscles controlling the wing, haltere, or neck (**Figure 4.3C**). Overall, axons in group C have the most direct connections to wing motor neurons. This particular morphology, however, was not identifiable from previous literature, so we found genetic drivers that labeled the axon morphology using the FlyLight MCFO library[26].

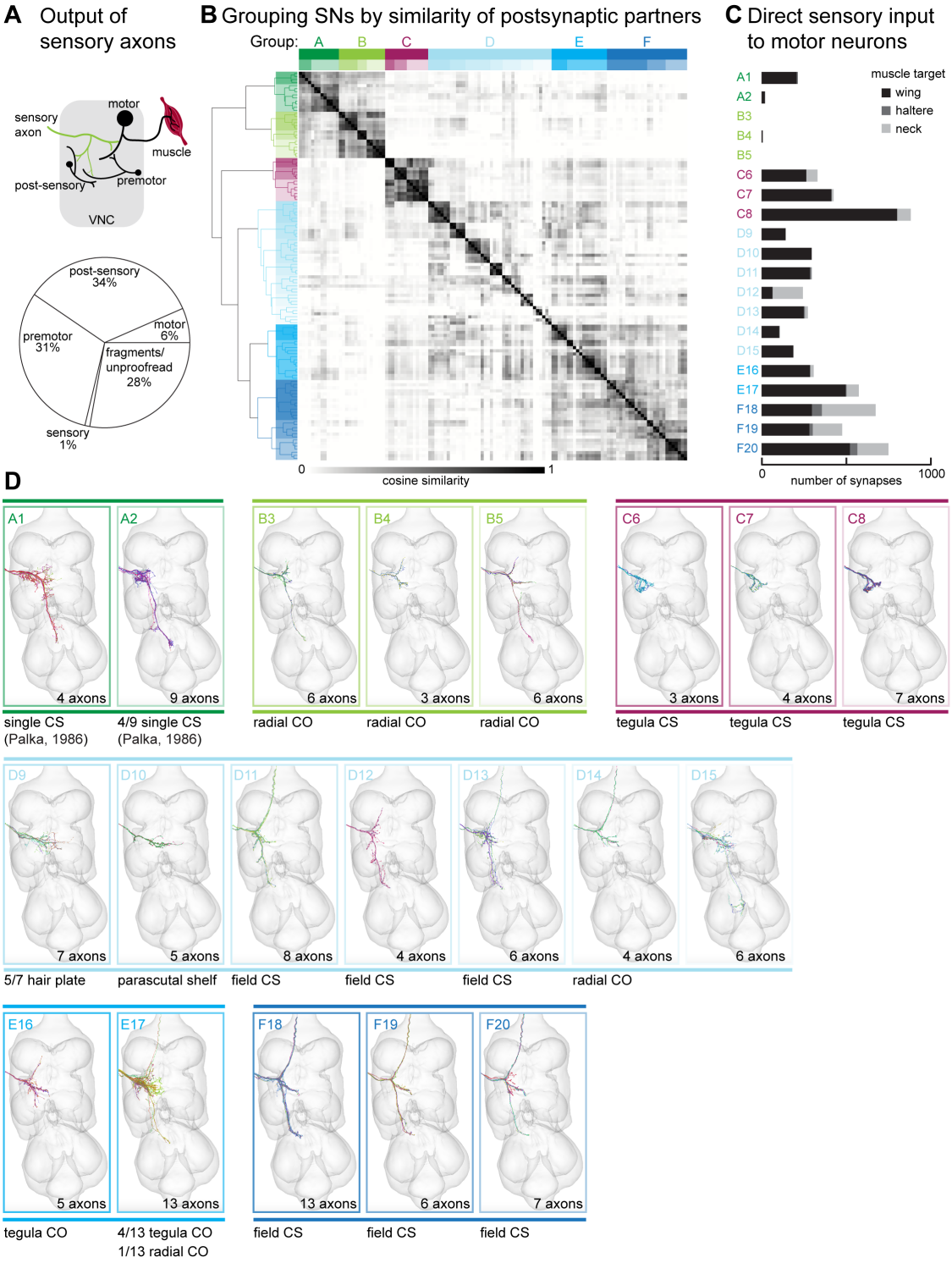

Figure 4.3: Postsynaptic connectivity of wing sensory axons. (A) (above) Cartoon showing the different downstream targets of sensory axons. (below) Proportion of synapses from all left wing sensory neurons (excluding bristles) to each target cell class. **(B)** Agglomerative clustering dendrogram and cosine similarity matrix of sensory axon postsynaptic similarity. **(C)** Number of predicted synapses from each connectivity group onto motor neurons. **(D)** Each morphology group identified in **B**, along with number of axons and peripheral sensory structure, if identified.

4.3.1 Campaniform sensilla on the tegula

Groups C6, C7, and C8 were immediately of interest because they make the highest number of synapses directly onto motor neurons (group C, **Figure 4.3C**). These 14 neurons have thick axons that project into the VNC but stay in the wing neuropil (**Figure 4.4A**). Imaging the periphery of multiple sparse driver lines crossed to GFP revealed that these axons originate from the population of 18 campaniform sensilla on the tegula (**Figure 4.4B-C**). The mismatch in number of axons and number of campaniform sensilla suggests that some of these sensilla have axons with different morphologies, which is discussed below. No functional studies of the tegula have yet been done in *Drosophila*, but it is an important sensory structure for flight in locusts[27]. The high amount of direct connectivity onto wing motor neurons (especially the tonic b1 MN), suggests that campaniform sensilla on the tegula could be the wing sensory afferents responsible for setting the phase of muscle activation during each wing stroke[1].

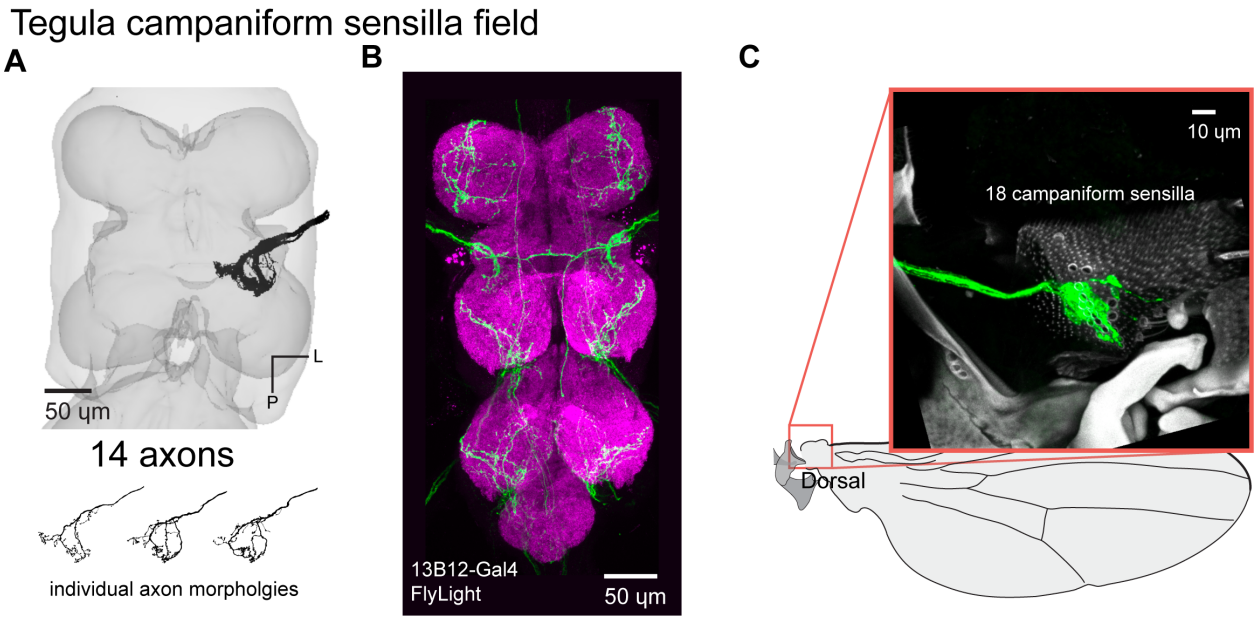

Figure 4.4: Tegula campaniform sensilla. (A) 3D reconstructed axons. Above: population of axons with similar morphology (black) and reconstructed VNC tissue (gray). Below: three example individual axons to demonstrate the variation in axon branching. **(B)** Axon branching pattern in VNC. Maximum projection from FlyLight Z-Stack of the driver line R13B12-GAL4. Projection that is crossing the midline is a projection from the posterior dorsal medial nerve. **(C)** Expression in the periphery. Maximum projection from confocal Z-Stack showing sensory neurons that innervate the campaniform sensilla field on the tegula. The driver line also labels two tegula hair plate neurons, but their axon location is distinct.

4.3.2 Hair plate on the tegula

A population of five axons enter the VNC and immediately branch ventrally and dorsally, crossing the midline, to the tectulum as well as the ovoid where leading edge bristle sensilla also terminate (**Figure 4.5A-B**). In the periphery, they innervate what appears to be a hair plate on the tegula, although a hair plate has not yet been described as such on the wing. It can be seen in a detailed anatomical drawing of the wing, where the hairs are described as thicker and shorter than other bristles on the wing[19]. As noted in detailed drawing, we observed five stubby short hairs in a row (**Figure 4.5C**). Hair plates are a specialized class of bristle sensilla, found at joints on legs. They are thought to be activated by extreme

positions of a joint[16,28].

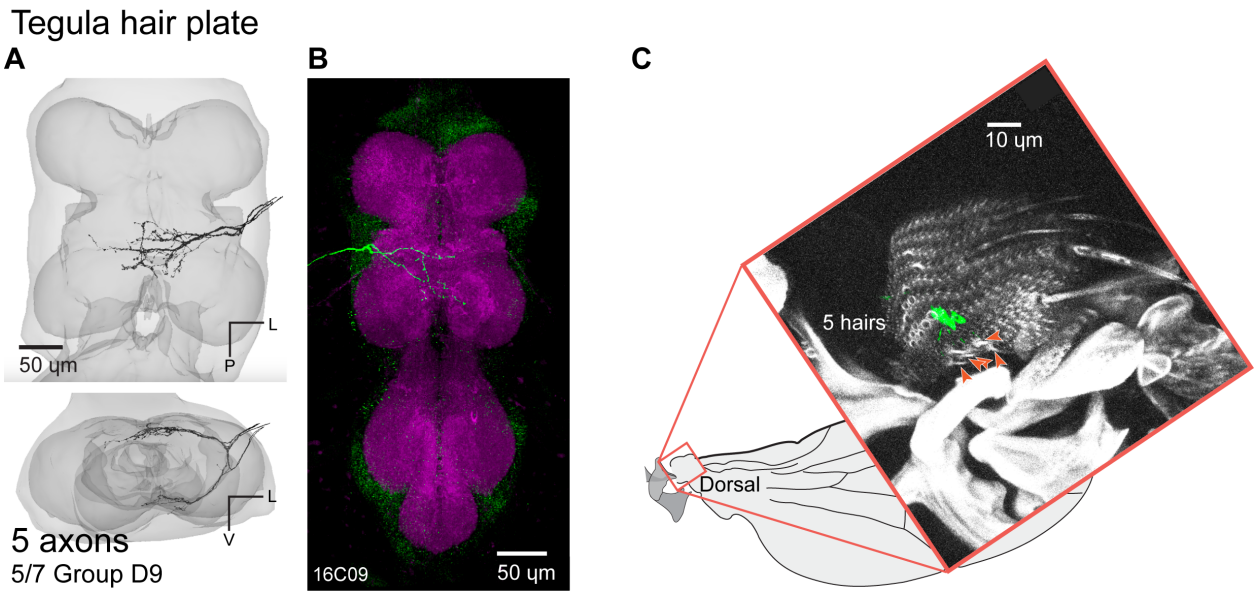

Figure 4.5: Tegula hair plate. (A) 3D reconstructed axons. Above: population of axons with similar morphology (black) and reconstructed VNC tissue (gray). Below: rotated view to show how the axons split to scoop around the dorsal and ventral edges of the wing neuropil. **(B)** Axon branching pattern in VNC. Maximum projection from FlyLight Z-Stack of images of the driver line R16C09-GAL4. **(C)** Expression in the periphery. Maximum projection from confocal Z-Stack showing sensory neurons that innervate the hairs of the tegula hair plate. Arrowheads indicate hair plate hairs.

4.3.3 Chordotonal organ in the tegula

In addition to campaniform sensilla and different classes of bristle sensilla, each of which has an external component for transducing sensory information, the tegula also features a chordotonal organ. These neurons bundle together and attach at the distal, anterior end of the tegula. So far, nine axons from two similar morphology groups have been identified as belonging to the tegula chordotonal organ (**Figure 4.6A-B**). Unlike every other known chordotonal organ in the fly, the tegula chordotonal organ does not express inactive, although they do have actin-rich cap cells, which are not present in campaniform sensilla (**Figure 4.6C**). It is possible that neurons in the tegula chordotonal organ exhibit different axon

morphologies, which would allow neurons with the same receptive fields to send the same signals to different parts of the central nervous system in parallel.

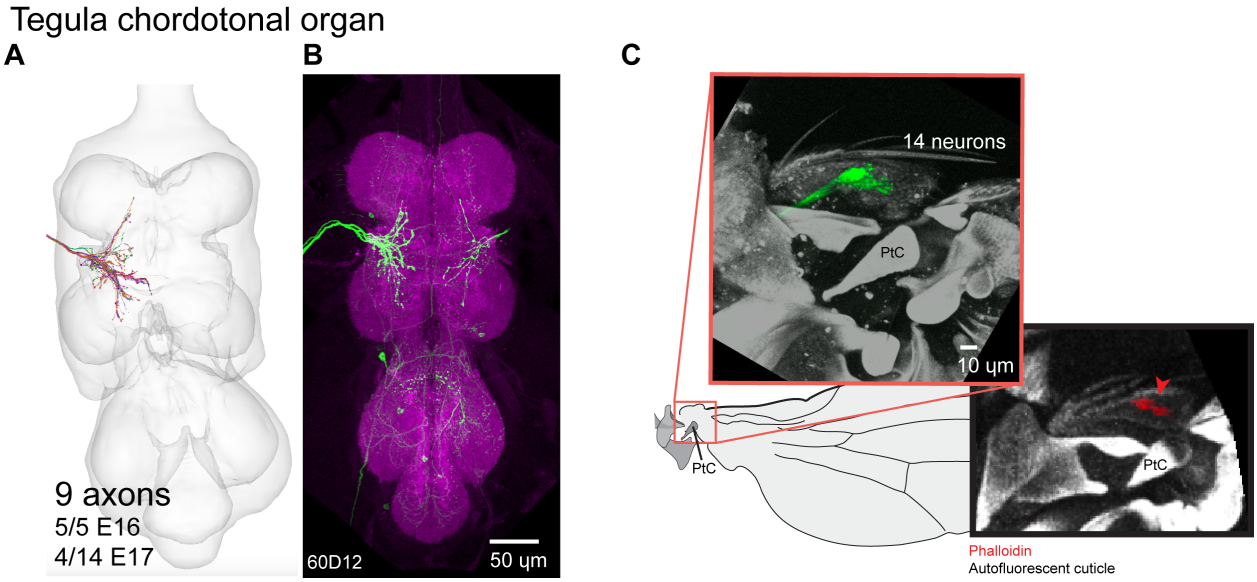

Figure 4.6: Chordotonal organ in the tegula. (A) 3D reconstructed axons. Axons from two connectivity groups, E16 and E17, both originate from the tegula chordotonal organ. **(B)** Axon branching pattern in VNC. Maximum projection from FlyLight Z-Stack of images of the driver line R60D12-GAL4. **(C)** Expression in the periphery. (top) Maximum projection from confocal Z-Stack showing sensory neurons that innervate the chordotonal organ in the tegula. (bottom) Phalloidin labeling the actin-rich cap cells that are part of chordotonal organs. Pterale C (PtC) is labeled in the wing cartoon and both images for orienting across images.

4.3.4 Chordotonal organ in the radial vein

A second, larger chordotonal organ sits in a pocket of the proximal radial vein (**Figure 4.7A**). As in the tegula, these neurons all attach at the same point (**Figure 4.7B**), so they likely share a receptive field, although it is possible that the neurons express different mechanosensitive channels from each other to encode different types of stress on the cuticle. The cell bodies sit on the posterior side of the radial vein and their dendrites and cap cells stretch to insert on the anterior side of the radial vein. These neurons are distinguishable from the neurons in the radial vein innervating campaniform sensilla because they don't

stretch toward the surface of the vein as the campaniform sensilla neurons do to reach the domes. There are at least four different morphologies of radial chordotonal axons, though likely more exist to account for all of the cell bodies. Some axons have a long process into the haltere neuropil (**Figure 4.7C-D**) while others branch dorsally to stay in the tectulum. These distinct morphologies may allow for parallel streams of information from the radial chordotonal organ.

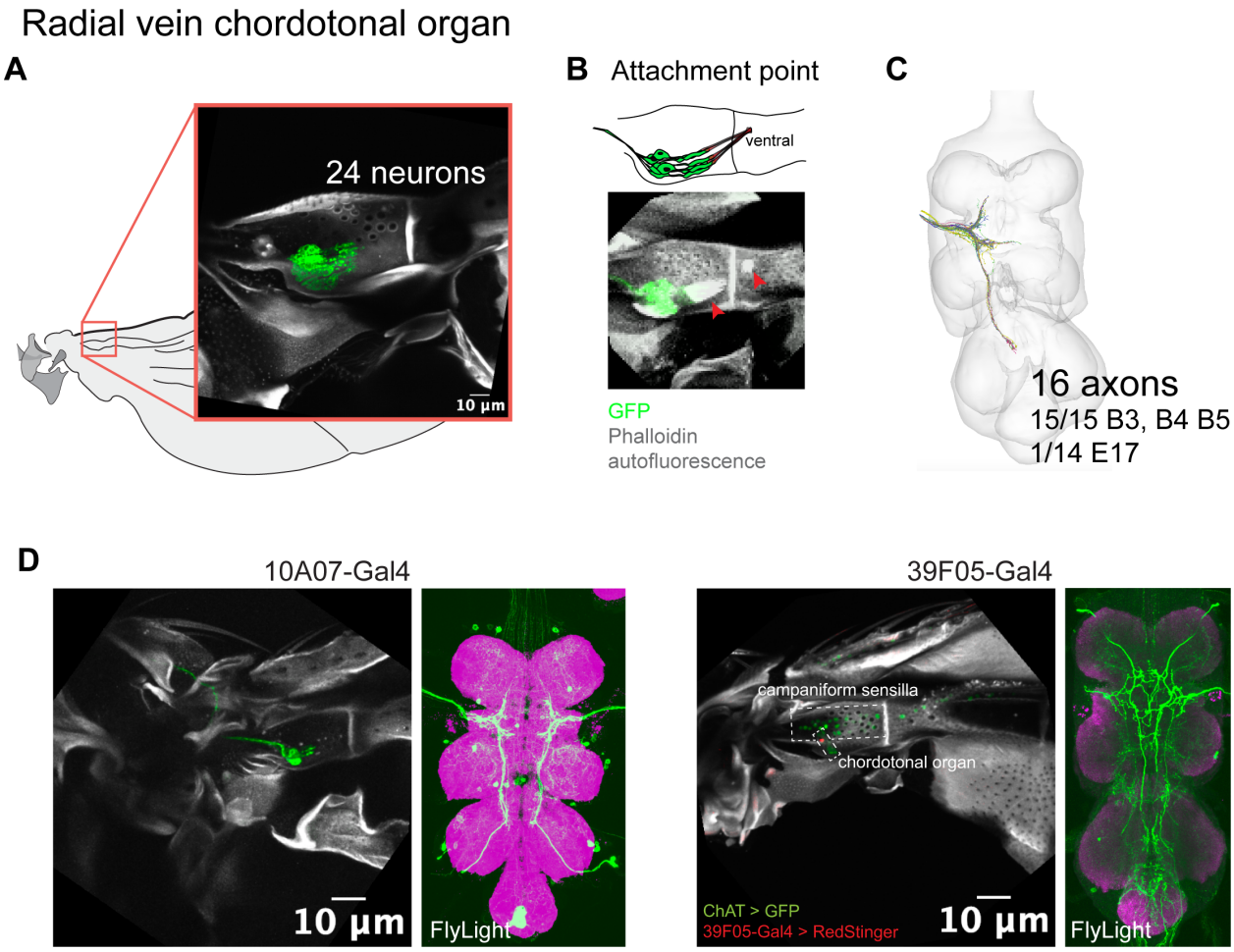

Figure 4.7: Radial chordotonal organ. **(A)** All neurons in the radial vein chordotonal organ expressing membrane-bound GFP (R15F10-Gal4 >UAS-GFP). **(B)** The radial vein chordotonal organ attaches to the ventral inner wall of the radial vein. **(C)** Reconstructed axons that were identified as originating in the radial vein chordotonal organ. **(D)** Example matchings between periphery and VNC. For other driver lines that label radial chordotonal neurons, see Table 1.

4.3.5 Parascutal Shelf

A population of five axons extends a single process along the far-dorsal tectulum, and two of the axons cross the midline (**Figure 4.8A-B**). These axons originate from a cluster of five neurons at the wing hinge which surround the parascutal shelf, just medial to the anterior nodal wing process. Other than the three campaniform sensilla on the anterior nodal wing process, These are the only cells at the wing hinge that are express choline acetyltransferase (ChAT), an indicator of sensory neurons in the periphery (**Figure 4.8C**)[29]. There are no ChAT+ cells at the base of, or innervating, sclerite Pterale C, which was previously hypothesized to be a sensory structure[5]. This hypothesis was based on spikes recorded from a sharp electrode placed at the base of Pterale C in response to vibrating the wing. We did observe that the entire nerve of sensory axons from the radial vein passes under Pterale C, so action potentials traveling along this nerve is likely what was being intercepted in the Pterale C recordings. The function of the parascutal shelf sensory neurons can only be speculated as of now, but their axons are premotor. Based on their location they could signal wing opening and closing.

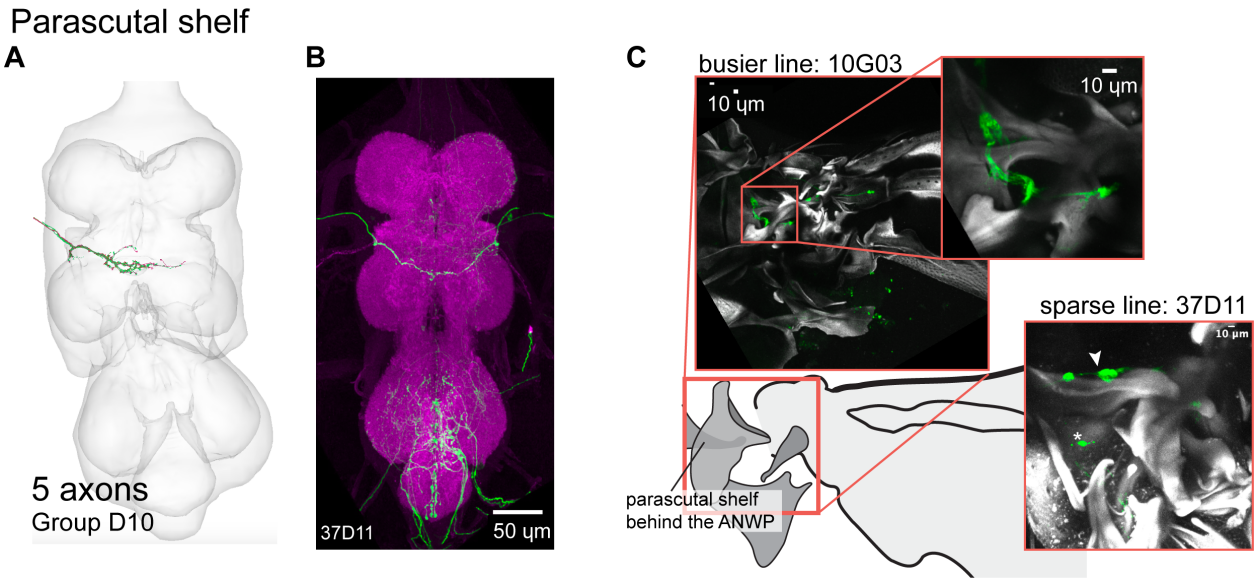

Figure 4.8: Sensory axons near the parascutal shelf. (A) 3D reconstructed axons, all five belong to the D10 connectivity group. **(B)** Axon branching pattern in VNC. Maximum projection from FlyLight Z-Stack of images of the driver line R37D11-GAL4. **(C)** Expression in the periphery. Top: maximum projection from confocal Z-Stack of a busier driver line, R10G03-GAL4, to show the morphology of the sensory neurons at the base of the parascutal shelf. Below: maximum projection from confocal Z-Stack of the sparse driver line R37D11-GAL4 >UAS-GFP showing neurons labeled at the base of the parascutal shelf. The asterisk marks the anterior nodal wing process campaniform sensilla neurons.

4.3.6 Campaniform sensilla from the same field can have different axon morphologies

Campaniform sensilla are classified as being within the same field if they are situated in the same location and if their domes orient along the same axes[3]. By definition, then, each campaniform sensilla within the same field likely encodes the same information. Whether or not this information is all routed to the same places, though, is an open question. To determine whether neurons that innervate campaniform sensilla in the same field also share postsynaptic partners, we identified Gal4 driver lines that express sparsely in the wing nerve (less than five ADMN axons) and imaged the periphery. We found three lines that label one or two different campaniform sensilla in the ventral radius C field (v.Rad.C) and compared the VNC expression of axons from the wing nerve (**Figure 4.9A**). In one line, the axon

extends two thin processes down to the haltere neuropil (**Figure 4.9B**); in another, one process goes to the haltere neuropil and a second reaches into t1 (**Figure 4.9C**). In the third line, one process ascends to the brain (**Figure 4.9D**). This quantification shows that neurons that innervate campaniform sensilla within the same field can have different morphologies. Experimentally, this means that mapping axon morphology to the periphery for field campaniform sensilla will be more difficult. Biologically, this suggests that redundant peripheral information is routed to different locations throughout the central nervous system in parallel.

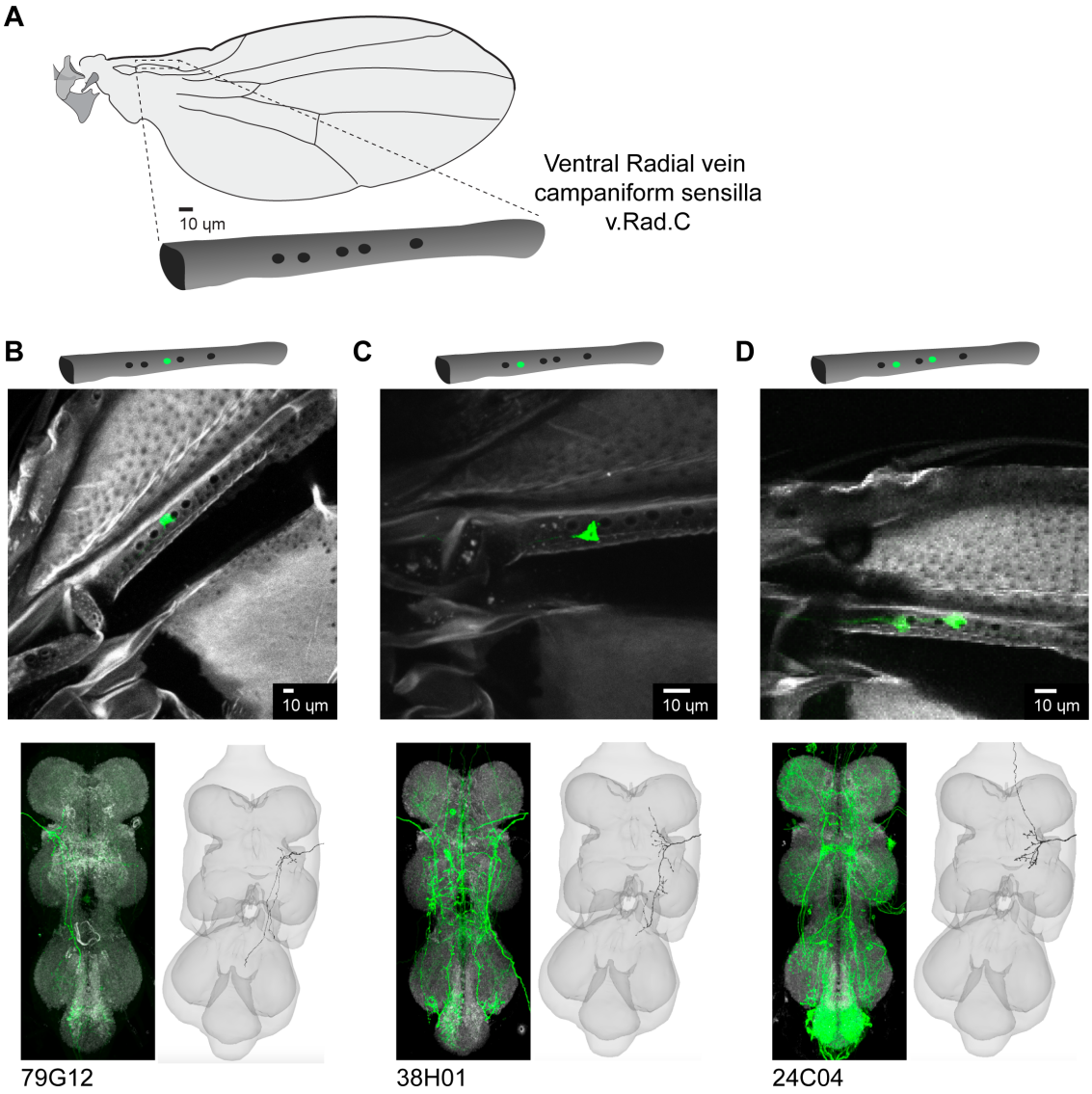

Figure 4.9: Different axon morphologies within a single campaniform sensilla field. **(A)** The v.Rad.C field of campaniform sensilla. The v.Rad.C field of campaniform sensilla is on the ventral side of the more distal part of the radial vein. The field has four to five domes, the fifth dome is proposed to be its own individual dome as it is farther apart from the other four and its orientation is slightly different[18]. **(B)** Peripheral expression in specific campaniform sensilla from sparse driver lines. Above: cartoon showing which dome is innervated for each driver line. Below: Maximum projection from confocal z-stack showing expression in the periphery from each sparse driver line. In the first line, only the neuron innervating the third dome is labeled. The second driver line labels the neuron innervating the second dome. The third line labels neurons innervating both the second and fourth dome. **(C)** Axon morphologies in the VNC. Left: Maximum projection from FlyLight Z-Stack MCFO. Right: 3D reconstructed axon that matches the morphology in the MCFO image. Sparse driver lines are labeled below each MCFO image.

4.3.7 Ultrastructure of electrotonic synapses

In addition to morphology and connectivity, the 3D volume of EM images of the VNC reveals the ultrastructure of neurons and synapses. While identifying neurons in FANC, we observed a notable feature regarding the premotor sensory neurons, namely that axon terminals at known locations of gap junctions had densely packed mitochondria (**Figure 4.10A**)[30]. How or if these mitochondria support functions such as signal transduction is currently unknown, but gap junction connections ensure lower latency signal transduction[31]. Further, very recent work suggests that axonal mitochondria consume ATP and therefore may have a different function than other mitochondria[32]. If experiments validate the prediction that gap junctions are accompanied by dense mitochondria packing at the terminal, new models can be trained to identify similar locations throughout this and other EM datasets to account for electrical synapses along with chemical synapses, and ultimately create more accurate wiring diagrams of the nervous system. We identified a population of wing sensory neurons whose terminals also feature densely packed mitochondria, suggesting that these sensory neurons may make electrotonic synapses as well (**Figure 4.10B**). Notably, these neurons were also identified with making the most direct connections onto motor neurons (see section on campaniform sensilla on the tegula).

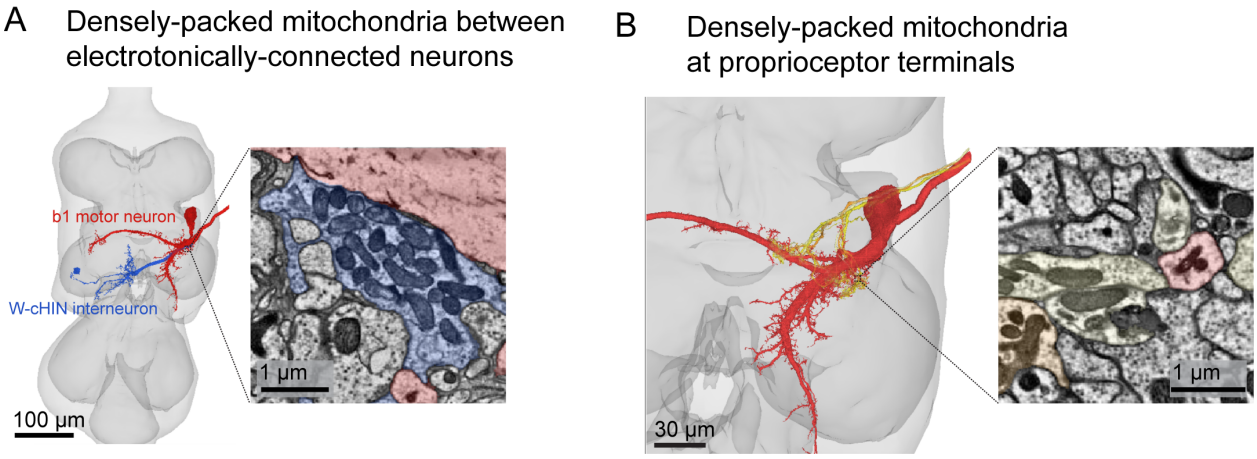

Figure 4.10: Ultrastructure of electrotonic synapses. **(A)** An example interneuron with known electrical synapse. FANC images reveal dense mitochondria at terminals near the b1 motor neuron. **(B)** Tegula campaniform sensilla also have densely packed mitochondria, suggesting that they may also play a role in fast sensory feedback during flight.

4.4 Discussion

In this project, we reconstructed each sensory axon in the left ADMN wing nerve from an EM dataset of the *Drosophila* VNC (FANC). We found a wider variety of morphologies than was expected based on previous studies. We matched particular morphologies to the sensory structure they originate from by finding driver lines that label those morphologies and imaging the periphery. This work is ongoing, but this abridged atlas features all of the sensory structures of the wing hinge other than campaniform sensilla on the wing blade. Single campaniform sensilla have already been mapped to central projections[14,13], and we found that within the same field, campaniform sensilla can have different axon morphologies. Along with this manuscript, a library of confocal Z-Stacks and an annotation table linked to the FANC dataset will be made available to make this information as accessible as possible to the wider community (see **Methods**).

Connecting the nervous system and the body

The nervous system exists to move and sense the body. Due to technical constraints, though, the two are often studied independently. Connectomes are a powerful tool for tackling connectivity questions, but their interpretability is limited by the quality of single-cell annotations. For the most part, neuron morphologies are stereotyped from fly to fly, so annotations in one dataset can be extended to others without further experiments. This transfer has already been successful for leg motor neurons[33]. By identifying the peripheral structures of wing sensory axons, we aim to increase the interpretability of any future work with neural circuits that feature sensory input from wings.

Visual signatures of electrotonic synapses

Although connectomes are described as "wiring diagrams," they currently only account for chemical synapses connections between neurons. Neurons, however, also communicate with each other via long-range neuromodulatory signaling and electrotonic synapses, neither of which are captured by the algorithms which detect visual signatures of chemical synapses[12]. There are, however, a handful of places in the fly VNC where electrotonic synapses have been experimentally validated[30,34]. Inspection of EM images revealed that the presynaptic terminals of these neurons are densely packed with mitochondria. This striking feature is also seen in the terminals of the tegula campaniform sensilla neurons, which synapse directly onto the tonic wing steering motor neuron b1. If these densely packed mitochondria pockets are indeed a visual signature of electrotonic synapses, then new algorithms can be trained to recognize them and predict other electrotonic synapses throughout the dataset. This, in turn, would create more-complete "wiring diagrams," as well as better inform signal propagation models based on connectomes.

Direct sensory input to wing motor neurons

Many wing sensory neurons synapse directly onto wing motor neurons, providing a mechanism for rapid feedback-driven motor control. Four wing motor neurons receive over 10% of their synaptic input from sensory neurons, including haltere input. Each of these four motor neurons is also classified as firing tonically throughout flight (e.g. not only during turning maneuvers). Integrating direct sensory input provides a mechanism for low latency motor control, which is a necessity in a motor system oscillating above 200 Hz. From the wing, directly premotor neurons primarily originate from the field of campaniform sensilla on the tegula. Future experiments and modeling is needed to show exactly what this field is sensitive to, but based on their direct connections and thick axons, it is likely that these are the sensory neurons in the wing nerve responsible for resetting the phase of b1 firing[1,2].

Heterogeneous axons from the same field of campaniform sensilla

Campaniform sensilla can be found in "fields" in which domes with roughly the same size and shape are clustered together. Previously, the central projections of all of the wing field campaniform sensilla were thought to follow the same basic morphology of three branches, one short branch to the tectulum and two long branches that project anteriorly to the brain and posteriorly to the haltere neuropil[13]. In the FANC dataset, however, there were only 36 axons that followed this pattern and there are 53 campaniform sensilla in the nine fields along the wing. We reasoned that some of the axons with uncharacterized morphologies must belong to campaniform sensilla in fields as well. Whether or not distinct morphologies mapped onto separate fields, though, was an open question. By imaging sparse lines that labeled one or two neurons in the same field and nothing else in the wing, we saw that neurons that innervate campaniform sensilla in the same field can have different axon morphologies in the VNC such that one will ascend to the brain while others project to the haltere neuropil. This finding is also in line with previous work that attempted to genetically isolate single fields of campaniform sensilla being largely unsuccessful. This organization may offer a

functional advantage of sending the same signal to multiple parts of the nervous system in parallel, or, put another way, the same postsynaptic neurons can integrate information across different fields of campaniform sensilla.

Outlook

By mapping peripheral sensory structures to their central axons, we aim to increase the interpretability of connectomic datasets. Our findings that campaniform sensilla on the tegula are the primary premotor wing sensors are just the very beginning of what can be done to map wing sensorimotor circuits in these new datasets. For example, another connectomic dataset exists of a male VNC[22]. Because male flies use their wings to court females, wing sensorimotor circuits may be a rich model for studying sexually dimorphic circuits. Since the wing is in motion, it is likely impossible to record activity of single sensory neurons during flight, but by uncovering their connectivity within the VNC we may begin to make hypotheses about their functions and test targeted predictions in quiescent flies.

4.5 Acknowledgements

Thank you to Anne Sustar, Su-Yee Lee, Leila Elabbady, and Brandon Pratt for thoughtful feedback on this chapter.

4.6 Methods

Resource availability

VNC images are publicly available via FlyLight[25]. An annotation table for FANC left wing sensory neurons is available to the FANC community.

Materials availability

The genetic driver lines used in this study are listed in **Table S4.1** and are available from the Bloomington Drosophila Stock center.

EM image collection and neuron reconstruction

The 3D reconstructed axons came from the FANC dataset[12], for details on segmentation, see Azevedo et al, 2022[21]. Following automatic segmentation, neurons were proofread to include a complete backbone and as many branches as could confidently be reattached. Neurons were annotated using CAVE[35].

There are 364 bristly neurons from the left wing, but they were not counted in this survey. They are easily separated from other axons because they project only ventrally. Additionally, sensory neurons from the PDMN were not accounted for, as these have already been mapped to single thorax bristles[23,24].

Reconstructed axon morphology groups

To group axons by similar connectivity, we computed the cosine similarity of synaptic weights onto postsynaptic partners. We included fragments but used a three synapse threshold for connections. Cosine similarity and agglomerative clustering were computed with the python library Scikit-learn[36].

Samples

We used *Drosophila melanogaster* raised on standard cornmeal and molasses medium at 25 C in a 14:10 hour light:dark cycle. We used female flies 2-7 days post-eclosion for imaging.

Sample preparation

Wing images

Wings were fixed in 4% formaldehyde (PFA) PBS solution for 20-60 minutes followed by rinsing in PBS with 0.2% Triton X-100 (PBT) four times over the course of 75 minutes. For most samples, native fluorescence was imaged, so the wings were then mounted onto slides in Vectashield without DAPI. For a subset of samples, after rinsing, some wings were incubated in 1:50 Alexa Fluor 635-nm Phalloidin (Thermofisher A34054) in a PBS solution with the

following reagents to improve tissue penetrance: 1% triton X-100, 0.5% DMSO, 0.05 mg/ml Escin (Sigma-Aldrich, E1378) and 3% normal goat serum. Wings were then incubated for ten days at 4 C with occasional gentle nutating. Following incubation, a second rinsing procedure was performed before mounting the wings on slides with Vectashield.

Wing hinge images

For wing hinge images, a full adult fly was hemisected. First, flies were killed by freezing flies briefly on ice, then dipping in 95% ethanol. Next they were frozen in Tissue-Tek O.C.T. Compound on dry ice for 3 minutes. Flies were then sliced along the anterior-posterior axis with a razor blade and transferred to a series of wells of 3mL 4% formaldehyde (PFA) PBS solution until the O.C.T. melted away. Half-flies were then transferred to a 0.6 mL tube with fresh fixative for 45 minutes before following the same washing procedure detailed above. Instead of Vectashield, half-flies were mounted using the FocusClear-MountClear system (CelExplorer FC-101 and MC-301).

Confocal Imaging and image post-processing

Mounted wings and wing hinges were imaged on a Confocal Olympus FV1000. Images were processed in FIJI[37].

Peripheral identifications

Sensory structures were identified from confocal image stacks by closely scrutinizing the images to see exactly where GFP-labeled neurons were in relation to wing veins. Campaniform sensilla were the most straightforward sensory structures to identify thanks to the recent comprehensive atlas[18]. The chordotonal organs were identified by their actin-rich attachment cells labeled by phalloidin. The structure on the tegula was identified as a hair plate due to the appearance of the hairs.

4.7 Supplementary Materials

Peripheral structure	Radial CO	Tegula CO	ANWP CS	tegula CS field	d.Rad.A	d.Rad.B	d.Rad.C	v.Rad.A	v.Rad.B	v.Rad.C	d.Rad.D	d.Rad.E	dS-1 & 2	d.HCV	GSR	TSM-1 & 2	ACV	L3-1	L3-2	L3-3	v.HCV	L3-V	parascutal shelf	tegula hp	tegula hairs	edge bristles
# of neurons	~24	~14	3	18	4	7	18	4	3	5	4	8	2	1	1	2	1	1	1	1	1	1	5	5	6	
R10A07-Gal4	4																									
R10F07-Gal4	7					1																				
R10G03-Gal4							2																			
R13B12-Gal4				8																				2		
R26B11-Gal4																2										
R15F10-Gal4	24																									
R16C09-Gal4																								4		
R21A01-Gal4		5																								
R21C09-Gal4							2	4		1																
R24C04-Gal4	6									2																
R25C01-Gal4																										
R26D04-Gal4							5	2		3		2														
R26F04-Gal4					4	7	17		2		4	2														
R35B08-Gal4	3																									
R36C09-Gal4	4																									
R37D11-Gal4			1																			5		2		
R38H01-Gal4										3																
R39F05-Gal4	1																									
R42G08-Gal4				2																						
R45D07-Gal4																					1	4				
R48H11-Gal4	4																									
R49F11-Gal4	7																									
R54H12-Gal4			2	2									2									3				
R60D12-Gal4		10																								
R60G04-Gal4		5																								
R64C04-Gal4	4				1		1																			
R70G12-Gal4																								2		
R72C01-Gal4	6																									
R73F02-Gal4				2																						
R75B09-Gal4		4	2	13		2																				
R76E12-Gal4	8																									
R79G12-Gal4										1																
R83B04-Gal4																						5				

Table 4.1

References

[1] A. Fayyazuddin and M. H. Dickinson. “Convergent mechanosensory input structures the firing phase of a steering motor neuron in the blowfly, Calliphora”. In: *Journal*

of Neurophysiology 82.4 (Oct. 1999), pp. 1916–1926. ISSN: 0022-3077. DOI: 10.1152/jn.1999.82.4.1916.

[2] Gerhard Heide. "Neural mechanisms of flight control in Diptera". In: *BIONA-report* 2 (1983), pp. 35–52.

[3] J. W. S. Pringle. *Insect Flight*. Google-Books-ID: hPOsN4QExQMC. Cambridge University Press, Dec. 1957. 146 pp. ISBN: 978-0-521-05995-4.

[4] John C. Tuthill and Rachel I. Wilson. "Mechanosensation and Adaptive Motor Control in Insects". In: *Current biology: CB* 26.20 (Oct. 24, 2016), R1022–R1038. ISSN: 1879-0445. DOI: 10.1016/j.cub.2016.06.070.

[5] Jaleel A. Miyan and Arthur W. Ewing. "A wing synchronous receptor for the Dipteran flight motor". In: *Journal of Insect Physiology* 30.7 (Jan. 1, 1984), pp. 567–574. ISSN: 0022-1910. DOI: 10.1016/0022-1910(84)90085-4. URL: https://www.sciencedirect.com/science/article/pii/0022191084900854 (visited on 02/19/2024).

[6] Michael H. Dickinson. "Directional Sensitivity and Mechanical Coupling Dynamics of Campaniform Sensilla During Chord-Wise Deformations of the Fly Wing". In: *Journal of Experimental Biology* 169.1 (Aug. 1, 1992), pp. 221–233. ISSN: 0022-0949. DOI: 10.1242/jeb.169.1.221. URL: https://doi.org/10.1242/jeb.169.1.221 (visited on 02/20/2024).

[7] M. H. Dickinson and J. Palka. "Physiological properties, time of development, and central projection are correlated in the wing mechanoreceptors of Drosophila". In: *Journal of Neuroscience* 7.12 (Dec. 1, 1987). Publisher: Society for Neuroscience Section: Articles, pp. 4201–4208. ISSN: 0270-6474, 1529-2401. DOI: 10.1523/JNEUROSCI.07-12-04201.1987. URL: https://www.jneurosci.org/content/7/12/4201 (visited on 02/20/2024).

[8] Florian T. Muijres et al. "Flies Evade Looming Targets by Executing Rapid Visually Directed Banked Turns". In: *Science* 344.6180 (Apr. 11, 2014). Publisher: American

Association for the Advancement of Science, pp. 172–177. DOI: 10.1126/science.1248955. URL: https://www.science.org/doi/full/10.1126/science.1248955 (visited on 02/14/2024).

[9] W. Nachtigall, A. Wisser, and D. Eisinger. "Flight of the honey bee. VIII. Functional elements and mechanics of the "flight motor" and the wing joint – one of the most complicated gear-mechanisms in the animal kingdom". In: *Journal of Comparative Physiology B* 168.5 (July 1, 1998), pp. 323–344. ISSN: 1432-136X. DOI: 10.1007/s003600050152. URL: https://doi.org/10.1007/s003600050152 (visited on 02/14/2024).

[10] Michael H Dickinson and Michael S Tu. "The Function of Dipteran Flight Muscle". In: *Comparative Biochemistry and Physiology Part A: Physiology* 116.3 (Mar. 1, 1997), pp. 223–238. ISSN: 0300-9629. DOI: 10.1016/S0300-9629(96)00162-4. URL: https://www.sciencedirect.com/science/article/pii/S0300962996001624 (visited on 02/14/2024).

[11] Dana Shani Galili, Gregory S. X. E. Jefferis, and Marta Costa. "Connectomics and the neural basis of behaviour". In: *Current Opinion in Insect Science* (Sept. 13, 2022), p. 100968. ISSN: 2214-5753. DOI: 10.1016/j.cois.2022.100968.

[12] Jasper S. Phelps et al. "Reconstruction of motor control circuits in adult Drosophila using automated transmission electron microscopy". In: *Cell* 184.3 (Feb. 2021), 759–774.e18. ISSN: 00928674. DOI: 10.1016/j.cell.2020.12.013. URL: https://linkinghub.elsevier.com/retrieve/pii/S0092867420316834 (visited on 12/22/2023).

[13] Kathleen E. Whitlock and John Palka. "Development of wing sensory axons in the central nervous system of *Drosophila* during metamorphosis". In: *Journal of Neurobiology* 26.2 (Feb. 1995), pp. 189–204. ISSN: 0022-3034, 1097-4695. DOI: 10.1002/neu.480260204. URL: https://onlinelibrary.wiley.com/doi/10.1002/neu.480260204 (visited on 02/14/2024).

[14] J. Palka et al. “Central projections of identified Drosophila sensory neurons in relation to their time of development”. In: *Journal of Neuroscience* 6.6 (June 1, 1986). Publisher: Society for Neuroscience Section: Articles, pp. 1822–1830. ISSN: 0270-6474, 1529-2401. DOI: 10.1523/JNEUROSCI.06-06-01822.1986. URL: https://www.jneurosci.org/content/6/6/1822 (visited on 02/14/2024).

[15] K. M. Chapman, R. B. Duckrow, and D. T. Moran. “Form and Role of Deformation in Excitation of an Insect Mechanoreceptor”. In: *Nature* 244.5416 (Aug. 1973). Number: 5416 Publisher: Nature Publishing Group, pp. 453–454. ISSN: 1476-4687. DOI: 10.1038/244453a0. URL: https://www.nature.com/articles/244453a0 (visited on 02/14/2024).

[16] J. W. S. Pringle. “Proprioception In Insects: II. The Action Of The Campaniform Sensilla On The Legs”. In: *Journal of Experimental Biology* 15.1 (Jan. 1, 1938), pp. 114–131. ISSN: 0022-0949. DOI: 10.1242/jeb.15.1.114. URL: https://doi.org/10.1242/jeb.15.1.114 (visited on 02/14/2024).

[17] Eric S. Cole and John Palka. “The pattern of campaniform sensilla on the wing and haltere of Drosophila melanogaster and several of its homeotic mutants”. In: *Development* 71.1 (Oct. 1, 1982), pp. 41–61. ISSN: 0950-1991. DOI: 10.1242/dev.71.1.41. URL: https://doi.org/10.1242/dev.71.1.41 (visited on 02/14/2024).

[18] Gesa F. Dinges et al. “Location and arrangement of campaniform sensilla in Drosophila melanogaster”. In: *Journal of Comparative Neurology* 529.4 (2021). _eprint: https://onlinelibrary.wile pp. 905–925. ISSN: 1096-9861. DOI: 10.1002/cne.24987. URL: https://onlinelibrary.wiley.com/doi/abs/10.1002/cne.24987 (visited on 02/14/2024).

[19] Fudalewicz-Niemczyk, Władysława. *L’innervation et les organes sensoriels des ailes des Diptčres et comparaison avec l’innervation des ailes d’insectesd’autres ordres.* 1963. 112 pp. URL: http://archive.org/details/actazoolcrac-8-12 (visited on 02/14/2024).

[20] Laurence H. Field and Thomas Matheson. "Chordotonal Organs of Insects". In: *Advances in Insect Physiology*. Ed. by P. D. Evans. Vol. 27. Academic Press, Jan. 1, 1998, pp. 1–228. DOI: 10.1016/S0065-2806(08)60013-2. URL: https://www.sciencedirect.com/science/article/pii/S0065280608600132 (visited on 02/14/2024).

[21] Anthony Azevedo et al. *Tools for comprehensive reconstruction and analysis of Drosophila motor circuits*. Pages: 2022.12.15.520299 Section: New Results. Dec. 15, 2022. DOI: 10.1101/2022.12.15.520299. URL: https://www.biorxiv.org/content/10.1101/2022.12.15.520299v1 (visited on 12/12/2023).

[22] Shin-ya Takemura et al. *A Connectome of the Male Drosophila Ventral Nerve Cord*. Pages: 2023.06.05.543757 Section: New Results. June 6, 2023. DOI: 10.1101/2023.06.05.543757. URL: https://www.biorxiv.org/content/10.1101/2023.06.05.543757v1 (visited on 02/14/2024).

[23] A. Ghysen. "The projection of sensory neurons in the central nervous system of *Drosophila*: Choice of the appropriate pathway". In: *Developmental Biology* 78.2 (Aug. 1, 1980), pp. 521–541. ISSN: 0012-1606. DOI: 10.1016/0012-1606(80)90351-6. URL: https://www.sciencedirect.com/science/article/pii/0012160680903516 (visited on 02/14/2024).

[24] Ibrahim Kays, Vedrana Cvetkovska, and Brian E. Chen. "Structural and functional analysis of single neurons to correlate synaptic connectivity with grooming behavior". In: *Nature Protocols* 9.1 (Jan. 2014). Number: 1 Publisher: Nature Publishing Group, pp. 1–10. ISSN: 1750-2799. DOI: 10.1038/nprot.2013.157. URL: https://www.nature.com/articles/nprot.2013.157 (visited on 02/19/2024).

[25] Arnim Jenett et al. "A GAL4-driver line resource for Drosophila neurobiology". In: *Cell Reports* 2.4 (Oct. 25, 2012), pp. 991–1001. ISSN: 2211-1247. DOI: 10.1016/j.celrep.2012.09.011.

[26] Geoffrey W Meissner et al. "A searchable image resource of Drosophila GAL4 driver expression patterns with single neuron resolution". In: *eLife* 12 (Feb. 23, 2023). Ed. by Ilona C Grunwald Kadow and Claude Desplan. Publisher: eLife Sciences Publications, Ltd, e80660. ISSN: 2050-084X. DOI: 10.7554/eLife.80660. URL: https://doi.org/10.7554/eLife.80660 (visited on 02/19/2024).

[27] Harald Wolf. "The Locust Tegula: Significance for Flight Rhythm Generation, Wing Movement Control and Aerodynamic Force Production". In: *Journal of Experimental Biology* 182.1 (Sept. 1, 1993), pp. 229–253. ISSN: 0022-0949. DOI: 10.1242/jeb.182.1.229. URL: https://doi.org/10.1242/jeb.182.1.229 (visited on 02/20/2024).

[28] James R. Trimarchi, Ping Jin, and Rodney K. Murphey. "Controlling the Motor Neuron". In: *International Review of Neurobiology*. Ed. by R. Adron Harris {and} Peter Jenner Ronald J. Bradley. Vol. 43. Neuromuscular Junctions in Drosophila. Academic Press, 1999, pp. 241–264. DOI: 10.1016/S0074-7742(08)60548-6. URL: http://www.sciencedirect.com/science/article/pii/S0074774208605486 (visited on 03/31/2017).

[29] Kouji Yasuyama and Paul M. Salvaterra. "Localization of choline acetyltransferase-expressing neurons in Drosophila nervous system". In: *Microscopy Research and Technique* 45.2 (1999). _eprint: https://onlinelibrary.wiley.com/doi/pdf/10.1002/%28SICI%291097-0029%2819990415%2945%3A2%3C65%3A%3AAID-JEMT2%3E3.0.CO%3B2-0, pp. 65–79. ISSN: 1097-0029. DOI: 10.1002/(SICI)1097-0029(19990415)45:2<65::AID-JEMT2>3.0.CO;2-0. URL: https://onlinelibrary.wiley.com/doi/abs/10.1002/%28SICI%291097-0029%2819990415%2945%3A2%3C65%3A%3AAID-JEMT2%3E3.0.CO%3B2-0 (visited on 02/28/2024).

[30] James R. Trimarchi and R. K. Murphey. "The shaking-B2 Mutation Disrupts Electrical Synapses in a Flight Circuit in AdultDrosophila". In: *Journal of Neuroscience* 17.12 (June 15, 1997). Publisher: Society for Neuroscience Section: Articles, pp. 4700–

4710. ISSN: 0270-6474, 1529-2401. DOI: 10.1523/JNEUROSCI.17-12-04700.1997. URL: https://www.jneurosci.org/content/17/12/4700 (visited on 02/15/2024).

[31] Amir Fayyazuddin and Michael H. Dickinson. "Haltere Afferents Provide Direct, Electrotonic Input to a Steering Motor Neuron in the Blowfly, Calliphora". In: *Journal of Neuroscience* 16.16 (Aug. 15, 1996). Publisher: Society for Neuroscience Section: Articles, pp. 5225–5232. ISSN: 0270-6474, 1529-2401. DOI: 10.1523/JNEUROSCI.16-16-05225.1996. URL: https://www.jneurosci.org/content/16/16/5225 (visited on 02/29/2024).

[32] Yusuke Hirabayashi et al. *Most axonal mitochondria in cortical pyramidal neurons lack mitochondrial DNA and consume ATP*. Pages: 2024.02.12.579972 Section: New Results. Feb. 13, 2024. DOI: 10.1101/2024.02.12.579972. URL: https://www.biorxiv.org/content/10.1101/2024.02.12.579972v1 (visited on 02/27/2024).

[33] H. S. J. Cheong et al. *Transforming descending input into behavior: The organization of premotor circuits in the Drosophila Male Adult Nerve Cord connectome*. Pages: 2023.06.07.543976 Section: New Results. Jan. 26, 2024. DOI: 10.1101/2023.06.07.543976. URL: https://www.biorxiv.org/content/10.1101/2023.06.07.543976v2 (visited on 02/15/2024).

[34] Tyler Kennedy and Kendal Broadie. "Newly Identified Electrically Coupled Neurons Support Development of the Drosophila Giant Fiber Model Circuit". In: *eNeuro* 5.6 (Dec. 2018), ENEURO.0346–18.2018. ISSN: 2373-2822. DOI: 10.1523/ENEURO.0346-18.2018.

[35] Sven Dorkenwald et al. *CAVE: Connectome Annotation Versioning Engine*. Pages: 2023.07.26.550598 Section: New Results. July 28, 2023. DOI: 10.1101/2023.07.26.550598. URL: https://www.biorxiv.org/content/10.1101/2023.07.26.550598v1 (visited on 10/16/2023).

[36] Fabian Pedregosa et al. “Scikit-learn: Machine Learning in Python”. In: *Journal of Machine Learning Research* 12.85 (2011), pp. 2825–2830. ISSN: 1533-7928. URL: http://jmlr.org/papers/v12/pedregosa11a.html (visited on 02/19/2024).

[37] Johannes Schindelin et al. “Fiji: an open-source platform for biological-image analysis”. In: *Nature Methods* 9.7 (July 2012), pp. 676–682. ISSN: 1548-7105. DOI: 10.1038/nmeth.2019. URL: https://www.nature.com/articles/nmeth.2019 (visited on 10/16/2019).

Chapter 5

CONCLUDING REMARKS

5.0.1 Overview

All together, these chapters address the anatomy of neural circuits for sensing and controlling a wing. During flight, these neural circuits allow a fly to rapidly adjust its musculature in response to a dynamic environment. Chapters 2 and 4 detail how a connectome's outputs and inputs were identified, respectively, and chapter 3 analyzes the synaptic structure of a middle layer of the nervous system. By examining these networks, we found that groups of premotor neurons preferentially target specific groups of motor neurons, but developmental identity of premotor neurons does not determine which groups they target. By identifying the muscle outputs of these motor neurons, we were able to uncover the different synaptic architectures of premotor-to-muscle "motor modules" that exist within one animal to support different ranges of motion at different types of joints. Especially revealing were the groupings of motor neurons that innervate wing muscles directly connected to the wing hinge. The biomechanics of the wing hinge are still an enigma, so we did not know if the motor neurons received independent streams of input or would be grouped together. The modules we observed often mapped on to experimentally-informed predictions, while some offered new synergies to directly test.

The public resources created along the way in the form of motor neuron morphology to muscle mapping, wing sensory axon morphology to sensory organ mapping, and hemilineage annotation for VNC interneurons, will hopefully expand and accelerate future research on a range of sensorimotor behaviors in adult *Drosophila*.

Functional implications of VNC anatomy

What matters about the nervous system is how it functions: what it actually does. Anatomy can only go so far in generating hypotheses about function. In some cases, anatomy describes what we observe experimentally, as in the case of common input to b1 and b2 wing motor neurons, and their correlated timing of firing during flight[1]. In other cases, anatomy misses important pieces of the puzzle, as the leg motor neurons that receive the most synaptic input actually tend to fire last, because they are larger and thus have lower resistance to electrical input[2]. Connectomics is a powerful engine for generating predictions, but these predictions must eventually be verified experimentally. As sparse genetic tools for *Drosophila* continue to expand, these experiments will become more feasible and interpretable.

By combining connectomic analysis and findings from past literature, a number of predictions regarding VNC function can be made based on these projects. One such prediction is the consequence of non-proportional synaptic input to direct wing motor neurons. We predict that direct wing motor neurons that receive common input are a flexible motor synergy, in which they are often activated together but with variable recruitment orders, such that which premotor neurons are active determine the precise spike timing within a steering motor module. This level of flexibility may reflect the relatively low number of muscles involved in controlling the wing in relation to the relatively high number of degrees of freedom at the wing hinge joint, or it may allow for the behavior flexibility of using wings for both flight and courtship - or both.

Evolutionary insights from VNC anatomy

Nervous systems don't develop *de novo*. They are the product of millions of years of evolution. Previously, it was thought that asynchronous flight evolved independently at least seven times[3]. Recently, however, genetic evidence suggests a more likely theory, that asynchronous flight has evolved once, but some species have reverted back to synchronous flight[4]. The wealth of literature recording from locust central circuits may support this theory. In-

terneurons in the locust flight system either reset the wingbeat phase or shift the firing phase of a motor neuron, but not both[5]. This division suggests that central circuits for decoupling power and steering existed before the specialized musculature for stretch-activated muscles. Further, some of the flight interneurons in locusts closely resemble wing premotor neurons identified in FANC, including the premotor interneuron in **Figure 2.5**, which resembles locust interneuron 301.[5] These morphologies can be mapped to their developmental identity, or hemilineage, based on stereotyped features such as cell body location and primary neurite tract[6,7,8]. One theory holds that these hemilineages constitute an evolutionary "toolkit" or "groundplan" from which behavior develops[9]. As the connectomes of more species are analyzed, we may be able to glean clues about how neural circuit anatomy lays the groundwork for evolutionary adaptations. For example, there are flightless insects whose evolutionary ancestors had wings, e.g. snow flies (*chionea*). Are hemilineages that mainly contact wing motor neurons present in these animals? Are they co-opted into different circuits, reduced in connectivity, or not present at all?

Another unexpected similarity we observed between the locust and the fly was the prominence of the tegula for sensory feedback. In locusts, stimulation of the tegula resets the wingstroke[10]. In *Drosophila*, however, the role of the tegula as a sensor has never been directly tested. We found that the tegula has a chordotonal organ and a hair plate, as well as the field of campaniform sensilla that provides the most direct synaptic input to wing motor neurons. In locusts, the tegula features a field of mechanosensitive hairs, not campaniform sensilla[11]. These hairs, unlike the hairs along the anterior edge of the wing, are innervated by single neurons, so they may share a genetic blueprint with campaniform sensilla[12]. The circuitry, as well, is different between the two species. In locusts, the tegula axons contact premotor neurons[13], whereas in *Drosophila* the tegula axons contact both premotor neurons and motor neurons. How these circuits have changed to support the different flight control strategies necessary for synchronous vs. asynchronous flight may reveal critical steps in the evolution of neural circuits for flight.

Relevance to human neural circuits

The ventral nerve cord is analogous to the vertebrate spinal cord. Both integrate sensory signals and distribute commands to muscles. The VNC, however, contains orders of magnitude fewer neurons and is not encased in bone, making it more feasible to study. There's a lot we don't know about how the spine is organized, and studying more accessible organisms can motivate more targeted research about spinal neural circuits. We found that in the fly, a majority of direct synaptic input is from local interneurons, and only about 10% of synaptic input is from the brain. These proportions may be a fundamental principle of how nervous systems develop, and could help guide our understanding of disease. For example, students are often taught that Parkinson's disease is "caused" by the death of Dopamine cells in the Substantia Nigra brain area, based on lesion experiments[14]. Despite the prevalence of the disease, like many diseases its "cause" is unknown, and it is instead diagnosed based on symptoms[15]. It is possible that changes observed in the brain of PD patients originate in the spinal cord, in the premotor or motor areas responsible for many of the symptoms. By studying accessible nerve cords, we may be able to uncover fundamental principles or how nervous systems are organized that could lead to better treatment and prevention of diseases.

5.0.2 Outlook

Sensorimotor neural circuits are the anatomical implementation of how an animal responds to its environment. Although a connectome shows every single neuron, it only captures the nervous system at a single point in time. To gain insight about how these circuits develop and change in response to experience, connectome analysis needs to be combined with creative experiments. Addressing these questions in *Drosophila* feels possible, thanks to the wealth of literature, genetic resources, and large collaborative communities. This dissertation focuses on creating community resources for interpreting connectomes. My aim is that these resources can contribute to future discoveries that expand our understanding of sensorimotor circuits.

References

[1] Gerhard Heide. "Neural mechanisms of flight control in Diptera". In: *BIONA-report* 2 (1983), pp. 35–52.

[2] J. E. Zengel et al. "Membrane electrical properties and prediction of motor-unit type of medial gastrocnemius motoneurons in the cat". In: *Journal of Neurophysiology* 53.5 (May 1, 1985), pp. 1323–1344. ISSN: 0022-3077. DOI: 10.1152/jn.1985.53.5.1323. URL: https://www.physiology.org/doi/abs/10.1152/jn.1985.53.5.1323 (visited on 07/10/2019).

[3] Robert Dudley. *The Biomechanics of Insect Flight: Form, Function, Evolution*. Google-Books-ID: hTIMhD9BF1kC. Princeton University Press, Sept. 29, 2002. 506 pp. ISBN: 978-0-691-09491-5.

[4] Jeff Gau et al. "Bridging two insect flight modes in evolution, physiology and robophysics". In: *Nature* 622.7984 (Oct. 2023). Number: 7984 Publisher: Nature Publishing Group, pp. 767–774. ISSN: 1476-4687. DOI: 10.1038/s41586-023-06606-3. URL: https://www.nature.com/articles/s41586-023-06606-3 (visited on 03/01/2024).

[5] R. M. Robertson and K. G. Pearson. "Interneurons in the flight system of the locust: distribution, connections, and resetting properties". In: *The Journal of Comparative Neurology* 215.1 (Mar. 20, 1983), pp. 33–50. ISSN: 0021-9967. DOI: 10.1002/cne.902150104.

[6] Haluk Lacin et al. "Neurotransmitter identity is acquired in a lineage-restricted manner in the Drosophila CNS". In: *eLife* 8 (Mar. 26, 2019). Ed. by K VijayRaghavan, Sonia Sen, and Matthias Landgraf. Publisher: eLife Sciences Publications, Ltd, e43701. ISSN: 2050-084X. DOI: 10.7554/eLife.43701. URL: https://doi.org/10.7554/eLife.43701 (visited on 10/21/2022).

[7] Elizabeth C. Marin et al. *Systematic annotation of a complete adult male Drosophila nerve cord connectome reveals principles of functional organisation*. Pages: 2023.06.05.543407 Section: New Results. June 6, 2023. DOI: 10.1101/2023.06.05.543407. URL: https://www.biorxiv.org/content/10.1101/2023.06.05.543407v1 (visited on 08/30/2023).

[8] James W. Truman et al. "Developmental architecture of adult-specific lineages in the ventral CNS of Drosophila". In: *Development* 131.20 (Oct. 15, 2004), pp. 5167–5184. ISSN: 0950-1991. DOI: 10.1242/dev.01371. URL: https://doi.org/10.1242/dev.01371 (visited on 11/08/2022).

[9] Robin M Harris et al. "Neuron hemilineages provide the functional ground plan for the Drosophila ventral nervous system". In: *eLife* 4 (July 20, 2015). Ed. by Leslie C Griffith. Publisher: eLife Sciences Publications, Ltd, e04493. ISSN: 2050-084X. DOI: 10.7554/eLife.04493. URL: https://doi.org/10.7554/eLife.04493 (visited on 10/21/2022).

[10] Harald Wolf. "The Locust Tegula: Significance for Flight Rhythm Generation, Wing Movement Control and Aerodynamic Force Production". In: *Journal of Experimental Biology* 182.1 (Sept. 1, 1993), pp. 229–253. ISSN: 0022-0949. DOI: 10.1242/jeb.182.1.229. URL: https://doi.org/10.1242/jeb.182.1.229 (visited on 02/20/2024).

[11] W. Kutsch, H. Hanloser, and M. Reinecke. "Light- and electron-microscopic analysis of a complex sensory organ: The tegula of Locusta migratoria". In: *Cell and Tissue Research* 210.3 (Sept. 1, 1980), pp. 461–478. ISSN: 1432-0878. DOI: 10.1007/BF00220202. URL: https://doi.org/10.1007/BF00220202 (visited on 03/01/2024).

[12] Eric C Lai and Virginie Orgogozo. "A hidden program in *Drosophila* peripheral neurogenesis revealed: fundamental principles underlying sensory organ diversity". In: *Developmental Biology* 269.1 (May 1, 2004), pp. 1–17. ISSN: 0012-1606. DOI: 10.1016/j.ydbio.2004.01.032. URL: https://www.sciencedirect.com/science/article/pii/S001216060400082X (visited on 02/21/2024).

[13] K. G. Pearson and H. Wolf. "Connections of Hindwing Tegulae with Flight Neurones in the Locust, Locusta Migratoria". In: *Journal of Experimental Biology* 135.1 (Mar. 1, 1988), pp. 381–409. ISSN: 0022-0949. DOI: 10.1242/jeb.135.1.381. URL: https://doi.org/10.1242/jeb.135.1.381 (visited on 03/01/2024).

[14] J. G. Greenfield and Frances D. Bosanquet. "The Brain-Stem Lesions in Parkinsonism". In: *Journal of Neurology, Neurosurgery & Psychiatry* 16.4 (Nov. 1, 1953). Publisher: BMJ Publishing Group Ltd Section: Articles, pp. 213–226. ISSN: 0022-3050, 1468-330X. DOI: 10.1136/jnnp.16.4.213. URL: https://jnnp.bmj.com/content/16/4/213 (visited on 02/29/2024).

[15] Melissa J. Armstrong and Michael S. Okun. "Diagnosis and Treatment of Parkinson Disease: A Review". In: *JAMA* 323.6 (Feb. 11, 2020), pp. 548–560. ISSN: 0098-7484. DOI: 10.1001/jama.2019.22360. URL: https://doi.org/10.1001/jama.2019.22360 (visited on 02/29/2024).